Polarization and Correlation Phenomena in the Radiative Electron Capture by Bare Highly-Charged Ions

Inaugural-Dissertation

zur Erlangung der

Doktorwürde der Naturwissenschaften

(Dr. rer. nat.)

vorgelegt beim Fachbereich Physik

der Universität Kassel

von

Andrey Surzhykov

aus Moskau, Russland

October 2003

Gedruckt mit Genehmigung des Fachbereichs Physik der
Universität Kassel.

1. Gutachter: PD Dr. S. Fritzsche
2. Gutachter: Prof. Dr. B. Fricke

weitere Miglieder der Prüfungskommission:

Prof. Dr. T. Baumert
Prof. Dr. F. Bosch

Tag der Disputation: 26 November 2003

Contents

vi

Chapter 1

Introduction

Owing to the recent experimental advances in heavy–ion accelerator and storage ring techniques, it becomes possible nowadays to produce, to accelerate and, then, to store highly stripped ions up to bare uranium U^{92+}. Within the last decade, these – heavy – ions have proved to be a unique tool in a large number of case studies in many areas of modern physics (see Figure 1.1). For example, in *nuclear and particle physics*, heavy ion collisions may help us to explore the properties of the heavy as well as superheavy elements or even (in the ultrarelativistic regime) of the quark–gluon plasma. Furthermore, the interaction of the intense ion beams with the solid targets allows to produce and to investigate dense plasma phenomena associated with high energy density matter, a topic of high interest in *astrophysics* as well as *plasma physics*. Apart from the fundamental research, heavy ions are widely used in different applications such as the cancer therapy in *biophysics* or, let us say, the interaction of the energetic ions with matter in *material sciences*.

Of course, experiments with highly–charged ions have also opened up new and very promising opportunities in *atomic physics*. These opportunities are generally related to the studies of one– or few–electron systems in the exceptionally strong electromagnetic fields produced by the heavy nuclei. Such "extreme" conditions may lead, in particular, to the quite remarkable effects both in electronic *structure* of the few–electron ions as well as in their *collision* dynamics (Warczak 2003). Obviously, these two general aspects of atomic physics with heavy ions are strongly correlated with each other. While, for instance, ion collisions are usually applied in atomic structure studies in order to populate the excited states, the knowledge on the structure is highly required for the proper analysis of the collision experiments.

In atomic structure studies, for instance, the heavy ions provides us with the unique possibility to test quantum electrodynamics (QED) in a regime where its standard treatment, based on the perturbation expansion in terms of $\alpha \cdot Z$ parameters (Mohr *et al* 1998), is no longer a suitable tool. While, in particular, for the neutral hydrogen ($Z = 1$), the fine structure constant $\alpha = 1/137.036 \ll 1$ ensures the fast convergency of the perturbation expansion, for the high–Z system, where $\alpha \cdot Z$ approaches to unity, we have to deal with all orders of expansion coefficients. One of the most important tools for investigation of these higher order QED corrections is given by the measurements of the Lamb shift in heavy few–electron ions. In this contribution, for example, a number of experiments have been performed recently in order to study the *ground–*
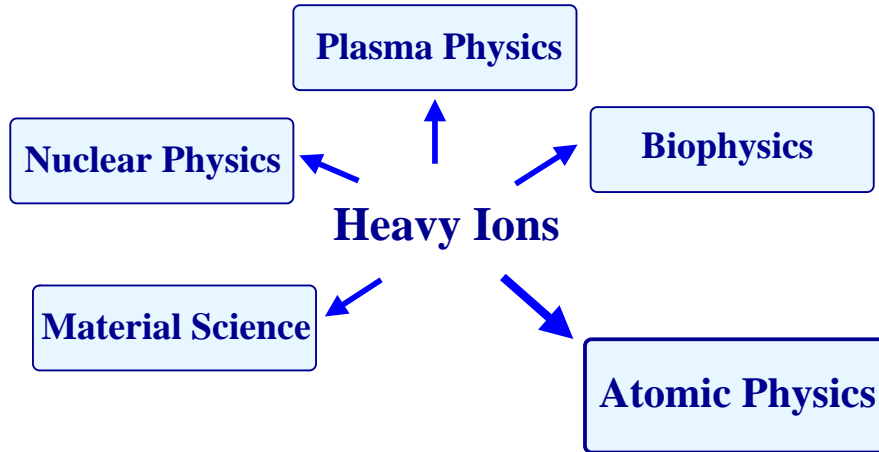
Figure 1.1: Heavy ion research in modern physics and related natural sciences (Metag 2000).

state Lamb shift in hydrogen– as well as helium–like uranium ions (Beyer *et al* 1995, Stöhlker *et al* 2000, Gumberidze 2003). These measurements provided new and very accurate results which are now well understood within the theoretical treatment (Beier 2000, Yerokhin and Shabaev 2001, Yerokhin *et al* 2003).

Beside of the electronic structure, the strong electromagnetic field of heavy nuclei strongly affect the *dynamical* behaviour of ions. In order to explore this second important aspect of heavy ion (atomic) physics, intensive experimental and theoretical studies have been focused recently on the *relativistic* collisions of high–Z projectile ions with low–Z target atoms (Eichler and Meyerhof 1995). However, since, these collisions give rise to a broad variety of recombination, ionization and excitation processes, we will restrict our discussion here to the particular case of studies with *bare* highly–charged ions. One of the most basic processes in collisions of such – bare – ions is the transfer of an electron between the low–Z target atom and a fast moving projectile. For not too high collision velocities, this process is governed by the so–called *nonradiative electron capture* (NRC), at which the energy and momentum transfer in collision is shared between projectile, target and the captured electron. The nonradiative capture, however, possesses a dramatic velocity dependence $\sigma_{NRC} \sim v^{-12}$ (Oppenheimer 1928) and, hence, typically plays no role at projectile energies of more than $T_p \sim 100$ MeV/u. At such highly energetic collisions, the electron transfer is accompanied by the simultaneous emission of a photon carrying away the excess energy and momentum. This process, typically denoted as the radiative electron capture (REC), attracts nowadays much experimental as well as theoretical attention. It is related, in particular, to the developments in the field of the ion storage rings where the electron recombinations are the dominant (ion) loss processes. Another and even more fundamental interest arises from the fact that, for high–Z projectiles and low–Z targets, the REC process is almost identical to the radiative recombination (RR) of the ion with a *free* electron which, in turn, is the inverse of the photoelectric effect (cf Figure 1.2). Therefore, the measurements on the radiative electron capture by heavy ions allow us to study the strong filed effects in the photoionization which is, in fact, one of the most fundamental interaction processes between light and matter (Ichihara *et al* 1994, Stöhlker *et al* 1999).
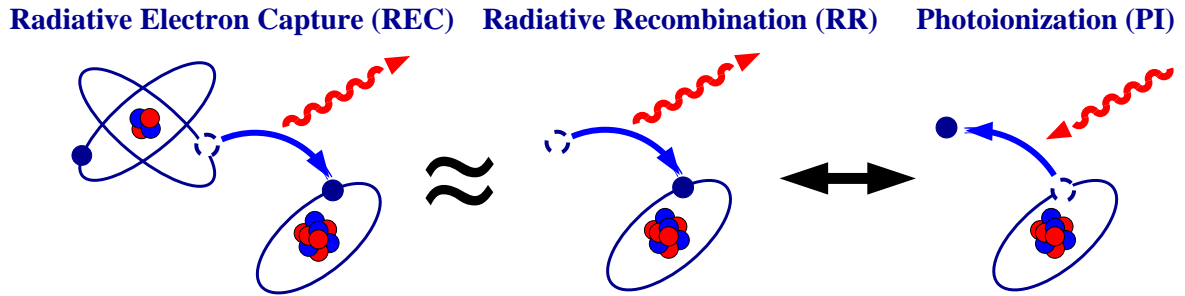
Radiative Electron Capture (REC)   Radiative Recombination (RR)   Photoionization (PI)

Figure 1.2: In the relativistic collisions of high–Z projectiles with low–Z target atoms, an electron may be radiatively captured into a bound ion state. Since a loosely bound target electron may be considered as quasi–free, the radiative electron capture (REC) is almost identical to the radiative recombination (RR) of a projectile ion with free electron, which is the time–inverse photoionization process (PI).

In this contribution, the radiative electron capture by bare high–Z ions has been intensively studied during the last decade at the GSI (Gesellschaft für Schwerionenforschung) storage ring in Darmstadt. Such measurements become possible nowadays due to the considerable progress in the precision x–ray spectroscopy. In particular, application of the efficient x–ray detectors allowed to explore not only the *total* REC cross sections but also the *angular distributions* of the emitted recombination photons (Stöhlker 1999, Stöhlker *et al* 2000). These – angular resolved – measurements proved to be an extremely precise tool for investigation of the relativistic and magnetic interaction effects in the electron capture processes. The proper *theoretical* description of these higher–order effects requires, however, the fully relativistic treatment for both the electronic wavefunctions as well as the electron–photon interaction operator (Pratt *et al* 1977, Eichler and Meyerhof 1995). In **Chapter 2**, therefore, we will discuss in detail the basic relations of this exact relativistic treatment and then emphasize the general agreement between the theoretical computations and the experimental data.

The former experimental and theoretical studies on the total and, especially, angle–differential REC cross sections have certainly revealed an important knowledge on the dynamics of electron recombination in the presence of the strong electromagnetic fields. This knowledge, however, is still incomplete mainly because both (the total and angle–differential) cross sections are not sensitive to the magnetic (spin) states of the projectile ion and target atom as well as to the polarization of the emitted radiation. In order to get an access to this – highly precise – magnetic substate information, a new generation of electron capture experiments is currently under the way at the GSI storage ring (Stöhlker *et al* 2003a). In these experiments, one may explore the *polarization* of the emitted x–ray photons as well as the different *correlation* phenomena arising in the REC into excited ionic states.

In this contribution, we outline here the recent progress in polarization and correlation studies on the radiative electron capture into highly–charged ions. The theoretical background of such studies is given by the exact relativistic treatment which is (in the moment) the most accurate description of the REC process. In particular, following this approach, below we will make no difference between the REC and the radiative recombination (RR) processes, assuming, therefore, a target electron as quasi–free. Exact relativistic treatment, however,

3

has to be placed in a proper framework that would provides us with a simple access to the polarization and correlation properties of particles. Most naturally, this framework is given by the *density matrix theory* whose basic principles are summarized in **Chapter 3**. Starting from these principles, we theoretically describe the *two–step* REC process in which a quasi–free electron is radiatively captured into an excited ion state that later decays under the emission of a characteristic photon. Explicit expressions are derived for the observable properties of the recombination and the subsequent decay x–ray photons as well as for the magnetic sublevel population of the residual (hydrogen–like) ion. While, of course, these expressions may be employed for the description of an arbitrary one–, two– and even multi–step recombination process, in **Chapter 4** we consider only *two cases* which are, in fact, typical for nowadays experiments (Stöhlker 1999, Warczak 2003). In the first case, which is a trivial example of one–step recombination, an electron is captured into the K–shell of bare projectile ion. Since, however, the total as well as angle–differential K–REC cross sections have been well studied before, we restrict our treatment to the *polarization* of the emitted x–rays. In our theoretical analysis, emphasis is placed on the effect of the spin–polarization of the incident particles on the linear polarization of the recombination photons. We show, in particular, that non–zero polarization of the electron target leads to an overall rotation of the linear polarization of light out of the reaction plane. This theoretical finding may have an considerable impact for the experimental studies both in atomic and nuclear physics where the problem of "measuring" the polarization of the target atoms (or electrons) and ion beams attracts now much interest.

Beside of the recombination into the ground ionic state, we also implement the density matrix approach in order to study the second typical experimental situation: electron capture into the $2p_{3/2}$ level and the subsequent Lyman–α_1 ($2p_{3/2} \rightarrow 1s_{1/2}$) decay. For such two–step recombination process, we explore in detail not only the *individual* properties of the first and second steps but also the *correlated* photon emission which may be observed in the coincidence (e, 2γ) experiment. It is shown, in particular, that similar to the linear polarization of the recombination photons, the photon–photon correlations appear to be much sensitive to the polarization of the incident particles and provides, therefore, an alternative route for the polarization studies on the heavy ion beams. In **Chapter 5** we give a summary of these theoretical results and their implication for the future experimental research, while, finally, six – most important – works on electron recombination which have been published by us during the last three years are included in **Chapter 8**.

Chapter 2

Radiative electron capture: Present status of studies

Theoretical studies on the radiative electron capture (as well as the radiative recombination) have a very long tradition. Since the early days of the development of quantum mechanics this process has been known as the time–reversed photoionization. On this basis, and by applying the principle of the detailed ballance, Stobbe in 1930 presented a general formalism for describing the radiative recombination into arbitrary projectile states within the framework of a nonrelativistic dipole approximation. This – nonrelativistic – approach has been reviewed in later theoretical studies which have incorporated the *relativistic* effects in the photoionization and, consequently, the radiative recombination processes. For example, the first order relativistic Born approximation has been applied in 1931 by Sauter in order to calculate the K–shell (photoionization as well as recombination) total and angle–differential cross sections. The Sauter theory, however, provided unsatisfactory results for the photoionization of the medium–Z and high–Z atoms and, hence, was modified in the beginning of sixties by Gavrila (1960) and Nagel (1960) who included the next order Born corrections. Of course, owing to the computational difficulties, these corrections have still based on the *approximate* wavefunctions for both bound and continuum (relativistic) electrons. However, in the light of the recent progress in computer technologies, the rigorous relativistic calculations became possible which included both *exact* relativistic electron wavefunctions as well as all multipoles in the electron–photon interaction operator (Pratt *et al* 1973, Eichler and Meyerhof 1995).

Although theoretically the radiative electron capture has been known for a long period, the emission of the recombination photons was observed for the first time only in the early seventies by Raisbeck and Yoiu (1971), Schnopper *et al* (1972) and Kienle *et al* (1973) and since then became a subject of intensive experimental studies. In the beginning, however, most of these experimental efforts were focused on the radiative electron capture by the light–Z and medium–Z projectile ions (Tanis *et al* 1978, Spindler *et al* 1979, Tawara *et al* 1982, Anholt *et al* 1984) for which the relativistic and high–order multipole effects were rather small. Only with the recent experimental advances in heavy–ion accelerators and ion storage rings, more possibilities arise to study the relativistic collision of *high–Z* projectile ions with low–Z target atoms (or free electrons). For such collisions, for example, a large number of measurements have been carried
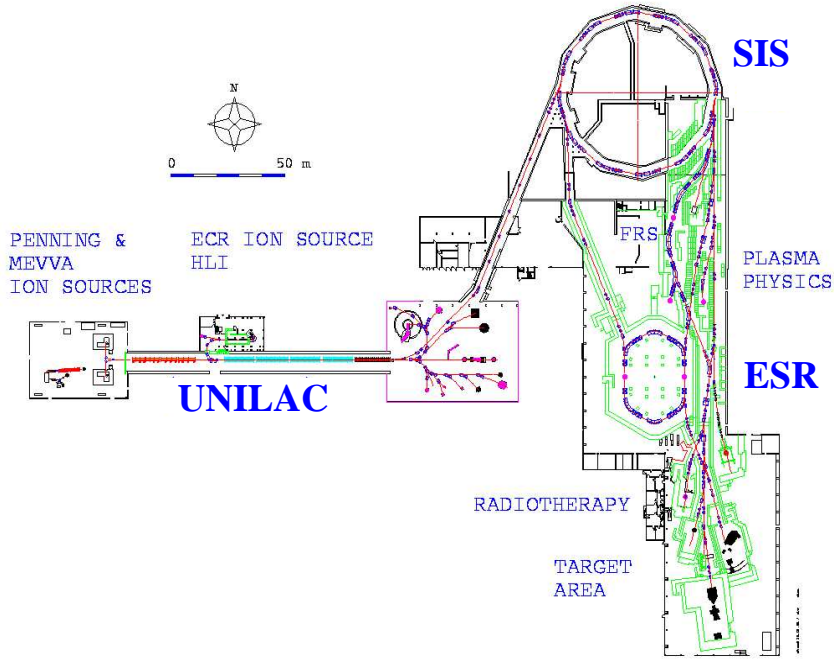
Figure 2.1: Layout of the heavy ion synchrotron/storage ring facility SIS/ESR (from `www.gsi.de`).

out at the GSI storage ring in Darmstadt in order to explore the total and angle–differential recombination cross sections (Stöhlker *et al* 1995, Stöhlker 1999). These experimental findings, whose brief outline is given in Section 2.1, are now well understood within the framework of (above mentioned) exact relativistic description. The basic relations of this treatment as applied to the electron capture process are summarized then in Section 2.2.

2.1 Experimental studies at the ESR storage ring

During the last ten years, the radiative electron capture into the bound states of highly–charged projectile ions has been intensively studied at the GSI laboratory in Darmstadt. This experimental facility was established more than 30 years ago in order to provide the heavy ion research in the atomic, nuclear, plasma, solid state physics as well as in the related natural sciences. Nowadays, GSI is the complex accelerator structure which consists of the linear accelerator UNILAC (UNIversal Linear ACcelerator), the heavy ion synchrotron SIS (Schwerionensynchrotron), and the experimental storage ring ESR (cf Figure 2.1). The accelerator facilities UNILAC and SIS are usually applied in order to produce (in the required charge states) and to accelerate the beams of the ions which later can be accumulated into the ESR storage ring. In fact, the ESR offers the unique opportunities to store fully stripped heavy ions up to bare uranium U^{92+} at energies between 50 and 560 MeV/u and to employ them for a broad range of atomic as well as nuclear physics experiments (Blasche and Franzke 1994, Mokler and Stöhlker 1996). The measurements on the radiative electron capture, for example, are typically performed at the ESR internal jet target (Reich *et al* 1997) where the thin gaseous targets from H_2 up to Xe are used with the densities of about $\rho \sim 10^{12}$ particles/cm^3. In the reaction cham-
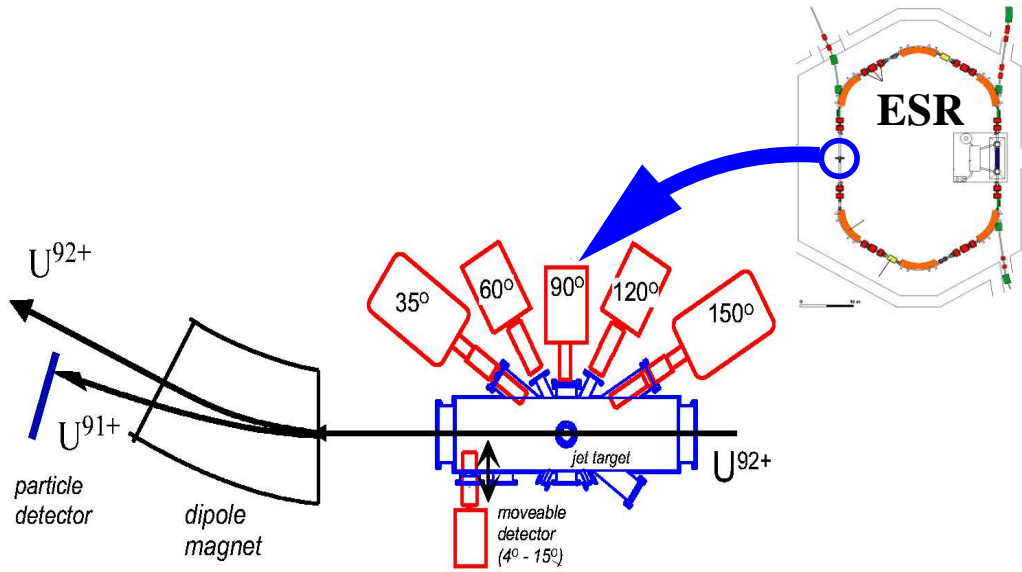
6

Figure 2.2: The internal ESR jet–target allows to explore the projectile x–ray emission at various observation angles from nearly 0° to 150° with respect to the ion beam. Emitted photons are observed in coincidence with the down–charged ions, detected by the particle counter behind the dipole magnet.

ber of this target, as seen from Figure 2.2, the stored projectile ions cross a perpendicularly oriented molecular or atomic supersonic gas jet and, therefore, may (radiatively) capture the loosely bound target electrons. The associated photon emission is then observed by the set of the x–ray detectors which are viewing the gas–jet/beam interaction zone at the different angles from almost 0° up to 150°. Moreover, in order to ensure that the photon is emitted due to the electron recombination, the signal from the x–ray detector is always counted in coincidence with the signal from the particle detector which registers the down–charged particles (cf Figure 2.2).

In recent years, the experimental set–up 2.2 has been successfully implemented in order to explore the total as well as the angle–differential cross sections for the electron capture into the $K-$ and L–shells of bare high–Z projectile ions (Stöhlker *et al* 1995, Brinzanescu 2000). For instance, Figure 2.3 displays the measured angular distribution of the K–REC photons for the bare uranium projectile ions U^{92+} with energies $T_p = 88$ MeV/u and $T_p = 310$ MeV/u. The experimental data, moreover, are compared with the theoretical calculations based on the nonrelativistic dipole approximation (dashed line) as well as on the exact relativistic treatment (solid line). While the details on this – relativistic – treatment will be given in the next Section, here we will mention only a good agreement between the theory and experimental results. In particular, the strong photon emission is confirmed for the forward directions which has to be attributed to the *spin–flip* electron transition arising due to interaction of the electron magnetic momentum with the magnetic field of the fast moving projectile (Ichihara *et al* 1994, Stöhlker *et al* 1999). The spin–flip transition, however, clearly manifests itself only for the electron capture by high–Z relativistic ions which, therefore, prove to be a very sensitive tool for studying the *magnetic* interaction effects in the ion–atom (ion–electron) collisions.
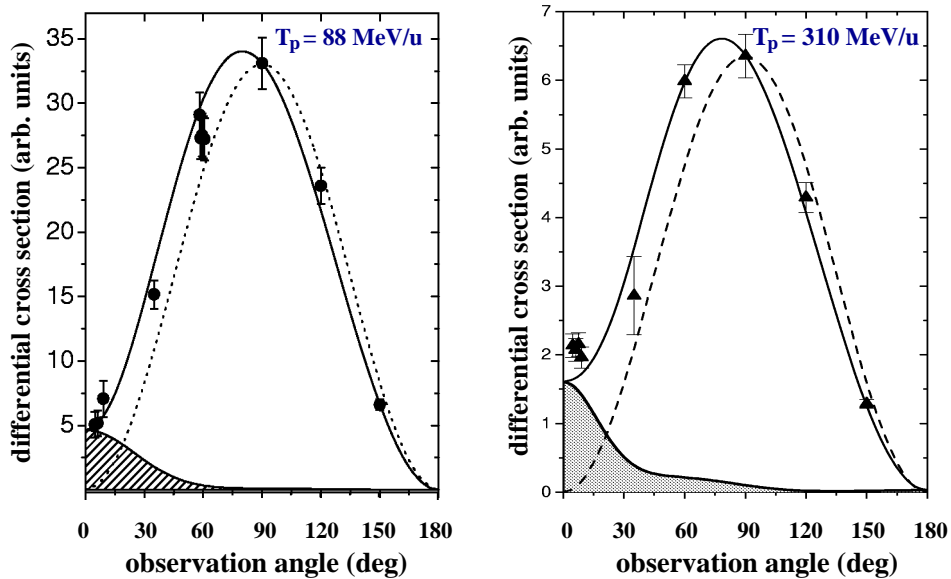
Figure 2.3: Experimental angular distributions of the photons emitted in the K–REC into bare uranium ions ions with projectile energies $T_p = 88$ MeV/u (left panel) and $T_p = 310$ MeV/u (right panel). The solid line represents the theoretical predictions based on the exact relativistic treatment (Brinzanescu 2000, Stöhlker *et al* 1999, 2001).

Beside the measurements on the REC (total and angle–differential) cross sections, the gas–jet target facility has also been employed to study the characteristic photon emission following the electron recombination into the excited ion states. Special emphasis has been placed, in particular, on the electron capture into the $2p_{3/2}$ state of bare uranium ions and the subsequent Lyman–α_1 $(2p_{3/2} \rightarrow 1s_{1/2})$ decay. From the observed emission pattern of the decay radiation (cf Figure 4.4), the information on the magnetic sublevel population of the $2p_{3/2}$ state was extracted (Stöhlker *et al* 1997). However, when compared with the theoretical calculations based on the exact relativistic description (Eichler 1994, Eichler *et al* 1998), these experimental findings showed a remarkable variance, which could not be attributed neither to additional cascade feeding processes nor to further corrections to the electron capture process. As it will be discussed later in Section 4.2, such derivation indicates the *magnetic* effects in the bound–bound electron transitions which become sizable for high–Z projectile ions.

2.2   Theoretical treatment: Exact relativistic description

The experimental results on the REC total cross sections and the angular distributions of the recombination photons are well reproduced nowadays by the theoretical computations based on the *exact relativistic treatment*. Within this approach, when applied to the collisions of high–Z projectiles with low–Z ions, the loosely bound target electrons are usually regarded as *quasi–free*. Therefore, it is a good approximation to substitute the REC process by the radiative recombination (RR) of a *free* electron into a bound state of projectile ion which is usually considered in its rest frame (projectile frame). Beyond this assumption, the description of the electron capture is rigorous by using exact relativistic wavefunctions for both initial–free and

final–bound electrons and by including retardation, i.e. all multipole orders of the photon field (Ichihara *et al* 1994, Eichler and Meyerhof 1995). In Subsection 2.2.1 we employ these exact wavefunctions to evaluate the matrix element for the free–bound electron transition which then can be used for calculations of the RR cross sections. Since, however, the cross sections are obtained within the projectile frame, their Lorentz transformation to the laboratory frame is required and briefly discussed in Subsection 2.2.2.

2.2.1 Evaluation of the free–bound transition amplitude

Obviously, the computations of the radiative recombination cross sections can be traced back to the evaluation of the *transition amplitude* for the capture of a free electron into a bound ionic state under the simultaneous emission of recombination photon. Within the first–order perturbation theory, this amplitude is given by (Pratt *et al* 1964, Alling and Johnson 1965)

$$M_{b\mathbf{p}}^{RR}(m_s, \lambda_{RR}, \mu_b) = \int d^3\mathbf{r}\, \psi_{j_b\mu_b}^{\dagger}(\mathbf{r})\, \alpha\, \hat{\mathbf{u}}_{\lambda_{RR}}^{*}\, \mathrm{e}^{-i\,\mathbf{k}_{RR}\mathbf{r}}\, \psi_{\mathbf{p}m_s}(\mathbf{r}) \tag{2.1}$$

where $\psi_{\mathbf{p}m_s}(\mathbf{r})$ and $\psi_{j_b\mu_b}(\mathbf{r})$ denote the Dirac–Coulomb wavefunctions for the incident free electron with well defined asymptotic momentum $\mathbf{p}$ and spin projection m_s and for the final hydrogen–like bound state $|n_b\, j_b\, \mu_b\rangle$, respectively. Moreover, the (relativistic) electron–photon interaction is described by the transition operator $\alpha\, \hat{\mathbf{u}}_{\lambda_{RR}}\, e^{i\,\mathbf{k}_{RR}\mathbf{r}}$ where $\mathbf{k}_{RR}$ is the wavevector of the emitted (recombination) photon and the unit vector $\hat{\mathbf{u}}_{\lambda_{RR}}$ refers to photon's right–hand ($\lambda_{RR} = +1$) and left–hand ($\lambda_{RR} = -1$) circular polarization (Berestetskii *et al* 1971).

For the further simplification of the transition amplitude (2.1), we need to decompose both, the photon as well as the free–electron wave functions into partial waves in order to make later use of the techniques of Racah's algebra. However, as discussed previously in a number of works (Eichler *et al* 1998, Surzhykov *et al* 2002a, Klasnikov *et al* 2003), we first have to decide about a proper quantization axis (z–axis) for this decomposition, depending – of course – on the particular process under consideration. For the radiative recombination of a projectile ion (at rest) with a free moving electron, the only really *preferred* direction of the overall system is given by the electron momentum $\mathbf{p}$ which we will adopt below as the quantization axis. To evaluate the transition amplitude (2.1) for such choice of the quantization axis, we shall start from the rotation of the photon field (Rose 1957)

$$\hat{\mathbf{u}}_{\lambda_{RR}}\, \mathrm{e}^{i\,\mathbf{k}_{RR}\mathbf{r}} \;=\; \sqrt{2\pi}\, \sum_{L=1}^{\infty}\, \sum_{M=-L}^{M=+L} i^L\, \sqrt{2L+1}\, \mathcal{A}_{LM}^{\lambda_{RR}}(\mathbf{r})\, D_{M\lambda_{RR}}^{L}(\mathbf{k}_{RR} \to \mathbf{z}), \tag{2.2}$$

which is – most conveniently – expressed in terms of its (electric and magnetic) multipole components (Eichler *et al* 1998):

$$\mathcal{A}_{LM}^{\lambda_{RR}}(\mathbf{r}) = \mathbf{A}_{LM}^{(m)}(\mathbf{r}) \;+\; i\lambda_{RR}\, \mathbf{A}_{LM}^{(e)}(\mathbf{r})\,. \tag{2.3}$$

Each of these multipoles may be written, respectively, as

$$\begin{aligned}
\mathbf{A}_{LM}^{(m)}(\mathbf{r}) &= j_L(kr)\, \mathbf{T}_{L,L}^{M}, \\
\mathbf{A}_{LM}^{(e)}(\mathbf{r}) &= j_{L-1}(kr)\, \sqrt{\frac{L+1}{2L+1}}\mathbf{T}_{L,L-1}^{M} - j_{L+1}(kr)\, \sqrt{\frac{L}{2L+1}}\mathbf{T}_{L,L+1}^{M},
\end{aligned} \tag{2.4}$$

9

where $j_L(kr)$ is the spherical Bessel function and $\mathbf{T}^M_{L,\Lambda}$ is the vector spherical harmonics of rank L (Edmonds 1996).

By inserting now the right–hand side of expansion (2.2) into the matrix element (2.1), we can represent the transition amplitude

$$
\begin{aligned}
M^{RR}_{b\mathbf{p}}(m_s, \lambda_{RR}, \mu_b) &= \sqrt{2\pi} \sum_{L=1}^{\infty} \sum_{M=-L}^{M=+L} i^{-L} \sqrt{2L+1}\, D^{L*}_{M\lambda_{RR}}(\mathbf{k}_{RR} \to \mathbf{z}) \\
&\times \int d^3\mathbf{r}\, \psi^{\dagger}_{j_b\mu_b}(\mathbf{r})\, \alpha\, \mathcal{A}^{\lambda_{RR}*}_{LM}(\mathbf{r})\, \psi_{\mathbf{p}m_s}(\mathbf{r})
\end{aligned} \tag{2.5}
$$

in terms of its electric and magnetic *multipole* matrix elements which, however, still include a continuum electron wavefunction with definite momentum $\mathbf{p}$ and helicity m_s. Therefore, this wavefunction also has to be represented as the partial wave decomposition which, for the particular choice of the quantization axis along the electron momentum $\mathbf{p}$, simply reads as (Eichler and Meyerhof 1995):

$$
\psi_{\mathbf{p}m_s}(\mathbf{r}) = \sum_{\kappa} i^l\, e^{i\Delta_\kappa} \sqrt{4\pi(2l+1)}\, \langle l0\, 1/2 m_s \,|\, j m_s \rangle\, \psi_{E\kappa m_s}(\mathbf{r}) \tag{2.6}
$$

where the summation runs over all partial waves $\kappa = \pm 1, \pm 2...$, i.e. over all possible values of the Dirac's angular momentum quantum number $\kappa = \pm(j + 1/2)$ for $l = j \pm 1/2$. In this notation, the (nonrelativistic angular) momentum l represents the parity of the partial waves and Δ_κ is the phase shift which arises due to the Coulomb potential of a *pointlike* nucleus (Bethe and Maximon 1954). Moreover, the partial waves

$$
\psi_{E\kappa m_s}(\mathbf{r}) = \frac{1}{r} \left(\begin{array}{c} P_{E\kappa}(r)\, \chi^{m_s}_{\kappa}(\hat{r}) \\ i\, Q_{E\kappa}(r)\, \chi^{m_s}_{-\kappa}(\hat{r}) \end{array} \right) \tag{2.7}
$$

separate into a radial and an angular parts, where the two radial functions $P_{E\kappa}(r)$ and $Q_{E\kappa}(r)$ are often called the *large* and *small* components of the partial wave and the corresponding angular parts $\chi^{m_s}_{\kappa}(\hat{r})$ and $\chi^{m_s}_{-\kappa}(\hat{r})$ are the standard Dirac spin–angular functions (Edmonds 1996, Varshalovich *et al* 1988).

Applying the decomposition (2.6) of the continuum electron wave and by making use of the Wigner–Eckart theorem (Zare 1998, Balashov *et al* 2000), the amplitude (2.5) may be finally expressed as:

$$
\begin{aligned}
M^{RR}_{b\mathbf{p}}(m_s, \lambda_{RR}, \mu_b) &= \sqrt{8}\,\pi \sum_{L=1}^{\infty} \sum_{M=-L}^{M=+L} \sum_{\kappa} i^{-L+l}\, e^{i\Delta_\kappa} \sqrt{(2L+1)(2l+1)}\, D^{L*}_{M\lambda_{RR}}(\mathbf{k}_{RR} \to \mathbf{z}) \\
&\times \langle l0\, 1/2 m_s \,|\, j m_s \rangle\, \langle j m_s\, LM \,|\, j_b \mu_b \rangle\, \left\langle n_b\, j_b \left\| \alpha\, \mathcal{A}^{\lambda_{RR}*}_L \right\| E\kappa j \right\rangle ,
\end{aligned} \tag{2.8}
$$

where $\left\langle n_b\, j_b \left\| \alpha\, \mathcal{A}^{\lambda_{RR}*}_L \right\| E\kappa j \right\rangle$ are the *reduced* matrix elements for the free–bound electron transition (Surzhykov *et al* 2002b). We can further simplify these matrix elements by using the calculus of the irreducible tensor operators (Edmonds 1996, Balashov *et al* 2000). That is, according to Equations (2.3) and (2.4), the reduced *free–bound* matrix element is written

$$
\begin{aligned}
\left\langle n_b\, j_b \left|\left| \alpha\, \mathcal{A}_L^{\lambda_{RR}*} \right|\right| E\kappa j \right\rangle &= \left\langle n_b\, j_b \left|\left| \alpha\, j_L(kr)\, \mathbf{T}_{L,L}^* \right|\right| E\kappa j \right\rangle \\
&\quad - i\lambda_{RR} \left[\sqrt{\frac{L+1}{2L+1}}\, \left\langle n_b\, j_b \left|\left| \alpha\, j_{L-1}(kr)\, \mathbf{T}_{L,L-1}^* \right|\right| E\kappa j \right\rangle \right. \\
&\qquad\qquad \left. - \sqrt{\frac{L}{2L+1}}\, \left\langle n_b\, j_b \left|\left| \alpha\, j_{L+1}(kr)\, \mathbf{T}_{L,L+1}^* \right|\right| E\kappa j \right\rangle \right] \quad (2.9)
\end{aligned}
$$

in terms on the (reduced) magnetic and electric multipole matrix elements which, in turn, can be decomposed into the radial and angular parts as (Eichler *et al* 1998):

$$
\begin{aligned}
\left\langle n_b\, j_b \left|\left| \alpha\, j_\Lambda(kr)\, \mathbf{T}_{L,\Lambda}^* \right|\right| E\kappa j \right\rangle &= -i \int dr\, Q_{n_b\, j_b}(r)\, j_\Lambda(kr)\, P_{E\,\kappa}(r) \left\langle \chi_{-\kappa_b} \left|\left| \sigma\, \mathbf{T}_{L,\Lambda}^* \right|\right| \chi_\kappa \right\rangle \\
&\quad + i \int dr\, P_{n_b\, j_b}(r)\, j_\Lambda(kr)\, Q_{E\,\kappa}(r) \left\langle \chi_{\kappa_b} \left|\left| \sigma\, \mathbf{T}_{L,\Lambda}^* \right|\right| \chi_{-\kappa} \right\rangle . \quad (2.10)
\end{aligned}
$$

The angular part of the amplitude (2.10) is given by the matrix element of the rank L spherical tensor $\sigma\, \mathbf{T}_{L,\Lambda}^* = [Y_\Lambda^* \otimes \sigma]_L$ that can be evaluated (for the arbitrary κ_1 and κ_2) to

$$
\left\langle \chi_{\kappa_1} \left|\left| \sigma\, \mathbf{T}_{L,\Lambda}^* \right|\right| \chi_{\kappa_2} \right\rangle = \sqrt{\frac{3}{2\pi}}\, [j_1, L, \Lambda, l_2]^{1/2}\, \left\langle l_2 0, \Lambda 0 \,|\, l_1 0 \right\rangle
\begin{Bmatrix} l_2 & 1/2 & j_2 \\ \Lambda & 1 & L \\ l_1 & 1/2 & j_1 \end{Bmatrix} , \qquad (2.11)
$$

by using a proper decomposition in terms of orbital and spin sub–states (Edmonds 1996, Varshalovich *et al* 1998). Moreover, for a pointlike nucleus and use of exact Dirac–Coulomb wavefunctions, the radial integrals in Equation (2.10) can also be expressed *analytically* by means of the hypergeometric functions $_2F_1(a, b; c; z)$ (Trautmann *et al* 1983, Valluri *et al* 1984). These (analytical) evaluations for both the radial and the angular matrix elements have been carried out by using the two computer–algebraic packages RACAH (Fritzsche 1997, Fritzsche *et al* 2001) and DIRAC, where the latter one represents a toolbox of Maple procedures designed for studying the properties and dynamical behaviour of hydrogen–like ions (Inghoff *et al* 2001).

2.2.2 Lorentz transformation of the cross sections

We may apply now the free–bound transition amplitude (2.8) in order to calculate the characteristics of the radiative recombination process. For example, the angle–differential cross section for the capture of an unpolarized electron into a bound $|n_b\, j_b\rangle$ state of bare projectile ion is given by the well–known formula (Eichler and Meyerhof 1995, Eichler *et al* 1996):

$$
\frac{d\sigma_{n_b\, j_b}^{RR}}{d\Omega_{RR}}(\theta_{RR}) = \frac{k_{RR}}{4\alpha} \left(\frac{\alpha^2}{\beta\gamma}\right)^2 \sum_{\lambda_{RR}\, m_s\, \mu_b} \left| M_{b\mathbf{p}}^{RR}(m_s, \lambda_{RR}, \mu_b) \right|^2 , \qquad (2.12)
$$

where we have averaged over the spin projections $m_s = \pm\, 1/2$ of the incident electron and summed over the magnetic sublevels μ_b of the residual ion as well as the polarizations $\lambda_{RR} = \pm 1$ of the emitted (recombination) photon. Moreover, the Lorentz factor $\gamma = 1/\sqrt{1-\beta^2}$ is related to the (relative) electron velocity $\beta = v/c$.
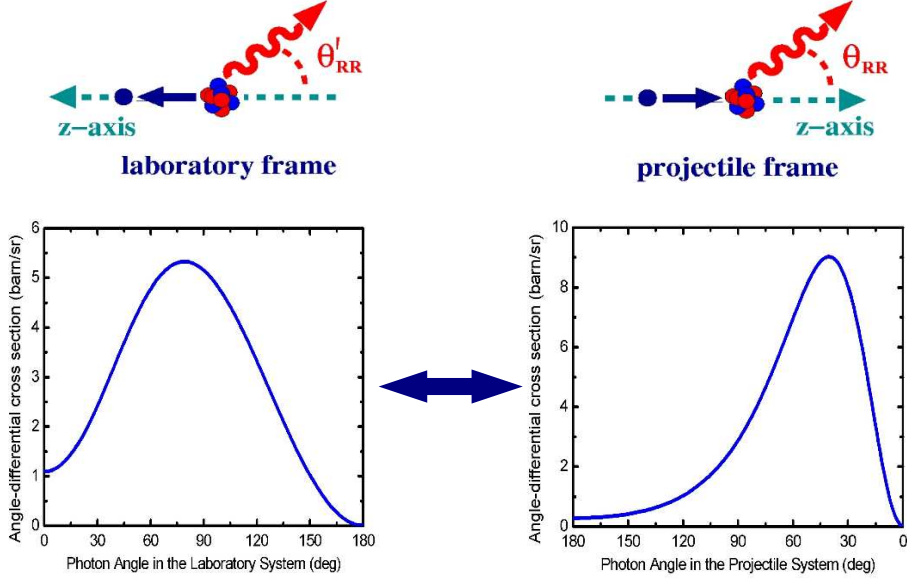
11

Figure 2.4: Angular distributions of the photons emitted in the radiative electron capture into the $K-$ shell of bare uranium ion with energy $T_p = 220$ MeV/u. Distributions are shown within the laboratory (left panel) and the projectile (right panel) frames.

Obviously, the angle–differential cross section (2.12) describes the emission of the recombination photons in the *projectile* system (i.e. the rest frame of the ion). However, as discussed in Section 2.1, the electron capture processes are typically observed in the *laboratory* system in which the projectile ions is moved with velocity β towards the target atoms (electrons). Since this is opposite to the direction of electron motion as seen from the projectile (cf Figure 2.4), we have first to replace the angle θ_{RR} of the photon emission with the $\pi - \theta_{RR}$ and then Lorentz–transform this – new – angle to the laboratory system (primed quantities):

$$\cos\theta_{RR} = \frac{\cos\theta'_{RR} - \beta}{1 - \beta\cos\theta'_{RR}}.\tag{2.13}$$

By means of the angle transformation (2.13), we may finally obtain

$$\frac{d\sigma^{RR}_{n_b j_b}}{d\Omega'_{RR}}(\theta'_{RR}) = \frac{1}{\gamma^2\left(1 - \beta\,\cos\theta'_{RR}\right)^2}\frac{d\sigma^{RR}_{n_b j_b}}{d\Omega_{RR}}(\theta_{RR})\tag{2.14}$$

the angular distribution of the recombination photons in the laboratory frame (Eichler and Meyerhof 1995). Figure 2.4 displays, for instance, the angle–differential cross sections for the K–shell recombination of bare uranium projectiles U^{92+} with energy $T_p = 220$ MeV/u which are calculated within the projectile as well as laboratory frames. As seen from these calculations, the Lorentz transformation partially cancels the forward shift of the photon emission pattern as measured in the projectile frame and therefore leads to the *nearly* symmetrical angular distribution in the laboratory frame (Spindler *et al* 1979, Stöhlker *et al* 2001). This cancellation effect, however, does not abolish the strong photon emission at the forward angles close to $\theta'_{RR} = 0°$ which, as mentioned above, is a clear signature of the magnetic interaction effects in relativistic heavy–ion collisions.

12

Chapter 3

Density matrix theory

The most natural framework for studying the polarization and correlation phenomena in the electron capture processes is given by the density matrix theory. Originally, this theory was introduced by von Neumann in 1927 to describe the statistical concepts in quantum mechanics and, hence, for the first time has been used mainly in statistical physics. In the middle of fifties, however, the applications of the density matrix have been gaining more and more importance in many other fields of physics. In atomic physics, for example, and combined particularly with the concept of spherical tensor, the density matrix approach was developed by Fano (1957). Since then, the density matrix has been utilized successfully in a large number of case studies on the polarization properties and the correlation between emitted particles and light (Blum 1981, Balashov *et al* 2000). Today, this formalism provides us with a tool of great elegance for our theoretical understanding of electron–atom and electron–ion collisions, the excitation of atomic autoionizing states (Balashov 1999), the polarization effects in the radiative and Auger decays (Berezhko and Kabachnik 1977), the theory of cascade processes, or even lifetime interferences in resonantly excited atoms (Kitajima *et al* 2002).

Since, however, the concept of the density matrix and statistical tensors as well as their applications in polarization and correlation studies have been presented in a number of works (Fano 1957, Fano and Racah 1959, Blum 1981, Slevin and Chwirot 1990), a rather short outline of the basic relations will be given in Section 3.1. While, of course, these relations are valid for any particular *representation* of the density matrix, the special interest in atomic physics is typically placed on the representation of the *angular momentum*. In this contribution, the most important cases of a *spin density matrix* of a (free and bound) electron as well as a photon are discussed in detail in Section 3.2. In particular, we will show how these density matrices are related to the (observable) polarization properties of both the electron and the photon beams and, therefore, can be easily implemented to study the polarization and correlation phenomena in electron–ion collision processes. In Section 3.3, for example, we will apply the basic concept of the spin density matrix in order to derive the angular distributions and polarization properties of the photons which are emitted in the two–step radiative recombination of a free (or quasi–free) electron into an excited state of the bare projectile ion.
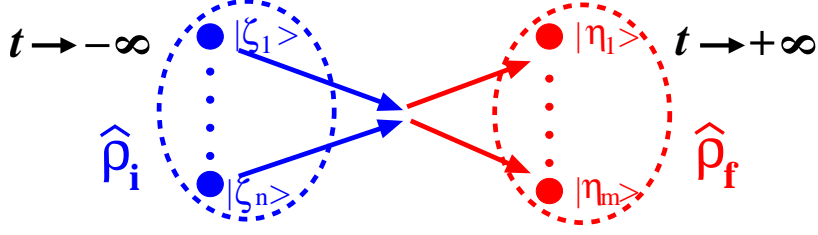
Figure 3.1: Time–independent treatment of the collision process; the statistical operators $\hat{\rho}_i$ and $\hat{\rho}_f$ describe the ensembles of particles of an "infinite time" before and after the collision.

3.1 Basic relations: Time–independent description

Within the density matrix theory, the state of a physical system is described in terms of so–called *statistical* (or *density*) operators (Fano 1957). These operators can be considered to represent, for instance, an ensemble of particles which are — altogether — in either a *pure* quantum state or in a *mixture* of different states with any degree of coherence. Then, the basic idea of the density matrix formalism is to *accompany* such an ensemble through the collision process, starting from an "initial" state which is prepared at an "infinite time" before the collision and reaching the "final" state of a system at an "infinite time" after the collision (cf Figure 3.1). Similar to the scattering theory, this collision process is described by so–called *transition* (or $\hat{T}$–) operator which connects the statistical operators of the initial $\hat{\rho}_i$ and the final $\hat{\rho}_f$ states by the standard rule (Blum 1981, Balashov *et al* 2000):

$$\hat{\rho}_f = \hat{T} \, \hat{\rho}_i \, \hat{T}^+ \ . \tag{3.1}$$

Instead of applying (operator) Equation (3.1), in practice, it is often more convenient to re–write the statistical operators in a matrix form. Of course, the matrix of the statistical operator (or so–called *density matrix*) will depend on the particular representation. Using, for instance, the representation of the individual quantum numbers $\{\zeta_i\}_{i=1...n}$ and $\{\eta_i\}_{i=1...m}$ for both the initial and final states of the system (see Figure 3.1), the final state density matrix may be obtained from Equation (3.1) as:

$$
\begin{aligned}
\left\langle \eta_1 \, ... \, \eta_m \,|\, \hat{\rho}_f \,|\, \eta_1' \, ... \, \eta_m' \right\rangle \;=\; & \sum_{\zeta_1 \, ... \, \zeta_n} \sum_{\zeta_1' \, ... \, \zeta_n'} \left\langle \eta_1 \, ... \, \eta_m \left| \hat{T} \right| \zeta_1 \, ... \, \zeta_n \right\rangle \\
\times \;\; & \left\langle \zeta_1 \, ... \, \zeta_n \,|\, \hat{\rho}_i \,|\, \zeta_1' \, ... \, \zeta_n' \right\rangle \left\langle \zeta_1' \, ... \, \zeta_n' \left| \hat{T}^+ \right| \eta_1' \, ... \, \eta_m' \right\rangle \ , \quad (3.2)
\end{aligned}
$$

where $\left\langle \eta_1 \, ... \, \eta_m \left| \hat{T} \right| \zeta_1 \, ... \, \zeta_n \right\rangle$ is the amplitude of transition from the state $|\zeta_1 \, ... \, \zeta_n\rangle$ to the state $|\eta_1 \, ... \, \eta_m\rangle$. Obviously, the particular form of this transition amplitude depends on the representations $\{\zeta_i\}$ and $\{\eta_i\}$ as well as on the considered collision process (i.e. on the particular form of the transition operator $\hat{T}$).

Equations (3.1) and (3.2) are basic expressions of the density matrix theory. Assuming that the initial state of system is well–defined, these Equations provide the *complete* information about the system in the final state and, hence, can be used to derive all physical characteristics of the system such as mean values and distributions of observables. Obviously, however, the outcome

14

of some considered experiment will depend on the particular set–up and the capability of the detectors for *resolving* the individual properties of the particles. In the density matrix theory, this set–up of the experiment is typically described in terms of a (so–called) *detector operator* $\hat{P}$ which characterizes the detector system as a whole. In fact, this detector operator can be considered to project out all those quantum states of the final–state system which leads to a "count" at the detectors; in the language of the density matrix the probability for an "event" at the detector is simply given by the trace of the detector operator with the matrix (3.2):

$$W = Tr(\hat{P}\ \hat{\rho}_f) = \sum_{\eta_1\ \dots\ \eta_n} \left\langle \eta_1\ \dots\ \eta_n \left| \hat{P}\ \hat{\rho}_f \right| \eta_1\ \dots\ \eta_n \right\rangle\ . \tag{3.3}$$

Apart from deriving the observable quantities of the system, however, the final state density matrix (3.2) may be also used in order to *separate* the density matrices of the subsystems or individual particles from one another. For instance, the density matrix of a single (k–th) particle may be found by taking trace of the final state matrix (3.2) over the quantum numbers of all particles except, certainly, the considered one:

$$\left\langle \eta_k \left| \hat{\rho}_f^{(k)} \right| \eta_k' \right\rangle = \sum_{\eta_1 \dots \eta_{k-1},\ \eta_{k+1} \dots \eta_m} \left\langle \eta_1\ \dots\ \eta_k\ \dots\ \eta_m \left| \hat{\rho}_f \right| \eta_1\ \dots\ \eta_k'\ \dots\ \eta_m \right\rangle\ . \tag{3.4}$$

In some practical applications, using the relation (3.4) is even more convenient than the "detector operator" technique (3.3). For instance, in the next Section we show that the density matrix of photons (in the helicity representation) is *directly* related to their polarization properties and, therefore, it is not necessary to "build up" the set of detectors in order to "measure" the polarization of light.

3.2   Spin density matrix and statistical tensors

As already mentioned in the previous Section, the density matrix of a system depends on the given representation. In atomic physics, for example, the polarization properties of particles are usually described in terms of the density matrix in representation of the *angular momentum* (spin, orbital or/and total). Obviously, the dimension and the particular form of such *spin density matrix* will be defined by the value of the angular momentum and by the physical properties of a considered particle. In the following, therefore, we consider the spin density matrices for three typical cases: a free electron (Subsection 3.2.1), an electron into a bound hydrogenic state (Subsection 3.2.2) and a photon (Subsection 3.2.3).

3.2.1   Spin density matrix of a free electron

Within the exact relativistic description (2.1), a free electron is described by well defined (and fixed) asymptotic momentum $\mathbf{p}$ and spin projection m_s on the quantization axis. Since an electron (with spin $S = 1/2$) has only two allowed spin projections $m_s = \pm\ 1/2$, its spin density matrix is a 2×2 matrix and, hence, may be parameterized by three real parameters (Kessler 1985, Balashov *et al* 2000):

$$\langle \mathbf{p}m_s\ |\hat{\rho}_e|\ \mathbf{p}m_s \rangle\ =\ \frac{1}{2} \begin{pmatrix} 1 + P_z & P_x - iP_y \\ P_x + iP_y & 1 - P_z \end{pmatrix}\ . \tag{3.5}$$

In fact, parameters $P_{x,y,z}$ are the cartesian coordinates of the polarization unit vector $\mathbf{P}$ of an electron beam and, therfore, depend on the choice of coordinate system. In the radiative recombination, for instance, the coordinate system is usually adopted in a way that the quantization axis (z–axis) is chosen along the electron momentum $\mathbf{p}$ (Surzhykov *et al* 2002b). For such choice of the quantization axis, parameter P_z reflects the degree of *longitudinal* polarization and two parameters P_x and P_y denote the *transversal* polarization of electrons.

3.2.2 Spin density matrix and statistical tensors of a bound electron

In contrast to a free electron function $|\mathbf{p}\,m_s\rangle$ which is built up as a superposition of the partial waves $|E\,\kappa\,m_s\rangle$ with the different angular momenta and parities (cf Equation (2.6)), an electron into a bound hydrogenic state has well specified principal n_b as well as Dirac's $\kappa_b = \pm(j_b + 1/2)$ quantum numbers. The polarization properties of such bound electron may be described, therefore, by the spin density matrix $\langle n_b\,j_b\,\mu_b|\,\hat{\rho}_e\,|\,n_b\,j_b\,\mu_b'\rangle$ with $\mu_b, \mu_b' = -j_b, -j_b + 1, \,...\,\, j_b$ in the representation of the (total) angular momentum. Instead of using this density matrix, however, it is often more convenient to represent ionic (or atomic) bound states in terms of so–called *statistical tensors*. Although, from a mathematical viewpoint, these statistical tensors are equivalent to the spin density matrix, they are constructed to represent the spherical tensors of rank k and component q. Hence, the statistical tensors can be expressed as a linear combination of the density matrix elements (Percival and Seaton 1957, Blum 1981)

$$\hat{\rho}_{kq}(j_b) = \sum_{\mu_b \mu_b'} (-1)^{j_b - \mu_b'}\,\langle j_b \mu_b\; j_b - \mu_b' \,|\, kq\rangle\,\langle n_b\,j_b\,\mu_b|\,\hat{\rho}_e\,|\,n_b\,j_b\,\mu_b'\rangle \tag{3.6}$$

following the standard procedure for the coupling of angular momenta. Owing to the properties of the Clebsch–Gordan coefficients, nonzero tensor components arise only for integer indices k, q with $0 \le k \le 2j_b$ and $q = -k, -k + 1, ..., k$, respectively.

In theory of atomic collisions, however, the statistical tensors (3.6) are usually normalized by means of *zero*–rank tensor (Blum 1981, Balashov *et al* 2000):

$$\mathcal{A}_{kq}(j_b) = \frac{\hat{\rho}_{kq}(j_b)}{\hat{\rho}_{00}(j_b)}\;. \tag{3.7}$$

These – *reduced* – statistical tensors have a particular meaning of the population of the individual substates $|n_b\,j_b\,\mu_b\rangle$ relative to each other. For instance, the (relative) magnetic sublevel population of the $p_{3/2}$ state is described by the component $\mathcal{A}_{20}(j_b)$ of the second–rank tensor

$$\mathcal{A}_{20}(j_b = 3/2) = \frac{N_{j_b\,\mu_b = \pm 3/2} - N_{j_b\,\mu_b = \pm 1/2}}{N_{j_b\,\mu_b = \pm 3/2} + N_{j_b\,\mu_b = \pm 1/2}} \tag{3.8}$$

which is well known as the *alignment* parameter (Berezhko and Kabachnik 1977).

3.2.3 Spin density matrix of photon: Polarization parameters

Of course, apart from description of the spin states of electrons or/and atoms, the density matrix formalism may be also applied for studying the polarization of the photon beams. In the case of photon, however, the spin density matrix is usually defined in the *helicity representation*
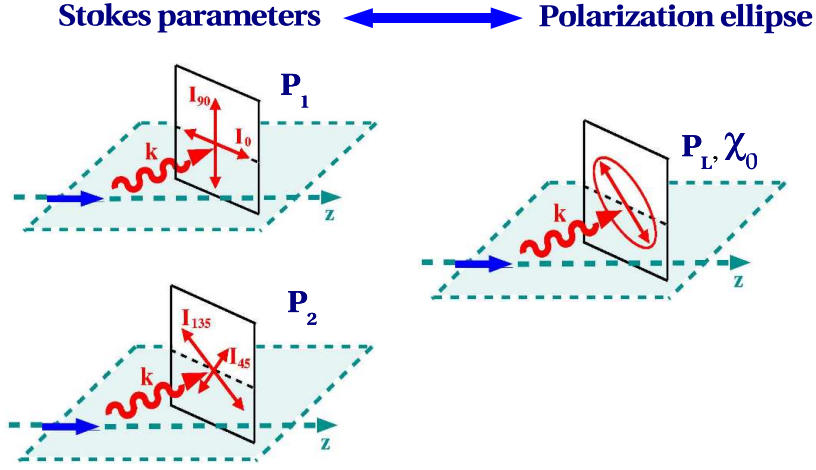
Figure 3.2: The Stokes parameters (3.10)–(3.11) and (parameters of the) polarization ellipse (3.12) are two equivalent sets in order to describe the linear polarization of light in the plane which is perpendicular to the photon momentum **k**.

$|\mathbf{k}\lambda\rangle$, where (helicity) λ is the spin projection of the photon onto the direction of its momentum **k**. Since for the photon (with the intrinsic spin $S = 1$), helicity takes only two values $\lambda = \pm 1$ (Berestetskii *et al* 1971), the spin density matrix is a 2×2 matrix and, therefore, similar to a free electron matrix (3.5), can be written in the form (Born and Wolf 1970):

$$\langle \mathbf{k}\lambda \ |\hat{\rho}_\gamma| \ \mathbf{k}\lambda'\rangle \ = \ \frac{1}{2} \begin{pmatrix} 1 + P_3 & P_1 - iP_2 \\ P_1 + iP_2 & 1 - P_3 \end{pmatrix}, \tag{3.9}$$

where P_1, P_2 and P_3 are so–called *Stokes parameters* of light. In optics, these parameters are often utilized in experiments in order to characterize the degree of polarization of the emitted light; while the Stokes parameter P_3 reflects the degree of *circular* polarization, the two parameters P_1 and P_2 together denote the (degree and direction of the) *linear* polarization of the light in the plane perpendicular to the photon momentum **k**. Experimentally, these Stokes parameters are determined simply by measuring the intensities of the light I_χ, linearly polarized under the different angles χ with respect to the reaction plane (as defined by the directions of the incoming beam and emitted photons). While the parameter

$$P_1 = \frac{I_0 - I_{90}}{I_0 + I_{90}}, \tag{3.10}$$

is obtained from the intensities *in parallel* and *perpendicular* to the reaction plane, the parameter P_2 follows a very similar intensity ratio, taken at $\chi = 45°$ and $\chi = 135°$, respectively:

$$P_2 = \frac{I_{45} - I_{135}}{I_{45} + I_{135}} . \tag{3.11}$$

Of course, the parameters P_1 and P_2 specify the linear polarization of light *completely*, i.e. both the degree of the polarization as well as its direction. In some applications, however, it is usually more convenient to use *another set* of polarization parameters. These parameters, for example, may represent the linear polarization of light in terms of *polarization ellipse*. Such an ellipse, defined in the plane perpendicular to the photon momentum **k**, is characterized

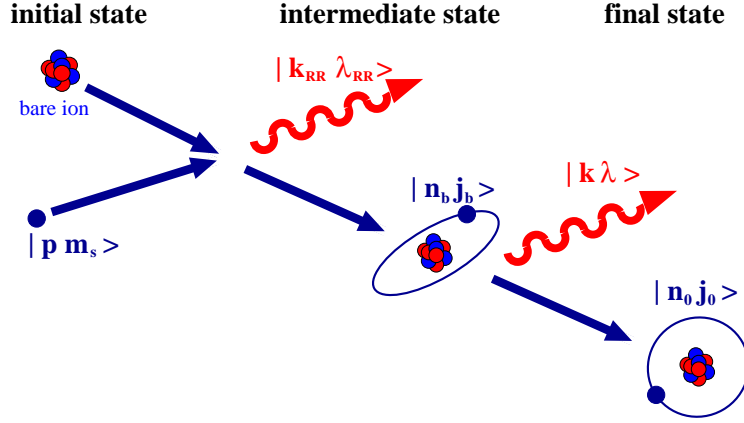**initial state**　　　**intermediate state**　　　**final state**

Figure 3.3: Two–step radiative recombination of an electron into a bare highly–charged ion. In the first step of such recombination process, a free electron $|\mathbf{p}m_s\rangle$ is captured into intermediate ion state $|n_b j_b\rangle$ under simultaneous emission of the recombination photon $|\mathbf{k}_{RR}\,\lambda_{RR}\rangle$. The subsequent decay of this intermediate (excited) state leads to the emission of the second – characteristic – photon $|\mathbf{k}\lambda\rangle$.

by the relative length P_L of its principal axis as well as by the angle χ_0 with respect to the reaction plane (cf Figure 3.2). While the angle χ_0 which can be expressed in terms of the Stokes parameters P_1 and P_2 as (Born and Wolf 1970, Balashov *et al* 2000):

$$\cos 2\chi_0 \;=\; \frac{P_1}{\sqrt{P_1^2 + P_2^2}}, \qquad \sin 2\chi_0 \;=\; \frac{P_2}{\sqrt{P_1^2 + P_2^2}} \;, \tag{3.12}$$

indicates the *direction* under which the linear polarization of light is maximal, the relative length of principal axis $P_L = \sqrt{P_1^2 + P_2^2}$ determines the *degree* of polarization in this direction.

3.3　Application to the two–step electron recombination

Of course, the basic relations (3.1) – (3.4) of the density matrix theory can be used for investigation of an arbitrary collision process. In the following, for example, we will employ this theory in order to study the *two–step* radiative recombination of bare high–Z ions. To this end, let us first consider the capture of a free electron into some "intermediate" ionic state, accompanied by the emission of the first – *recombination* – photon (cf Figure 3.3). For this capture process, in Subsection 3.3.1, we derive the angular distribution and the polarization parameters of the emitted light as well as the spin density matrix of the residual ("intermediate") ion. Obviously, this density matrix contains information about population of the "intermediate" ion state and, therefore, has to be applied later to consider its subsequent radiative *decay*. The properties of this radiative decay, such as – again – the angular distribution and polarization of the characteristic radiation are derived finally in Subsection 3.3.2.

3.3.1　Electron capture into bound state of bare ion

In the first step of the electron capture process, the "initial" state of the (combined) system is given by a (bare) ion *plus* a free electron with asymptotic momentum $\mathbf{p}$ and spin projection m_s (cf Figure 3.3). Since, for the sake of simplicity, we will restrict our treatment to the case

of a *zero nuclear spin* $I = 0$, the (spin) state of the initial system "electron + ion" is then equivalent to the statistical operator of a free electron $\hat{\rho}_i \equiv \hat{\rho}_e$.

In the "intermediate" state of a system, following electron capture, the statistical operator $\hat{\rho}_b$ has to describe both the residual (hydrogen–like) ion $|n_b\, j_b\, \mu_b\rangle$ and the recombination photon emitted with the wave vector $\mathbf{k}_{RR}$ and helicity λ_{RR}. This – intermediate state – operator can be obtained from the operator $\hat{\rho}_i$ of the initial state by following the standard rule (3.1):

$$\hat{\rho}_b = \hat{R}\,\hat{\rho}_i\,\hat{R}^+ = \hat{R}\,\hat{\rho}_e\,\hat{R}^+, \tag{3.13}$$

where the transition operator $\hat{R}$ describes the electron–photon interaction for the case of radiative recombination. Of course, the particular form of the transition operator $\hat{R}$ depends on the framework in which we describe the coupling of the radiation field to the atom. As appropriate for high–Z ions, below we will always refer to a *relativistic* treatment of the electron–photon interaction, which was discussed previously in Section 2.2 .

By means of the free electron operator $\hat{\rho}_e$ and relation (3.13), we may obtain the intermediate state density matrix in the representation of the individual angular momenta

$$\left\langle n_b\, j_b\, \mu_b,\ \mathbf{k}_{RR}\lambda_{RR}\,\middle|\, \hat{\rho}_b\,\middle|\, n_b\, j_b\, \mu_b',\ \mathbf{k}_{RR}\lambda_{RR}'\right\rangle \;=\; \sum_{m_s m_s'}\, \left\langle n_b\, j_b\, \mu_b,\ \mathbf{k}_{RR}\lambda_{RR}\,\middle|\, \hat{R}\,\middle|\, \mathbf{p}m_s\right\rangle$$

$$\times \left\langle \mathbf{p}m_s\,|\hat{\rho}_e|\,\mathbf{p}m_s'\right\rangle\, \left\langle \mathbf{p}m_s'\,\middle|\, \hat{R}^+\,\middle|\, n_b\, j_b\, \mu_b',\ \mathbf{k}_{RR}\lambda_{RR}'\right\rangle\ , \tag{3.14}$$

where transition amplitude $\left\langle n_b\, j_b\, \mu_b,\ \mathbf{k}_{RR}\lambda_{RR}\,\middle|\, \hat{R}\,\middle|\, \mathbf{p}m_s\right\rangle = C \cdot M_{\mathbf{b}\mathbf{p}}^{RR}(m_s, \lambda, \mu_b)$ for the recombination of a free electron under the simultaneous photon emission is given (except from kinematical factor) by the Equation (2.1). The density matrix (3.14) may be used now in order to derive the properties of both the emitted photon as well as the residual ion. As mentioned in Section 3.1, these properties may be "measured" in a most straightforward way by building up the proper detector operator $\hat{P}$ and, then, by taking trace of it product with the statistical operator (3.13). To determine, for instance, the angular distribution of the recombination photons, we may assume a detector in a given direction $\hat{n}_{RR}$ which is *insensitive* both to the polarization of such photons as well as to the spin substates of the residual ion

$$\hat{P}_{RR} = \sum_{\lambda_{RR}\mu_b} |\mathbf{k}_{RR}\lambda_{RR}\rangle\, |n_b\, j_b\, \mu_b\rangle\, \langle n_b\, j_b\, \mu_b|\, \langle \mathbf{k}_{RR}\lambda_{RR}|\ , \tag{3.15}$$

where the summation over (unobserved) helicities λ_{RR} and the magnetic quantum numbers μ_b of the ions are performed in order to define a proper detector (3.15). From this detector operator and the expression (3.14) we can immediately derive the angular distribution (2.12)

$$\frac{d\sigma_{n_b j_b}^{RR}}{d\Omega_{RR}}(\hat{n}_{RR}) \;=\; Tr(\hat{P}_{RR}\,\hat{\rho}_b) = \sum_{\lambda_{RR}\mu_b} \langle n_b\, j_b\, \mu_b,\ \mathbf{k}_{RR}\lambda_{RR}\,|\, \hat{\rho}_b\,|\, n_b\, j_b\, \mu_b,\ \mathbf{k}_{RR}\lambda_{RR}\rangle$$

$$= \frac{1}{2} \sum_{\lambda\mu_b m_s} \left|\left\langle n_b\, j_b\, \mu_b,\ \mathbf{k}_{RR}\lambda_{RR}\,\middle|\, \hat{R}\,\middle|\, \mathbf{p}m_s\right\rangle\right|^2 \tag{3.16}$$

of the photons which are emitted in the recombination of free *unpolarized* electrons into a hydrogenic bound state $|n_b\, j_b\rangle$.

19

Of course, another set of detector operators can be introduced in order to study the polarization of the emitted photons or, let us say, the magnetic sublevel population of the ion following electron capture. However, since these (polarization and alignment) properties are directly related to the spin density matrices of either the outgoing photons (3.9) or the residual ion (3.6), it is usually more convenient to retain at the density matrix of the final state (3.14). That is, by applying the standard technique (3.4), this final state density matrix can be spitted into independent matrices for the recombination photons and the final ions, respectively. For example, by taking trace over all *unobservable* quantum numbers of the residual ion we will immediately obtain the spin density matrix

$$\langle \mathbf{k}_{RR}\lambda_{RR} | \, \hat{\rho}_\gamma \, | \mathbf{k}_{RR}\lambda'_{RR} \rangle = Tr_b\left(\hat{\rho}_b\right) = \sum_{\mu_b} \langle n_b\, j_b\, \mu_b,\; \mathbf{k}_{RR}\lambda_{RR} | \, \hat{\rho}_b \, | n_b\, j_b\, \mu_b,\; \mathbf{k}_{RR}\lambda'_{RR} \rangle \quad (3.17)$$

of the recombination photons following electron capture into a bound (hydrogenic) state $|n_b\, j_b\rangle$ (Surzhykov *et al* 2001, 2003b). Then, by making use of this matrix and relation (3.9) we can easily find the Stokes parameters of the emitted radiation in a form:

$$P_1 = \frac{\langle \mathbf{k}_{RR}+1 | \, \hat{\rho}_\gamma \, | \mathbf{k}_{RR}-1 \rangle \; + \; \langle \mathbf{k}_{RR}-1 | \, \hat{\rho}_\gamma \, | \mathbf{k}_{RR}+1 \rangle}{\langle \mathbf{k}_{RR}+1 | \, \hat{\rho}_\gamma \, | \mathbf{k}_{RR}+1 \rangle \; + \; \langle \mathbf{k}_{RR}-1 | \, \hat{\rho}_\gamma \, | \mathbf{k}_{RR}-1 \rangle}, \qquad (3.18)$$

$$P_2 = i\, \frac{\langle \mathbf{k}_{RR}+1 | \, \hat{\rho}_\gamma \, | \mathbf{k}_{RR}-1 \rangle \; + \; \langle \mathbf{k}_{RR}-1 | \, \hat{\rho}_\gamma \, | \mathbf{k}_{RR}+1 \rangle}{\langle \mathbf{k}_{RR}+1 | \, \hat{\rho}_\gamma \, | \mathbf{k}_{RR}+1 \rangle \; + \; \langle \mathbf{k}_{RR}-1 | \, \hat{\rho}_\gamma \, | \mathbf{k}_{RR}-1 \rangle}, \qquad (3.19)$$

$$P_3 = \frac{\langle \mathbf{k}_{RR}+1 | \, \hat{\rho}_\gamma \, | \mathbf{k}_{RR}+1 \rangle \; - \; \langle \mathbf{k}_{RR}-1 | \, \hat{\rho}_\gamma \, | \mathbf{k}_{RR}-1 \rangle}{\langle \mathbf{k}_{RR}+1 | \, \hat{\rho}_\gamma \, | \mathbf{k}_{RR}+1 \rangle \; + \; \langle \mathbf{k}_{RR}-1 | \, \hat{\rho}_\gamma \, | \mathbf{k}_{RR}-1 \rangle}, \qquad (3.20)$$

where the trace of the photon density matrix (3.17) in the denominator of Equations (3.18)–(3.20) ensures the proper normalization of these polarization parameters (Balashov *et al* 2000).

While the density matrix of the recombination photons (3.17) follows the summation of the (intermediate–state) matrix (3.14) over the magnetic quantum numbers μ_b of the residual ion, the spin density matrix of such ion, in contrast, may be obtained by making trace over *unobservable* photon quantum numbers. Obviously, however, the choice of these – unobservable – quantities of emitted light depends on the particular set–up of experiment. If we suppose, for example, that recombination photons are not detected in the electron capture, the spin density matrix of the residual ion

$$\langle n_b\, j_b\, \mu_b \, | \, \hat{\rho}_b^{\text{ion}} \, | \, n_b\, j_b\, \mu'_b \rangle = \sum_{\lambda_{RR}} \int d\Omega_{\mathbf{k}_{RR}} \, \langle n_b\, j_b\, \mu_b,\; \mathbf{k}_{RR}\lambda_{RR} | \, \hat{\rho}_b \, | n_b\, j_b\, \mu'_b,\; \mathbf{k}_{RR}\lambda_{RR} \rangle \quad (3.21)$$

must include both the summation over the helicities $\lambda_{RR} = \pm\, 1$ as well as the integration $\int d\Omega_{\mathbf{k}_{RR}}$ over all photon directions. This integration, however, has to be omitted in order to describe the intermediate ionic states

$$\langle n_b\, j_b\, \mu_b \, | \, \hat{\rho}_b^{\text{ion}}(\hat{n}_{RR}) \, | \, n_b\, j_b\, \mu'_b \rangle = \sum_{\lambda_{RR}} \langle n_b\, j_b\, \mu_b,\; \mathbf{k}_{RR}\lambda_{RR} | \, \hat{\rho}_b \, | n_b\, j_b\, \mu'_b,\; \mathbf{k}_{RR}\lambda_{RR} \rangle \,, \quad (3.22)$$

following the emission of recombination radiation in a given direction $\hat{n}_{RR} = (\theta_{RR}, \phi_{RR})$ with respect to the incoming electron momentum (Surzhykov *et al* 2002b). Moreover, when comparing with Equation (3.16), we find that the spin density matrix (3.22) is normalized in such
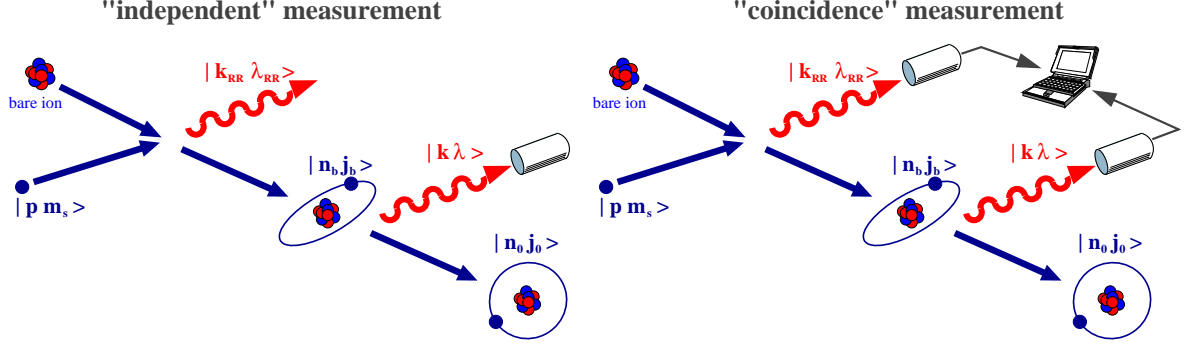
Figure 3.4: Two possible scenarios for studying the radiative decay of the excited ion state $|n_b j_b\rangle$ produced by the (radiative) electron capture. In the case of "independent" measurement, the only characteristic radiation is observed, while the recombination photons remain undetected. In contrast, both the recombination and subsequent decay photons are measured in "coincidence" scenario.

a way that its trace is equal to the angle–differential cross for the electron recombination into (hydrogen–like) ion state $|n_b j_b\rangle$:

$$Tr\, \hat{\rho}_b^{\text{ion}}(\hat{n}_{RR}) = \frac{d\sigma_{n_b j_b}^{RR}}{d\Omega_{RR}}(\hat{n}_{RR}). \tag{3.23}$$

From this relation we may immediately find also the normalization of the (angle–independent) density matrix (3.21): $Tr\, \hat{\rho}_b^{\text{ion}} = \sigma_{n_b j_b}^{RR}$, where $\sigma_{n_b j_b}^{RR} = \int d\Omega_{\mathbf{k}_{RR}} \frac{d\sigma_{n_b j_b}^{RR}}{d\Omega_{RR}}(\hat{n}_{RR})$ is the total recombination cross section (Ichihara and Eichler 2000).

3.3.2 Subsequent radiative decay

The density matrices (3.21) and (3.22) describe the intermediate ion state $|n_b j_b\rangle$ following electron capture for two different cases: while the matrix (3.21) characterizes the population of the ion as averaged over all photon angles, the matrix (3.22) is related to only those substates which arise from photon emission in a fixed direction $\hat{n}_{RR} = (\theta_{RR}, \phi_{RR})$. Obviously, these two situations have to be taken into account in order to accommodate the system through the subsequent decay which leads to emission of the (second) characteristic photon (cf Figure 3.4). For example, if only the properties of the characteristic radiation are studied while the recombination photons remain undetected, the theoretical treatment of the radiative decay have to be started from the density matrix in a form (3.21). In contrast, the simultaneous measurement of both the recombination and the subsequent decay radiation in the *coincidence* scenario is described by the density matrix (3.22) which contains information about the emission angles $\hat{n}_{RR} = (\theta_{RR}, \phi_{RR})$ of the first–step (recombination) photon.

Since, however, the measurements of the second–step (characteristic) radiation *separately* from the recombination x–ray photons are more typical for present–day experiments (Stöhlker *et al* 1997, Stöhlker 1999), first we will consider the density matrix (3.21) and will utilize, once more, the relation $\hat{\rho}_0 = \hat{R}\, \hat{\rho}_b^{\text{ion}}\, \hat{R}^+$ (cf Equation (3.13)). Similarly to before, the statistical operator $\hat{\rho}_0$ has to describe the hydrogen–like ion in its final state $|n_0 j_0 \mu_0\rangle$ as well as the decay photon

with the wave vector $\mathbf{k}$ and helicity λ; in the representation of the individual momenta the matrix of this operator takes the form (Surzhykov *et al* 2002b)

$$\left\langle n_0\, j_0\, \mu_0, \mathbf{k}\,\lambda \;\middle|\; \hat{\rho}_0 \;\middle|\; n_0\, j_0\, \mu_0', \mathbf{k}\,\lambda' \right\rangle \;=\; \sum_{\mu_b \mu_b'} \left\langle n_0\, j_0\, \mu_0, \mathbf{k}\,\lambda \;\middle|\; \hat{R} \;\middle|\; n_b\, j_b\, \mu_b \right\rangle \left\langle n_b\, j_b\, \mu_b \;\middle|\; \hat{\rho}_b^{\,\mathrm{ion}} \;\middle|\; n_b\, j_b\, \mu_b' \right\rangle$$

$$\times \left\langle n_b\, j_b\, \mu_b' \;\middle|\; \hat{R}^+ \;\middle|\; n_0\, j_0\, \mu_0', \mathbf{k}\,\lambda' \right\rangle , \qquad (3.24)$$

where $\left\langle n_0\, j_0\, \mu_0, \mathbf{k}\lambda \;\middle|\; \hat{R} \;\middle|\; n_b\, j_b\, \mu_b \right\rangle$ represents the matrix element for the radiative *bound–bound* electron transition. Within the relativistic description, this matrix is very similar to the free–bound transition amplitude (2.1):

$$\left\langle n_0\, j_0\, \mu_0, \mathbf{k}\lambda \;\middle|\; \hat{R} \;\middle|\; n_b\, j_b\, \mu_b \right\rangle = C \cdot \int d^3\mathbf{r}\, \psi_{j_0\mu_0}^{\dagger}(\mathbf{r})\, \alpha\, \hat{\mathbf{u}}_\lambda^{*}\, \mathrm{e}^{-i\,\mathbf{kr}}\, \psi_{j_b\mu_b}(\mathbf{r}) . \qquad (3.25)$$

The only difference in (3.25) is that both (one–electron) wavefunctions represent bound ion states and, hence, only the photon filed has to be expanded into its multipole components (2.2). Therefore, evaluation of the transition amplitude (3.25) is completely resembling to the free–bound case and has been discussed elsewhere (Drake 1988, Pal'chikov 1998).

From the final state density matrix (3.24), the angular distribution of the de–excitation photons can be obtained, by applying the projection operator $\hat{P}_0 = \sum_{\lambda\,\mu_0} |\mathbf{k}\lambda\rangle\, |n_0\, j_0\, \mu_0\rangle\, \langle n_0\, j_0\, \mu_0|\, \langle\mathbf{k}\lambda|$ which "measures" the characteristic radiation in a given direction $\hat{n} = (\theta, \phi)$ being insensitive, however, to its polarization as well as to sublevel population of the final ion:

$$\frac{d\sigma^{dec}}{d\Omega}(\hat{n}) \;=\; Tr(\hat{P}_0\,\hat{\rho}_0) \;=\; \sum_{\lambda\mu_0} \langle n_0\, j_0\, \mu_0, \mathbf{k}\,\lambda \;|\; \hat{\rho}_0 \;|\; n_0\, j_0\, \mu_0, \mathbf{k}\,\lambda \rangle$$

$$= \sum_{\mu_b \mu_b'} \sum_{\lambda\mu_0} \left\langle n_0\, j_0\, \mu_0, \mathbf{k}\,\lambda \;\middle|\; \hat{R} \;\middle|\; n_b\, j_b\, \mu_b \right\rangle \left\langle n_b\, j_b\, \mu_b \;\middle|\; \hat{\rho}_b^{\,\mathrm{ion}} \;\middle|\; n_b\, j_b\, \mu_b' \right\rangle$$

$$\times \left\langle n_b\, j_b\, \mu_b' \;\middle|\; \hat{R}^+ \;\middle|\; n_0\, j_0\, \mu_0, \mathbf{k}\,\lambda \right\rangle . \qquad (3.26)$$

As seen from Equation (3.26), the angular distribution of the characteristic photons still contains knowledge about the electron recombination (i.e. the first step) which, obviously, arises from the intermediate state density matrix (3.21). This density matrix, however, is obtained in assumption that first (recombination) photon remains unobserved and, hence, may provide us only with some "averaged" information about electron capture. In order to investigate the radiative recombination in more details, we may consider the coincidence scenario of the experiment (cf Figure 3.4) in which both first– and second–step photons are measured simultaneously. Of course, the theoretical treatment of such photon–photon correlation phenomena is also provided by the relations (3.24) and (3.26) in which, however, the intermediate state density matrix (3.21) has to be substituted by its "angular–dependent" form (3.22): $\left\langle n_b\, j_b\, \mu_b \;\middle|\; \hat{\rho}_b^{\,ion} \;\middle|\; n_b\, j_b\, \mu_b' \right\rangle \rightarrow \left\langle n_b\, j_b\, \mu_b \;\middle|\; \hat{\rho}_b^{\,ion}(\hat{n}_{RR}) \;\middle|\; n_b\, j_b\, \mu_b' \right\rangle$. As the important consequence of this substitution, the angular distribution (3.26) depends now not only on the angles $\hat{n} = (\theta, \phi)$ of the decay photons but also on the direction $\hat{n}_{RR} = (\theta_{RR}, \phi_{RR})$ at which the recombination photons are detected: $\frac{d\sigma^{dec}}{d\Omega}(\hat{n}) \rightarrow \frac{d\sigma^{dec}}{d\Omega}(\hat{n}, \hat{n}_{RR})$ and, therefore, displays a general form of the photon–photon angular correlation function.

Similarly to the first step, the final state density matrix (3.24) may be applied not only to derive the observable properties of the characteristic radiation (such as angle–differential cross section (3.26)) but also in order to separate the spin density matrix of the decay photons:

$$\langle \mathbf{k}\lambda \,|\, \hat{\rho}_\gamma \,|\, \mathbf{k}\lambda' \rangle = Tr_0(\hat{\rho}_0) = \sum_{\mu_0} \langle n_0\, j_0\, \mu_0,\; \mathbf{k}\lambda \,|\, \hat{\rho}_0 \,|\, n_0\, j_0\, \mu_0,\; \mathbf{k}\lambda' \rangle \;. \qquad (3.27)$$

This density matrix can help us to analyze the Stokes (polarization) parameters of the characteristic radiation (cf Equations (3.18)–(3.20)), or even the *angular–polarization* phenomena if the polarization of the subsequent decay photons is measured in coincidence with (the angle of) the recombination radiation.

Chapter 4

Radiative electron capture: Advanced studies

Owing to the recent advances in the detector design, a new generation of experiments on the radiative electron capture became already or are likely to become possible within the next years. The main accent in these – advanced – studies will be placed either on the *polarization* properties of the recombination as well as the subsequent decay photons or on the *correlation* phenomena which arise in the electron capture into excited ionic states. In this contribution, below we will give the *classification* of these – polarization and correlation – measurements and will discuss in detail their possible outcome. Most naturally, such theoretical analysis can be done in the framework of the density matrix theory, whose basic relations (when applied to the electron recombination) are given in the Chapter 3. Following these relations, we will describe the (radiative) electron capture into bound states of bare projectile ions and the subsequent radiative decay as a *two–step* process (see Figure 3.3). In Sections 4.1 and 4.2, we then consider the angular distributions and the polarization properties of the emitted radiation, *independent* for each step. In contrast, the *simultaneous* studies of both, first and second, steps in the photon–photon coincidence measurements are discussed in Section 4.3. Finally, the prospectives of the electron recombination studies for the (initially) few–electron ions and ions with non–zero nuclear spins are summarized in Section 4.4.

4.1   Electron capture into a bound ion state (first step)

The capture of an electron into a bound state of bare highly–charged ion leads to the emission of the recombination photons *as well as* to the population of the residual ionic states. Therefore, in order to obtain the complete knowledge about such recombination process, we have to study the properties of *both* the residual (hydrogen–like) ions *and* the emitted light. For instance, the outgoing radiation is characterized (apart from the well known energies) by its angular distribution and polarization. Since, however, the angular distributions of the recombination photons have been intensively studied during recent years both in experiment and in theory (Eichler and Meyerhof 1995, Stöhlker *et al* 1994, 1995), below we will restrict our treatment to their polarization properties. To this end, in Subsection 4.1.1, we describe the relativistic
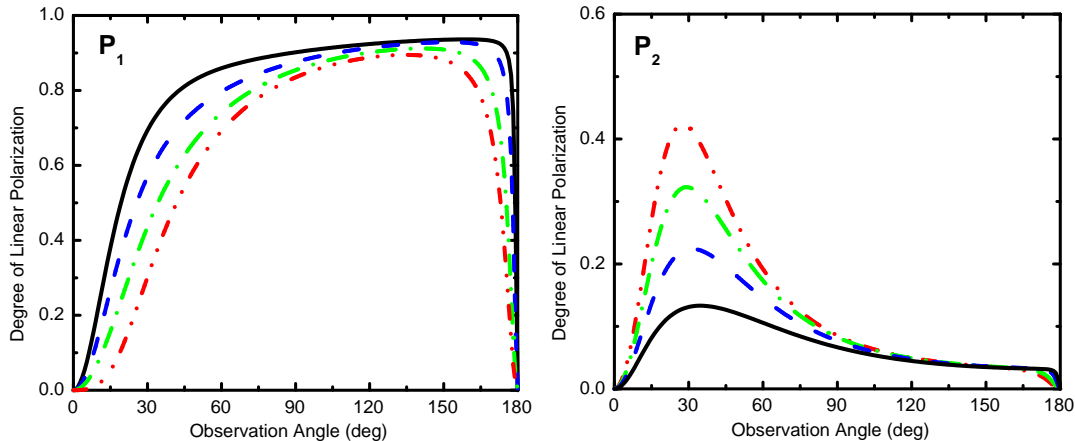
Figure 4.1: The Stokes parameters P_1 and P_2 of the recombination photons which are emitted in the electron capture into the K–shell of the bare uranium ions with projectile energies $T_p = 100$ (—), 200 (– –), 300 (– · –) and 400 (– · · –) MeV/u. The Stokes parameters P_2 are shown for the capture of completely polarized electrons. Calculations are presented in the laboratory frame.

computations for the *linear* polarization of emitted light following capture of electrons into the K shell of bare uranium projectile ions U^{92+}. In these computations, we place the particular emphasis on the effect of the incident electron spin–polarization which, as shown, remarkably modifies the linear polarization of the recombination x–ray photons.

Obviously, while the polarization and the angular distribution of the recombination photons are *observable* properties, the sublevel population of the residual ion can not be measured *directly* in experiment. However, this population is usually obtained from the measurements on the subsequent radiative decay of the ion (Stöhlker *et al* 1997, Surzhykov *et al* 2002a) if, of course, an electron is initially captured into excited state. In this contribution, we study the magnetic sublevel population of the excited states of highly–charged projectile ions as it arises from the electron recombination. Special attention is paid, in particular, to the alignment parameter of the $2p_{3/2}$ state of the (initially) bare uranium ions U^{92+}. In Subsection 4.1.2 this parameter is obtained for the *direct* electron capture into $2p_{3/2}$ state, while the cascade feeding from the higher–laying levels is discussed in Subsection 4.1.3.

4.1.1 Polarization of the recombination photons

Measurements on the polarization of hard x–rays emitted in the electron capture into highly–charged projectile ions become possible nowadays owing to the application of position sensitive solid–state detectors (Stöhlker *et al* 2003). For the recombination of bare uranium ions U^{92+}, for example, first experiments on the *linear* polarization of outgoing light have been performed at the GSI storage ring during the last year. As the preliminary results of these measurements (Tachenov *et al* 2003), strong linear polarization within the reaction plane was found for the K–shell recombination photons. These (preliminary) experimental data – as least qualitatively – are well reproduced now by the theoretical computations based on the relativistic Dirac's treatment (Surzhykov *et al* 2001). Left panel of Figure 4.1 displays, for example, the Stokes parameter P_1 (see Equation (3.10)) which is calculated for the electron capture into the K–shell
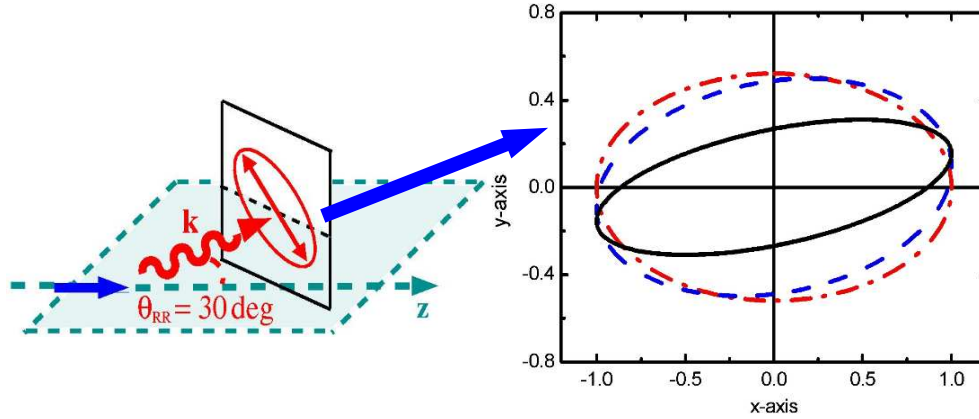
Figure 4.2: Rotation of the polarization ellipse of the recombination photons, calculated for three polarizations of the incident electrons: $P_z = 0.0$ (– - –), 0.3 (– –) and 1.0 (—) at the photon emission angle θ_{RR}=30°.

of bare uranium ions with energies in the range $100 \leq T_p \leq 400$ MeV/u. Moreover, as is typical for present–day experiments, we assume here that both projectile ions and target electrons (or atoms) are *unpolarized* and, therefore, the second Stokes parameter P_2 (3.11) is identically *zero* for all photon angles θ_{RR} (Eichler *et al* 2002, Surzhykov *et al* 2003b). Together with the fact that the P_1 parameter is positive and quite large for most emission angles (apart from the forward and backward directions), it implies that for projectile energies $T_p \leq 400$ MeV/u, the K–shell recombination photons are strongly linearly polarized *within* the reaction plane.

A rather different situation will arise, however, for the electron capture process in which either projectile ions or/and atomic target are spin–polarized. In the following, for example, we analyze the recombination of longitudinally polarized electrons with $P_z = 1.0$ into unpolarized uranium ions. As seen from right panel of Figure 4.1, this results in a non–vanishing Stokes parameter P_2 which peaks at around $\theta_{RR} = 30°$ and becomes larger for increasing projectile energies while the P_1 parameter remains unaffected by the electron polarization. Since the second Stokes parameter P_2 reflects the intensity ratio of light, linearly polarized at angles $\chi = 45°$ and $\chi = 135°$ with respect to the reaction plane (3.11), we may conclude that (non–zero) polarization of the incident electrons leads to an overall rotation of the linear polarization of the emitted photons *out of* the reaction plane. Most naturally, this rotation may be observed if instead of two Stokes parameters P_1 and P_2 we represent the linear polarization of light in terms of the *polarization ellipse* (3.12). Figure 4.2 displays, for example, such an ellipse as calculated for the photon emission angle $\theta_{RR} = 30°$ and for three different polarizations of the incident electrons: $P_z = 0.0$, 0.3 and 1.0. According to the increase of electron polarization P_z, the (rotation) angle of the principal axis of the polarization ellipse increases from $\chi = 0°$ for the unpolarized electors ($P_z = 0.0$) to almost $\chi = 30°$ for the capture of completely polarized electrons ($P_z = 1.0$). The measurements on the (rotation of) polarization ellipse of the recombination photons may serve, therefore, as a valuable tool for studying the polarization properties of either the electrons or, respectively, of the (nuclear) spin–polarized ion beams (Fritzsche and Surzhykov 2003, Surzhykov *et al* 2003b).
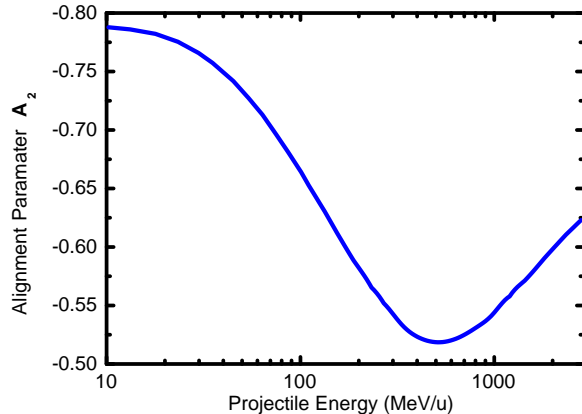
Figure 4.3: The alignment parameter $\mathcal{A}_2$ of the $2p_{3/2}$ state following the radiative recombination of a free electron into bare uranium ion U^{92+} as a function of projectile energy.

4.1.2 Electron capture into excited states: Alignment parameters

Of course, (future) experiments on the linear polarization of emitted x–ray photons will provide us with detailed knowledge on the electron recombination in the realm of high–Z ions. However, another way to learn more about the reaction mechanism is given by the measurements on the *population* of magnetic sublevels following electron capture into excited ion states (Stöhlker *et al* 1997, Eichler *et al* 1998). Apart from studying the collision dynamics, this sublevel population may also help to determine the polarization properties of the incident particles (Surzhykov *et al* 2003a). Such – polarization – phenomena, however, will be discussed later, while in this Section we restrict ourselves to the recombination of *unpolarized* electrons into an excited state $|n_b j_b\rangle$ of *unpolarized* ions. In particular, this capture process leads to an equal population of all pairs of sublevels with the same modulus of magnetic quantum number $|\mu_b|$. Moreover, if, for $j_b > 1/2$, the different pairs of magnetic substates are unequally populated, the ion is said to be *aligned*. In the density matrix theory, alignment of the atomic (or ionic) states is described in terms of one or several reduced statistical tensors $\mathcal{A}_{kq}$ (3.7), which are usually called *alignment parameters*. As it follows the definition (3.6), these parameters are related to the spin density matrix (3.21) of the residual ion following electron capture and, therefore, to the population cross sections $\sigma^{RR}_{n_b j_b \mu_b}$ of the various magnetic substates $|n_b j_b \mu_b\rangle$. In the case of electron capture into the $2p_{3/2}$ state, for instance, only one parameter $\mathcal{A}_2 \equiv \mathcal{A}_{20}$ is nonzero (apart, of course, $\mathcal{A}_{00} \equiv 1$), and can be expressed as (Eichler 1994):

$$\mathcal{A}_2 = \frac{\sigma^{RR}_{2p_{3/2}, \mu_b=\pm 3/2} - \sigma^{RR}_{2p_{3/2}, \mu_b=\pm 1/2}}{\sigma^{RR}_{2p_{3/2}, \mu_b=\pm 3/2} + \sigma^{RR}_{2p_{3/2}, \mu_b=\pm 1/2}} . \tag{4.1}$$

Since the alignment (4.1) depends on the recombination cross sections $\sigma^{RR}_{2p_{3/2}, \mu_b}$, we may also expect that it will depend on the collision parameters such as nuclear charge Z and energy T_p of the projectile ion. In Figure 4.3, for example, we display the parameter $\mathcal{A}_2$ for the capture of an electron into the $2p_{3/2}$ state of the bare uranium ion U^{92+}. The alignment parameter appears to be negative for all collision energies, referring to a predominant population of the sublevels with $|\mu_b| = 1/2$. As seen from the Figure, this population is strongest for the lowest energy, has a minimum around 500 MeV/u and increases again for the higher energies.

28

Collision energy	$\mathcal{A}_2$	$\tilde{\mathcal{A}}_2$	$\mathcal{A}_2/\tilde{\mathcal{A}}_2$
190.7 MeV/u	-0.587	-0.360	1.63
220.0 MeV/u	-0.568	-0.344	1.65
295.0 MeV/u	-0.542	-0.322	1.68
358.0 MeV/u	-0.528	-0.300	1.76
392.4 MeV/u	-0.523	-0.290	1.80

Table 4.1: The alignment parameters of the $2p_{3/2}$ state following the radiative recombination of a free electron into bare uranium ions U^{92+}. While the parameter $\mathcal{A}_2$ describes the sublevel population arising from the direct electron capture alone, the feeding transitions from higher levels are included in the parameter $\tilde{\mathcal{A}}_2$ (Stöhlker *et al* 1997, Bilyk *et al* 2003).

4.1.3 Cascade contributions

The alignment parameter (4.1) describes the relative sublevel population of the $2p_{3/2}$ state following *direct* electron capture. In practice, however, we may expect that apart from the direct recombination, the feeding transitions from the higher–laying levels will also contribute to the population of ionic substates. In order to study these – cascade – contributions we may consider the system of the (so–called) rate equations (Lin and Macek 1987, Bilyk *et al* 2003)

$$\frac{dN_i}{dt} = -\sum_j^< \lambda_{ij}\,N_i + \sum_k^> \lambda_{ki}\,N_k \,, \tag{4.2}$$

which describes the decay dynamics of the magnetic sublevels $|i\rangle \equiv |n_{b_i}\,j_{b_i}\,\mu_{b_i}\rangle$ produced with the initial population $N_i(0) = C \cdot \sigma^{RR}_{n_{b_i}\,j_{b_i}\,\mu_{b_i}}$. Moreover, in the system of equations (4.2), λ_{ij} is the decay rate for the $|i\rangle \to |j\rangle$ transition and Λ is the total number of (excited) sublevels which are considered in the decay cascade; the index j runs over all levels with total energy $E_j < E_i$ and k over all those with $E_k > E_i$.

By performing an integration of the system (4.2), we may find the occupation of the magnetic sublevels as a function of time $N_i = N_i(t)$. However, in experiments which are typically carried out at the ESR jet–target (Stöhlker *et al* 1997, Stöhlker 1999), no time dependence in the decay dynamics can be explored since the typical lifetimes of the excited ion states are in the order of $\tau \sim 10^{-14} \div 10^{-17}$ s. Such tiny lifetimes lead to an (almost) instantaneous decay of all levels if compared with the length of the target and, hence, to an *averaging* (over time) the sublevel populations as observed experimentally. Therefore, in order to "measure" alignment $\tilde{\mathcal{A}}_2$ of the $2p_{3/2}$ state which arises both from the direct electron capture as well as from the cascade feeding, we have to average solutions of the system (4.2) for the four magnetic sublevels $|2p_{3/2}\,,\mu_b = \pm 1/2, \pm 3/2\rangle$ and to employ then expression (3.8). In Table 4.1, for example, we display this alignment as calculated for the bare uranium ions with projectile energies in the range 190.7 MeV/u $\leq T_p \leq$ 392.4 MeV/u. Moreover, in order to emphasize the effect of cascade feeding we also present the parameter $\mathcal{A}_2$ which describes the sublevel population following the direct electron capture alone (4.1). As seen from the Table, the electron transitions from the upper levels lead to a considerable reduction of the "direct" alignment $\mathcal{A}_2$ and, therefore, has to

be taken into account for the proper analysis of experimental data. This reduction, moreover, enlarges for the higher projectile energies which has to be attributed to the relative increasing of the electron capture into the highly–excited levels with respect to the capture into $2p_{3/2}$ state (Ichihara and Eichler 2000).

4.2 Radiative decay (second step)

If, instead of the ground state, an electron is (radiatively) captured into some excited ion state, its subsequent decay will lead to the emission of one or several photons until the ground state is reached. Similarly to the recombination photons, such – subsequent – photon emission is characterized by its angular distribution and polarization. Both of these properties are closely related to the magnetic sublevel population of the excited ion state as it arises from the electron capture (Berezhko and Kabachnik 1977, Takacs *et al* 1996). However, as discussed previously in Section 3.3, apart from the collisional parameters such as nuclear charge Z and energy T_p of projectile ion, this population also reflects the set–up and efficiency of detectors which are used in order to study the electron recombination process. In the following, we assume that the recombination photons are not observed in a particular experimental scheme and, therefore, the subsequent radiative decay is studied *separately* from the first step (cf Figure 3.4). For such "separate" measurements, in particular, the population of the $2p_{3/2}$ state is described by the alignment parameter (4.1) which we will apply below in order to study both the angular distribution (Subsection 4.2.1) as well as the linear polarization (Subsection 4.2.2) of the Lyman–α_1 ($2p_{3/2} \rightarrow 1s_{1/2}$) transition in the hydrogen–like uranium ions U^{91+}.

4.2.1 Angular distribution of the decay photons

Several experiments have been carried out during recent years in order to study the angular distribution of the subsequent decay photons and, hence, to derive the magnetic sublevel population of the excited ion states following the electron capture (Stöhlker *et al* 1997, Stöhlker 1999). In particular, by measuring the anisotropic emission pattern of the Lyman–α_1 radiation (see left panel of Figure 4.4), an experimental *anisotropy* parameter β_{exp} may be elucidated from the least square adjustment of the general formula

$$W_{Ly}(\theta) \propto 1 + \beta_{\mathrm{exp}} \left(1 - \frac{3}{2} \sin^2 \theta \right) \tag{4.3}$$

for the angular distribution of characteristic photons which is presented here in the projectile (emitter) frame. The right panel of Figure 4.4 displays, for example, the anisotropy parameters (solid circles) as obtained for the hydrogen–like uranium ions U^{91+} produced in the $U^{92+} \rightarrow N_2$ collisions as a function of the projectile energy. However, deviations of up to 30 % were found when these experimental parameters β_{exp} were compared with the calculations (dashed line) based on the standard *electric dipole* approximation $\beta = \mathcal{A}_2/2$ where the $\mathcal{A}_2$ is the alignment of the $2p_{3/2}$ state (4.1). Originally, this discrepancy was quite surprising since, even for the hydrogen–like uranium, the electric dipole approximation for the coupling of the radiation field is known to provide theoretical decay rates with an accuracy of better than 1 % (Drake 1988, Pal'chikov 1998).
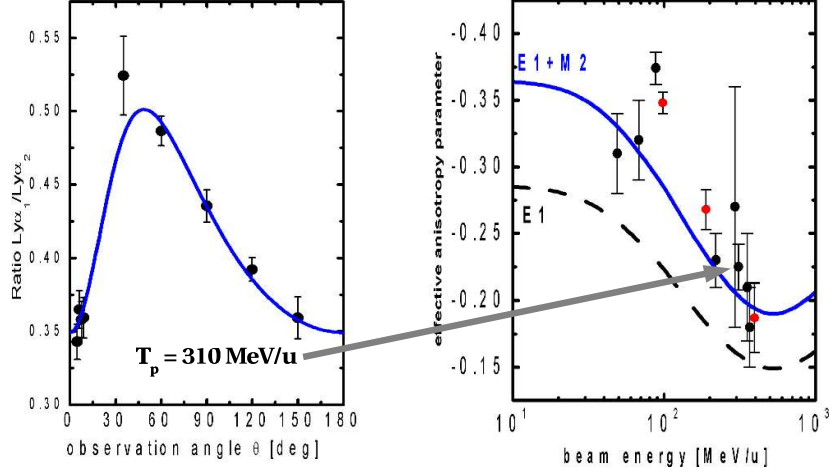
Figure 4.4: By employing the least square adjustment of Equation (4.3) to the experimental Lyman – α_1 angular distribution (left panel), we may obtain the effective anisotropy parameter β_{exp} for various collision energies (right panel). The experimentally determined anisotropy parameters (solid circles) are compared with theoretical predictions based on the electric dipole approximation (dashed line) and the exact approach (solid line) which includes the **E1**–**M2** multipole mixing term.

Note, however, that in computations on the total decay rates, the contributions from the different multipoles of the radiation field appear completely *additive*, while this is not the case for the angular distribution (as well as polarization) of the emitted photons. In the angular distribution of the Lyman–α_1 x–rays, for example, the incorporation of the – weaker – magnetic quadrupole (**M2**) decay branch beyond the electric dipole (**E1**) term leads to an *interference* between the transition (**E1** and **M2**) amplitudes which can be expressed in term of the so–called *structure function* (Surzhykov *et al* 2002a)

$$f(\mathbf{E1}, \mathbf{M2}) \propto \left[1 \ + \ 2\sqrt{3} \ \frac{\langle 1s_{1/2} \, ||\mathbf{M2}|| \, 2p_{3/2} \rangle}{\langle 1s_{1/2} \, ||\mathbf{E1}|| \, 2p_{3/2} \rangle} \right] , \tag{4.4}$$

where $\langle ||\mathbf{E1}|| \rangle$ and $\langle ||\mathbf{M2}|| \rangle$ are the reduced matrix elements for the bound–bound electric (magnetic) multipole transitions. The structure function (4.4) modifies the (electric dipole) anisotropy parameter β which has to be replaced now by the corresponding *effective* parameter

$$\beta \rightarrow \beta_{\text{eff}} = f(\mathbf{E1}, \mathbf{M2}) \, \cdot \, \mathcal{A}_{20}/2 \tag{4.5}$$

in order to take into account the **E1**–**M2** multipole mixing in the photon angular distribution.

In the *dipole approximation*, which incorporates only the **E1** term to the Lyman–α_1 transition, $f(E1, M2) \equiv 1$. As seen from Equation (4.4), the main correction to this approach arises from a mixed term of the **E1** and the magnetic quadrupole (**M2**) components which is proportional to the ratio of the corresponding amplitudes. For high–Z ions, this ratio is $\propto 0.1$, giving rise to a 20–30 % magnetic quadrupole correction over the *dipole approximation*. For hydrogen–like U^{91+} ions, for instance, the structure function is $f(E1, M2) = 1.28$, leading to a strongly modified anisotropy parameter (4.5). That is, as seen from Figure 4.4, the magnetic quadrupole term **M2** in the Lyman–α_1 transition shifts up the theoretical curve for the β_{eff} parameter (solid line) which is now in good agreement with the experimental data.
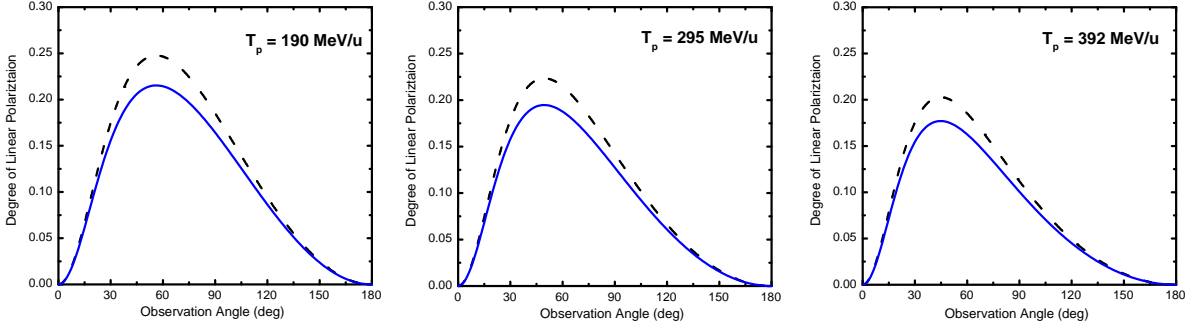
Figure 4.5: Linear polarization of the Lyman–α_1 radiation following the electron capture into $2p_{3/2}$ state of bare uranium ions with energies $T_p = 190$, 295 and 392 MeV/u. The dashed line represents the theoretical prediction from the electric dipole approximation, while the solid line incudes also the magnetic quadrupole decay channel (cf Equation 4.6). Results are presented within the laboratory frame (i.e. the rest frame of the electron target).

However, for the collision energies less than 100 MeV/u, Figure 4.4 still indicates remarkable discrepancy between experiment and theory. This discrepancy has to be attributed to the non-radiative electron capture (NRC) which, as discussed in Chapter 1, is the dominant population process in the low–energy region. We may explain, therefore, the "resonance" structure arising around $T_p \sim 90$ MeV/u by the additive contributions to the alignment of the $2p_{3/2}$ state from both the radiative and the nonradiative electron capture processes (Orsic–Muthig *et al* 2002).

4.2.2 Polarization of the decay photons

The radiative decay of the aligned ion state leads not only to the anisotropic angular distribution (see Equation 4.3) but also to the *non–zero* linear polarization of the characteristic x–ray photons. Similarly to the recombination light, this (linear) polarization can be described in terms of the two Stokes parameters P_1 and P_2. By combining the Equations (3.18) and (3.19) with the spin density matrix (3.27) of the characteristic decay photons, we may find that, for the Lyman–α_1 transition, the Stokes parameter P_1 is given in the emitter frame by

$$P_1(\theta) \propto \frac{-\frac{3}{2}\frac{\mathcal{A}_{20}}{2}\sin^2\theta\left[1 - \frac{2}{\sqrt{3}}\frac{\langle 1s_{1/2}||\mathbf{M2}||2p_{3/2}\rangle}{\langle 1s_{1/2}||\mathbf{E1}||2p_{3/2}\rangle}\right]}{1 + \frac{\mathcal{A}_{20}}{2}P_2(\cos\theta)\left[1 + 2\sqrt{3}\frac{\langle 1s_{1/2}||\mathbf{M2}||2p_{3/2}\rangle}{\langle 1s_{1/2}||\mathbf{E1}||2p_{3/2}\rangle}\right]}, \tag{4.6}$$

while the parameter P_2 is equivalent to *zero* for all emission angles (Surzhykov *et al* 2003c).

Equation (4.6) includes both, the electric dipole (**E1**) and magnetic quadrupole (**M2**) contributions to the Lyman–α_1 transition. However, in contrast to the angular distribution (4.3), the linear polarization of the decay photons is *less* affected by the **E1**–**M2** multipole mixing. As seen, for instance, from Figure 4.5, the magnetic quadrupole decay channel in the hydrogen–like uranium ions U^{91+} leads to a decrease of the linear polarization by approximately 15 % when compared with the electric dipole approach. This – relatively small – enhancement are likely to be measured within the next few years and will provide us, together with the angular distribution (4.3), with the precise information on the electronic structure of highly–charged heavy ions.

4.3 Photon–photon coincidence studies (first "plus" second steps)

So far, we have discussed the properties of the electron capture into an (excited) ion state and its subsequent radiative decay *separately* from each other. These – individual – studies were found to reveal a great deal of information about the interaction of electrons with the radiation field in the presence of strong electro–magnetic fields. However, even more detailed information about the capture process as well as the incident particles can be derived from the simultaneous measurements of the first– and second–step photons in an (e, 2γ) *coincidence* experiment (cf left panel of Figure 3.4). Perhaps, the most simple coincidence measurement concerns the angle–angle correlations whose theoretical background within the framework of the density matrix theory was briefly outlined in Subsection 3.3.2. In the following, we will apply this general theory to the electron capture into $2p_{3/2}$ state of uranium projectile U^{92+} and the study of the subsequent Lyman–α_1 angular distributions, where we assume that the recombination photons are detected *in coincidence*. In Subsection 4.3.1, for example, we show that the emission pattern of the decay photons strongly depends on the particular angle under which the (first) recombination photons are observed. As later discussed in Subsection 4.3.2, this dependence is sensitive to the spin–polarization of the incident electrons and, therefore, can be used to determine either polarization of the electron target and/or the projectile ions.

4.3.1 Photon–photon angular correlations

As mentioned in Subsection 4.1.2, the capture of unpolarized electrons into a bound ion state with total momentum $j_b > 1/2$ leads to an alignment of the magnetic sublevels $|n_b\, j_b\, \mu_b\rangle$. For the particular case of the $2p_{3/2}$ level, for instance, the alignment is described by the single parameter from Equation (4.1). This parameter, however, is obtained by assuming that the recombination photons are not observed in the given experiment and, hence, the population of the $2p_{3/2}$ state must be *averaged* over all possible photon angles. An alternative and more precise measurement may concern the investigation of the magnetic sublevel population which arises (only) from the emission of outgoing radiation in a given direction $\hat{n}_{RR} = (\theta_{RR}, \phi_{RR})$. Theoretically, this population is described by the (angle–dependent) spin density matrix (3.22) of the bound ionic state and, hence, is related to the *angular–differential* recombination cross sections [cf Equation (3.23)]. Instead of an "integral" alignment parameter (4.1) we may introduce the (so–called) *differential alignment* parameter (Surzhykov *et al* 2002b)

$$
\mathcal{A}_{20}(\hat{n}_{RR}) \;=\; \frac{\dfrac{d\sigma^{RR}_{2p_{3/2},\mu_b=\pm 3/2}}{d\Omega_{RR}}(\hat{n}_{RR}) \;-\; \dfrac{d\sigma^{RR}_{2p_{3/2},\mu_b=\pm 1/2}}{d\Omega_{RR}}(\hat{n}_{RR})}{\dfrac{d\sigma^{RR}_{2p_{3/2},\mu_b=\pm 3/2}}{d\Omega_{RR}}(\hat{n}_{RR}) \;+\; \dfrac{d\sigma^{RR}_{2p_{3/2},\mu_b=\pm 1/2}}{d\Omega_{RR}}(\hat{n}_{RR})}, \tag{4.7}
$$

which depends on the angles $\hat{n}_{RR} = (\theta_{RR}, \phi_{RR})$ under which the recombination photons are emitted. The left panel of Figure 4.6 displays, for instance, the parameter $\mathcal{A}_{20}(\hat{n}_{RR})$ calculated for the electron capture into $2p_{3/2}$ state of bare uranium ions U^{92+} with energies $T_p = 98$, 190 and 295 MeV/u. For these energies, the differential alignment (4.7) is positive in the forward and backward directions, referring to a predominant population of the $\mu_b = \pm\,3/2$ magnetic substates. In contrast, the emission of the recombination photons at the angles around $\theta_{RR} = 60°$ with respect to the beam direction mainly results – to more than 80 % – in a population
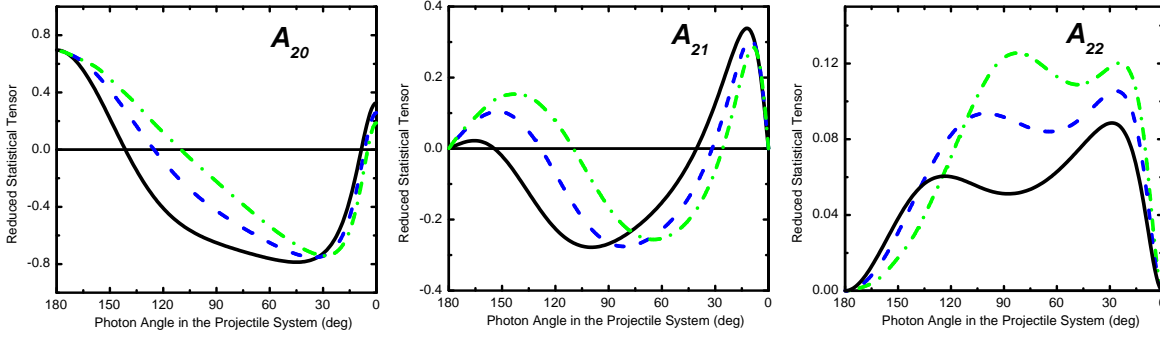
33

Figure 4.6: Components of the reduced statistical tensor $\mathcal{A}_{2q}$ as a function of the photon emission angle as measured in the projectile frame. All results are presented for the capture of unpolarized electrons into the $2p_{3/2}$ state of bare uranium ions with energies $T_p = 98$ (—), 190 ($-$ $-$) and 295 ($-$ $\cdot$ $-$) MeV/u.

of the $\mu_b = \pm\,1/2$ substates. Such almost exclusive population of the levels with $\mu_b = \pm\,1/2$ leads to a negative value of the "integral" parameter $\mathcal{A}_2$ (cf Figure 4.3) as obtained by the averaging of the differential alignment $\mathcal{A}_{20}(\hat{n}_{RR})$ over all photon angles.

Apart from the differential alignment $\mathcal{A}_{20}(\hat{n}_{RR})$, the magnetic sublevel population of the $2p_{3/2}$ state is also described by the tensor components $\mathcal{A}_{2\pm1}(\hat{n}_{RR})$ and $\mathcal{A}_{2\pm2}(\hat{n}_{RR})$ which, as seen from the definition (3.6), are related to the non–diagonal elements of the density matrix (3.22). Similarly to the differential alignment (4.7), these parameters depend on the projectile ion energy as well as on the emission angles of the recombination photons $\hat{n}_{RR} = (\theta_{RR}, \phi_{RR})$, cf Figure 4.6. They have to be *zero*, however, for $\theta_{RR} = 0°$ and $\theta_{RR} = 180°$ since the forward (as well as backward) photon emission does not break the initial axial symmetry of the collisional system and, therefore, cannot lead to the non–diagonal spin density matrix (Surzhykov *et al* 2002b). For the same reason the ("integral") parameters $\mathcal{A}_{2\pm1}$ and $\mathcal{A}_{2\pm2}$ are always *zero* if the recombination x–ray photons remain unobserved in the particular experiment and, hence, the integration over the photon angles $\int d\Omega_{RR}$ in the density matrix (3.21) also "restores" the axial symmetry of the system.

The reduced statistical tensors $\mathcal{A}_{2q}(\hat{n}_{RR})$ of the $2p_{3/2}$ state can be directly employed in order to derive the properties of the subsequent Lyman–α_1 ($2p_{3/2} \to 1s_{1/2}$) radiation. For instance, the emission pattern of the characteristic photons is given by the well–known formula:

$$W_{Ly}(\hat{n}, \hat{n}_{RR}) \propto 1 + \frac{1}{2}\sqrt{\frac{4\pi}{5}} \sum_{q=-2}^{2} Y_{2q}(\hat{n})\,\mathcal{A}_{2q}(\hat{n}_{RR})\,f(E1, M2) \qquad (4.8)$$

where $f(E1, M2)$ is the structure function (4.4). The angular distribution (4.8) represents the particular case of the photon–photon *angular correlation function* for the electron capture into $2p_{3/2}$ state and following Lyman–α_1 decay. This function depends not only on the emission angles of the subsequent decay photons but also on the angles $\hat{n}_{RR}$ under which recombination photons are observed. Figure 4.7 displays, for example, the angular distribution (4.8) for three different angles $\theta_{RR} = 0°$, $15°$ and $90°$ of the recombination photons with respect to the beam direction. Moreover, these angular distributions are presented for the case of *coplanar* geometry of the experiment, i.e. when both photons are detected within the same plane. As
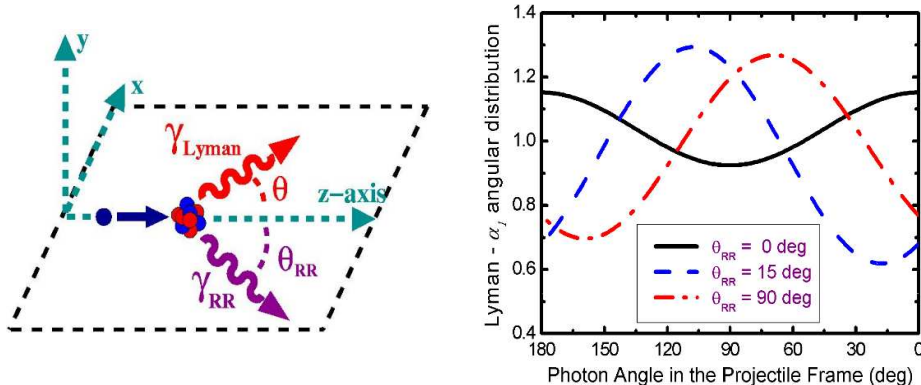
34

Figure 4.7: Angular distributions of the Lyman–α_1 radiation following the electron capture into $2p_{3/2}$ state of bare uranium projectile with energy $T_p = 220$ MeV/u. Distributions are presented within the projectile frame and for the coplanar geometry of coincidence experiment.

seen from the Figure, the Lyman–α_1 emission pattern is symmetric around the angle $\theta = 90°$ for a forward emission of the recombination photon ($\theta_{RR} = 0°$) as it can be expected from the *axial* symmetry of the overall system. In contrast, the emission of the recombination photon under any other angles ($\theta_{RR} \neq 0°$ and $180°$) breaks down this symmetry and, hence, gives rise to an asymmetric angular distribution of the decay photons.

Of corse, the measurements of the decay radiation simultaneously with the recombination x–ray photons are not a simple experimental task which, in fact, has not been realized so far. However, owing to the recent advances in x–ray detector technique, the two–photon coincidence experiments are likely to be carried out at the GSI storage ring within the next few years. These (future) x–x studies may help us, for instance, to distinguish between the different population mechanisms of the excited ion states, following either the direct (radiative) electron capture in this level or a cascade feeding from the upper levels as well as the nonradiative capture processes. Another important promise of such correlation measurements lays in the fact that they provide us with a tool for studying the polarization properties of the target electrons (atoms) and/or the projectile ions, a task which will be briefly discussed in the next Subsection.

4.3.2 Application to the polarization studies

The photon–photon angular correlation function (4.8) was derived for the particular case of both *unpolarized* target electrons and projectile ions. Of course, this function needs to be modified in order to describe, for example, the recombination of the electrons with a well defined polarization ($P_z \neq 0$) in respect to the beam direction. The capture of such – spin–polarized – electrons into the bare projectile ions leads to an *orientation* of the excited ionic state which, similarly to an alignment in the "unpolarized" case (see Subsection 4.1.2), can be described in terms of the reduced statistical tensors $\mathcal{A}_{kq}(\hat{n}_{RR})$. These tensors, however, have to reflect the polarization properties of the electron target and, therefore, are generally written as a sum of two parts, the "unpolarized" tensor as well as the "polarized" part weighted by
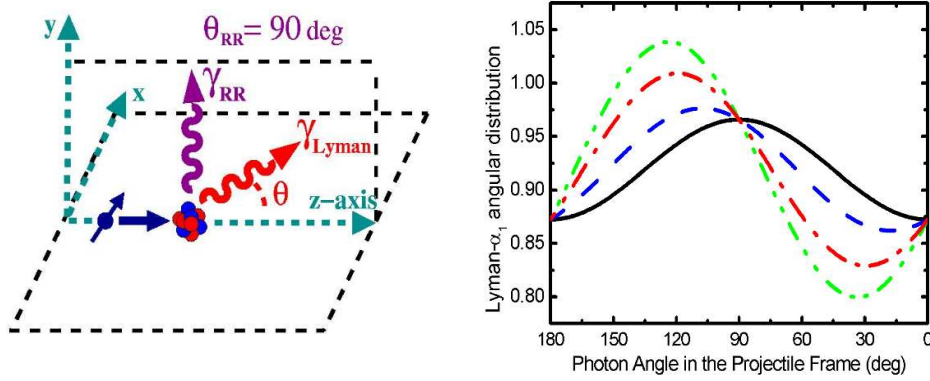
Figure 4.8: Angular distributions of the Lyman–α_1 radiation following the radiative capture of polarized electrons into $2p_{3/2}$ state of bare uranium projectiles with energy $T_p = 310$ MeV/u. Distributions are shown for four degrees of polarization of the incident electrons: $P_z = 0.0$ (—), 0.3 (– –), 0.7 (– - –) and 1.0 (– - - –). All results are presented within the projectile frame and for the perpendicular geometry of coincidence experiment.

the electron degree of polarization P_z (Surzhykov *et al* 2003a):

$$\mathcal{A}_{kq}(\hat{n}_{RR}) = \mathcal{A}_{kq}^{\text{unp}}(\hat{n}_{RR}) + P_z \cdot \mathcal{A}_{kq}^{\text{pol}}(\hat{n}_{RR}). \qquad (4.9)$$

Obviously, the "unpolarized" tensor $\mathcal{A}_{kq}^{\text{unp}}(\hat{n}_{RR})$ in the left side of Equation (4.9) refers to the capture of the unpolarized electrons ($P_z = 0$) and, hence, describes the *alignment* of the residual ion states. The deviation from this aligned population of the magnetic sublevels due to the capture of polarized electrons arises then from the "polarized" part $\mathcal{A}_{kq}^{\text{pol}}(\hat{n}_{RR})$ of the statistical tensor.

By inserting the (generalized) statistical tensors (4.9) into Equation (4.8) we can modify the photon–photon angular correlation function for the capture of spin–polarized electrons into $2p_{3/2}$ state of bare projectile ions and the following Lyman–α_1 decay. In particular, this correlation will reflect now the degree of electron polarization P_z which weights (cf Equation (4.9)) the five (imaginary) components of the "polarized" tensor $\mathcal{A}_{2q}^{\text{pol}}(\hat{n}_{RR})$, q = -2, ..., 2. However, one is typically interested in *reduction* of the number of these polarization parameters in order to perform, for instance, the analysis of the experimental data. This reduction may be achieved by the proper choice of the geometry in the set–up of a coincidence experiment. If, for instance, the Lyman–α_1 photons are observed perpendicular to the *reaction* plane (i.e. the plane which is formed by the directions of the beam and the recombination photons), the corresponding angular distribution simplifies to:

$$W_{Ly}(\theta, \phi = \pi/2; \ \hat{n}_{RR}) \ \propto \ 1 + \frac{1}{2}\sqrt{\frac{3}{2}}\left(\frac{1}{\sqrt{6}}\left(3\cos^2\theta - 1\right) \ \mathcal{A}_{20}^{\text{unp}}(\hat{n}_{RR}) \right.$$

$$\left. - \sin^2\theta \ \mathcal{A}_{22}^{\text{unp}}(\hat{n}_{RR}) - i \ P_z \cdot \sin 2\theta \ \mathcal{A}_{21}^{\text{pol}}(\hat{n}_{RR}) \right) \ f(E1, M2), \quad (4.10)$$

where only one term depends linearly on the degree of polarization P_z and component of the *polarized* tensor $\mathcal{A}_{21}^{\text{pol}}(\hat{n}_{RR})$. As seen from Equation (4.10), while the other two ("unpolarized")

terms describe the angular distribution of the Lyman–α_1 radiation which is *symmetrical* with respect to the plane perpendicular to the beam axis ($\theta = 90°$), this "polarized" term gives rise to an *asymmetrical* shift in the emission pattern and, hence, to a clear signature of the electron polarization P_z. Figure 4.8 shows, for example, the Lyman–α_1 angular distributions (4.10) following the capture of the (longitudinally) polarized electrons into the $2p_{3/2}$ state of bare uranium ions with energy $T_p = 310$ MeV/u. Moreover, these angular distributions are calculated for the emission of the first (recombination) photons perpendicular to the beam direction ($\theta_{RR} = 90°$) and for the four different degrees of polarization $P_z = 0.0, 0.3, 0.7$ and 1.0 of the incident electrons. As seen from the Figure, the asymmetrical shift in the Lyman–α_1 emission pattern increases proportionally to electron polarization P_z and, therefore, can be applied as a precise tool in coincidence (e, 2γ) experiments for studying the polarization properties of the incident particles (Surzhykov *et al* 2003a).

4.4 Outlook: Scenarios for the future studies

In this thesis, we have restricted our treatment of radiative recombination (or radiative electron capture) processes to the case of *bare, unpolarized* projectile ions. Such theoretical assumption corresponds to the typical experimental set–up at the GSI storage ring where the electron recombination of bare, unpolarized uranium ions U^{92+} have been observed during recent years. In the nearest future, however, a new series of measurements are likely to be carried out which will operate either with nuclear *spin–polarized* or/and *few–electron* ions. Theoretical investigations along these lines are currently under way in our group and are briefly summarized below. In Subsection 4.4.1 we discuss the extension of the density matrix approach for the polarization studies with the spin–polarized beams, while the further investigations on the electron capture into few–electron ions are reviewed in Subsection 4.4.2.

4.4.1 Studies on the spin–polarized ion beams

As discussed in Subsections 4.1.1 and 4.3.1, the polarization of the recombination x–ray photons as well as the correlated photon emission in (e, 2γ) coincidence experiments are strongly affected by the polarization properties of the incident particles. So far, however, we have considered only the case of polarized electrons while the ion beam has been assumed unpolarized throughout the theoretical analysis. Of course, much greater practical interest may concern the studies on the *nuclear spin* polarization of ion beams, a request which have been done recently by several groups. Since the spin–polarization of the target electrons and the projectile ions occurs rather symmetrical in the collisional process, similar effects on the polarization and correlation properties of the emitted light can therefore also be expected for the capture of electrons by polarized ions. The theoretical analysis of the ion polarization studies can be most easily performed within the density matrix approach as applied above to the electron recombination processes. This approach, however, has to be extended in order to include the spin density matrix of the projectile ions $\langle I_0\,M_0\,|\,\hat{\rho}_{\text{ion}}\,|\,I_0\,M_0'\rangle$, whose (proper) parameterization is required. For instance, while the longitudinal polarization of the 1/2–spin electron is described by the single parameter P_z (cf Equation (3.5)), the 9 parameters characterize the

polarization state of the projectile ion with the nuclear spin $I_0 = 9/2$. Obviously, in order to make possible the interpretation of the (future) experimental results, the number of these (independent) polarization parameters has to be reduced. As seen from Equation (4.10), for instance, such reduction can be easily achieved if the geometry of the x–ray detectors possesses proper *symmetry*. A more detailed theoretical analysis of the polarization effects as caused by the nuclear spin–polarized ions, will refer, therefore, to the studies on the "symmetrical" experimental schemes which would allow us to explore a few polarization parameters while the others remain unobserved.

4.4.2   Electron capture into the hydrogen–like ions

Until now, we have considered the electron capture into the bound states of *bare*, highly–charged ions. Such recombination process, as discussed in this thesis, appears now to be well understood both by experiment and theory. Less attention, in contrast, has been paid previously to the electron capture into initially *few–electron* heavy ions which, in fact, is more difficult to describe due to the interelectronic effects. A first step towards the interelectronic–interaction studies was carried out by Stöhlker and co–workes in 1994 who measured the angular distributions of the x–ray photons emitted in the radiative electron capture into the L–shell of *helium–like* uranium ions. These experimental findings, however, were found to be in a very good agreement with theoretical calculations employing the (final state) lithium–like uranium U^{89+} as the hydrogen–like system with the effective charge $Z_{eff} = 90.3$ that takes into account the electron screening effect. Moreover, later theoretical investigations have proved that such simple *screening–potential* approximation yields the dominant part of the interelectronic–interaction effects in the helium–like heavy ions at a wide region of projectile energies (Yerokhin *et al* 2000, Shabaev 2002).

The success of the one–electron treatment is obviously related to the fact that in the case of helium–like ions we consider the electron capture into the closed–shell configuration $(1s)^2$. In order to explore the electron–electron interactions in detail, therefore, we have to consider the capture into an open–shell system, the most simple example of which is given by the *hydrogen–like* ions. In this contribution, a series of experiments are likely to be carried out soon at the GSI storage ring to investigate the angle–differential cross sections for the K– as well as L–shell recombination of the initially hydrogen–like uranium ions. Theoretically, these angular distributions may be calculated within the framework of the Multi–configuration Dirac–Fock (MCDF) theory that incorporates (the main part of) the electron–electron interaction effects (Grant 1974, Fischer *et al* 2000). Moreover, when combining with the density matrix approach, the MCDF theory will allow us to study the *polarization* of the emitted x–ray photons which, as expected, is even more precise tool for studying the interelectronic effects. A detailed calculations of the angular distributions as well as polarization properties in the recombination of hydrogen–like heavy ions is currently under way for which the basis of the technical elements have been already prepared in the framework of the RATIP program (Fritzsche 2000, 2001).

Chapter 5

Summary

In summary, the interaction process between a photon and an electron in the presence of a strong nuclear Coulomb field is discussed from the viewpoint of the radiative recombination and the radiative electron capture of bare, highly–charged ions. For relativistic ion–atom collisions, this charge transfer process has been intensively explored recent years both in experiment and theory. However, while in the past most studies were focused on the total and angle–differential recombination cross sections, the today's challenge arises from measurements on the *polarization* and *correlation* properties of the emitted x–ray photons. The great promise of such advanced experiments lays in the fact that they provide an extremely precise tool to probe the subtle effects of relativity in heavy ion collisions. Moreover, apart from gaining more insight into the collision dynamics, these measurements may enable one to derive the polarization properties of the ion beams, a lane which was closed in the past but now attracts much interest, both in atomic and nuclear physics.

In this thesis, I have reviewed the advanced – polarization and correlation – studies on the radiative electron capture by highly–charged ions for which the most natural framework is given by density matrix theory. Within this theory, we derived the general relations for the description of the *two–step* recombination process at which an electron is (radiatively) captured into a bound ion state which later decays by emission of the second – characteristic – photon. Of course, these relations can be extended for any multi–step as well as one–step electron capture process. In the latter case, i.e. for the electron capture into the ground ion state, we investigated the *linear* polarization of the recombination x–ray photons which proved to be a valuable tool for the detection of the polarization of particles involved in heavy ion collisions. For instance, as seen from our computations for the recombination of bare uranium projectiles U^{92+}, spin–polarization of the incident electrons generally leads to a rotation of the linear polarization of light out of the reaction plane. These theoretical findings have evident consequences for future experimental research where polarization measurements on hard x–ray photons become possible due to recent developments in position sensitive solid–state detectors (Stöhlker *et al* 2003).

While the K–shell recombination is a trivial case of the *one–step* process, the best known example for the *two–step* recombination is given by the electron capture into the $2p_{3/2}$ state of bare ion and the subsequent Lyman–α_1 ($2p_{3/2} \rightarrow 1s_{1/2}$) decay. For this radiative decay

we applied the density matrix theory in order to study the angular distribution as well as the linear polarization of the characteristic photons. Both these (observable) properties are found to be considerably affected by the interference between the leading electric dipole decay channel **E1** and much weaker magnetic quadrupole transition **M2**. For the angular distribution of the Lyman–α_1 decay in hydrogen–like uranium, for instance, this **E1**–**M2** multipole mixing terms leads to a 30 % effect which removes the former deviation between the experimental and theoretical results for the alignment of the $2p_{3/2}$ ion state (Stöhlker *et al* 1997, Surzhykov *et al* 2002a). Moreover, similar interference terms are expected to have considerable impact for the interpretation of experimental data for any other atomic transition in the high–Z regime. Here we can mention, for example, the radiative decays following either L–shell vacancy production in heavy atoms (Papp and Palinkas 1988, Papp *et al* 1990) or the dielectronic recombination of high–Z projectile ions (Bhalla *et al* 1991, Chen and Scofield 1995, Gail *et al* 1998).

Beside of detailed but independent studies on the properties of the recombination (first step) and the subsequent decay (second step) photons we also explored the correlated photon emission which may be observed in x–x coincidence experiments. Emphasis was placed, in particular, on the photon–photon *angular* correlations which are, from an experimental viewpoint, the most simple case of the coincidence measurements. In this contribution, we performed detailed computations for the electron capture into $2p_{3/2}$ state of bare uranium ions and the subsequent Lyman–α_1 angular distributions, where we have assumed that the recombination photon is to be detected in coincidence. As shown above, the emission pattern of the characteristic radiation strongly depends not only on the particular angle, under which the recombination photon is observed, but also on the spin–polarization of the incident particles. Therefore, apart from the measurements on the linear polarization of the first–step (recombination) photons, the angle–angle angular correlations offer us a second possibility for studying the polarization properties of either the target atoms (or electrons) or, respectively, of the ion beams, if the electrons are captured by the nuclear spin–polarized ions.

Chapter 6

Zusammenfassung

In dieser Arbeit wird die Wechselwirkung zwischen einem Photon und einem Elektron im starken Coulombfeld eines Atomkerns am Beispiel des radiativen Elektroneneinfangs beim Stoß hochgeladener Teilchen untersucht. In den letzten Jahren wurde dieser Ladungsaustauschprozess insbesondere für relativistische Ion–Atom–Stöße sowohl experimentell als auch theoretisch ausführlich erforscht. In Zentrum standen dabei haupsächlich die totalen und differentiellen Wirkungsquerschnitte. In neuerer Zeit werden vermehrt Spin– und Polarisationseffekte sowie Korrelationseffekte bei diesen Stoßprozessen diskutiert. Man erwartet, dass diese sehr empfindlich auf relativistische Effekte im Stoß reagieren und man deshalb eine hervorragende Methode zu deren Bestimmung erhält. Darüber hinaus könnten diese Messungen auch indirekt dazu führen, dass man die Polarisation des Ionenstrahls bestimmen kann. Damit würden sich neue experimentelle Möglichkeiten sowohl in der Atom– als auch der Kernphysik ergeben.

In dieser Dissertation werden zunächst diese ersten Untersuchungen zu den Spin–, Polarisations– und Korrelationseffekten systematisch zusammengefasst. Die Dichtematrixtheorie liefert hierzu die geeignete Methode. Mit dieser Methode werden dann die allgemeinen Gleichungen für die Zweistufen–Rekombination hergeleitet. In diesem Prozess wird ein Elektron zunächst radiativ in einen angeregten Zustand eingefangen, der dann im zweiten Schritt unter Emission des zweiten (charakteristischen) Photons in den Grundzustand übergeht. Diese Gleichungen können natürlich auf beliebige Mehrstufen– sowie Einstufen–Prozesse erweitert werden. Im direkten Elektroneneinfang in den Grundzustand wurde die "lineare" Polarisation der Rekombinationsphotonen untersucht. Es wurde gezeigt, dass man damit eine Möglichkeit zur Bestimmung der Polarisation der Teilchen im Eingangskanal des Schwerionenstoßes hat. Rechnungen zur Rekombination bei nackten U^{92+} Projektilen zeigen z. B., dass die Spinpolarisation der einfallenden Elektronen zu einer Drehung der linearen Polarisation der emittierten Photonen aus der Streuebene heraus führt. Diese Polarisationdrehung kann mit neu entwickelten orts– und polarisationsempfindlichen Festkörperdetektoren gemessen werden. Damit erhält man eine Methode zur Messung der Polarisation der einfallenden Elektronen und des Ionenstrahls.

Die K–Schalen–Rekombination ist ein einfaches Beispiel eines Ein–Stufen–Prozesses. Das am besten bekannte Beispiel der Zwei–Stufen–Rekombination ist der Elektroneneinfang in den $2p_{3/2}$–Zustand des nackten Ions und anschließendem $Lyman$–α_1–Zerfall ($2p_{3/2} \rightarrow 1s_{1/2}$). Im Rahmen der Dichte–Matrix–Theorie wurden sowohl die Winkelverteilung als auch die lineare

Polarisation der charakteristischen Photonen untersucht. Beide (messbaren) Größen werden beträchtlich durch die Interferenz des E1–Kanals (elektrischer Dipol) mit dem viel schwächeren M2–Kanal (magnetischer Quadrupol) beeinflusst. Für die Winkelverteilung des Lyman–α_1 Zerfalls im Wasserstoff–ähnlichen Uran führt diese E1–M2–Mischung zu einem 30%–Effekt. Die Berücksichtigung dieser Interferenz behebt die bisher vorhandene Diskrepanz von Theorie und Experiment beim Alignment des $2p_{3/2}$–Zustands.

Neben diesen Ein–Teichen–Querschnitten (Messung des Einfangphotons oder des charakteristischen Photons) wurde auch die Korrelation zwischen den beiden berechnet. Diese Korrelationen sollten in X–X–Koinzidenz–Messungen beobbachtbar sein. Der Schwerpunkt dieser Untersuchungen lag bei der Photon–Photon–Winkelkorrelation, die experimentell am einfachsten zu messen ist. In dieser Arbeit wurden ausführliche Berechnungen der koinzidenten X–X–Winkelverteilungen beim Elektroneneinfang in den $2p_{3/2}$–Zustand des nackten Uranions und beim anschließenden Lyman–α_1–Übergang durchgeführt. Wie bereits erwähnt, hängt die Winkelverteilung des charakteristischen Photons nicht nur vom Winkel des Rekombinationsphotons, sondern auch stark von der Spin–Polarisation der einfallenden Teilchen ab. Damit eröffnet sich eine zweite Möglichkeit zur Messung der Polaristion des einfallenden Ionenstrahls bzw. der einfallenden Elektronen.

Chapter 7

Bibliography

Alling W R and Johnson W R 1965 *Phys. Rev.* **139** A1050

Anholt R, Andriamonje S A, Morenzoni E, Stoller Ch, Molitoris J D, Meyerhof W E, H. Bowman, Xu J S, Xu Z Z, Rasmussen J O and Hoffmann D H H 1984 *Phys. Rev. Lett.* **53** 234

Balashov V V 1999 *J. Phys. IV* **9** 21

Balashov V V, Grum–Grzhimailo A N and Kabachnik N M 2000 *Polarization and Correlation Phenomena in Atomic Collisions* (New York: Kluwer Academic Plenum Publishers)

Beier T 2000 *Phys. Rep. Lett.* **339** 79

Berezhko E G and Kabachnik N M 1977 *J. Phys.* B **10** 2467

Berestetskii V B, Lifshitz E M and Pitaevskii L P 1971 *Relativistic Quantum Theory* (Pergamon, Oxford).

Bethe H and Maximon L 1954 *Phys. Rev.* **93** 768

Beyer H F, Menzel G, Liesen D, Gallus A, Bosch F, Deslattes R, Indelicato P, Stöhlker Th, Klepper O, Moshammer R, Nolden F, Eickhoff H, Franzke B and Steck M 1995 *Z. Phys.* D **35** 169

Bhalla C P, Karim K R and Wilson M 1991 *Nucl. Instruments and Methods* B **56/57** 324

Bilyk V, Fritzsche S and Surzhykov A 2003 *J. Phys. B: At. Mol. Phys.* to be submitted

Blasche K and Franzke B 1994 *Status Report on SIS–ESR* Proc. 6th Europ. Part. Acc. Conf. (EPAC) (Singapore: World Scientific)

Blum K 1981 *Density Matrix Theory and Applications* (New York: Plenum)

Born M and Wolf E 1970 *Principles of Optics* (New York: Pergamon)

Brinzanescu O 2000 *X–Ray Emission of High–Z Projectiles in Collisions with Electrons and Atoms* (PhD Thesis, University of Heidelberg)

Chen M H and Scofield J H 1995 *Phys. Rev.* A **52** 2057

Drake G 1988 *Theory of Transitions, and the Electroweak Interaction* in: G. W. Series (Ed.), The Spectrum of Atomic Hydrogen: Advantages (Singapore: Word Scientific)

Edmonds A 1996 *Angular Momentum in Quantum Mechanics* (New Jersey: Princeton University Press)

Eichler J 1994 *Nucl. Phys.* A **572** 147

Eichler J and Meyerhof W 1995 *Relativistic Atomic Collisions* (San Diego: Academic Press)

Eichler J, Ichihara A and Shirai T 1995 *Phys. Rev.* A **51** 3025

Eichler J, Ichihara A and Shirai T 1996 *Phys. Rev.* A **54** 4954

Eichler J, Ichihara A and Shirai T 1998 *Phys. Rev.* A **58** 2128

Eichler J and Ichihara A 2002 *Phys. Rev.* A **65** 052716

Fano U 1957 *Rev. Mod. Phys.* **29** 74

Fano U and Racah G 1959 *Irreducible Tensorial Sets* (New York: Academic Press)

Fischer C F, Brage T and Jönsson P 2000 *Computational Atomic Structure; An MCDF Approach* (Bristol and Philadelphia: Institute of Physics Publishing)

Fritzsche S 1997 *Comput. Phys. Commun.* **103** 51

Fritzsche S 2000 *J. El. Spec. Rel. Phen.* **114–116** 1155

Fritzsche S 2001 *Comput. Phys. Commun.* **141** 163

Fritzsche S, Inghoff T, Bastug T and Tomaselli M 2001 *Comput. Phys. Commun.* **139** 314

Fritzsche S and Surzhykov A 2003 *AIP: Conference Proceedings* in press

Gail M, Grün N and Scheid W 1998 J. Phys. B: At. Mol. Phys. B **31** 4645

Gavrila M 1960 *Nuovo Cim.* **15** 691

Grant I 1974 *J. Phys.* B **7** 1458

Gumberidze A 2003 *Experimental Studies of the Ground State QED Corrections in H– and He–like Uranium* (PhD Thesis, University of Frankfurt on Main)

Ichihara A, Shirai T and Eichler J 1994 *Phys. Rev.* A **49** 1875

Ichihara A and Eichler J 2000 *At. Data Nucl. Data Tables* **74** 1

Inghoff T, Fritzsche S, Jacob T, Surzhykov A and Fricke B 2001 *Ein interaktives Programm zur Beshreibung wasserstoffähnlicher Ionen* (Energiereiche Atomare Stösse, 22 Arbeitsbericht)

Kessler J 1985 *Polarized Electrons* (New York: Pergamon)

Kienle P, Kleber M, Povh B, Diamond R M, Stephens F S, Grosse E, Maier M R and Proetel D 1973 *Phys. Rev. Lett.* **31** 1099

Kitajima M, Okamoto M, Hoshino M, Tanaka H, Fritzsche S, Kabachnik N M, Sazhina I P, Shimizu Y, Ueda K 2002 *J. Phys. B: At. Mol. Phys.* **35** 3327

Klasnikov A E, Artemyev A N, Beier T, Eichler J, Shabaev V M and Yerokhin V A 2002 *Phys. Rev.* A **66** 042711

Liesen D 2003 private communication

Lin C D and Macek J H 1987 *Phys. Rev.* A **35** 5005

Metag V 2000 *Research Highlights from 30 Years of GSI* (ceremony talk on the occasion of the 30th anniversary of GSI)

Mohr P J, Plunien G and Soff G 1998 *Phys. Rep.* **293** 227

Mokler P H and Stöhlker Th 1996 *Adv. in Atomic, Molecular, and Optical Physics* **37** 297

Nagel B 1960 *Ark. Fysik* **18** 1

Oppenheimer J R 1928 *Nucl. Phys.* **31** 349

Orsic–Muthig A, Stöhlker Th, Gumberidze A, Banas D, Fritzsche S, Laczko G, Kozhuharov C, Mann R, Hagmann S, Spillmann U, Surzhykov A and Tachenov S 2002 *GSI Scientific Report* 90

Pal'chikov V G 1998 *Phys. Scr.* **57** 581

Papp T and Palinkas J 1988 *Phys. Rev. A* **38** 2686

Papp T, Palinkas J and Sarkadi L 1990 *Phys. Rev. A* **42** 5452

Percival I C and Seaton M J 1958 *Philos. Trans. R. Soc. London* Ser. A **251** 113

Pratt R H, Levee R, Pexton R and Aron W 1964 *Phys. Rev.* **134** A898

Pratt R H, Akiva Ron and Tseng H K 1973 *Rev. Mod. Phys.* **45** 273

Raisbeck G and Yiou F 1971 *Phys. Rev. Lett.* **4** 1858

Reich H, Bourgeois W, Franzke B, Kritzer B and Varentsov V 1997 *Nucl. Phys.* A **696** 417

Rose M E 1957 *Elementary Theory of Angular Momentum* (New York: Wiley)

Sauter F 1931 *Ann. Phys.* **11** 454

Shabaev V M 2002 *Phys. Rep.* **356** 119

Schnopper H W, Betz H, Devaille J P, Kalata K, Sohval A R, Jones K W and Wegner H E 1972 *Phys. Rev. Lett.* **29** 898

Slevin J A and Chwirot S 1990 *J. Phys. B: At. Mol. Phys.* **23** 165

Spindler E, Betz H–D and Bell F 1979 *Phys. Rev. Lett.* **42** 832

Stobbe M 1930 *Ann. Phys.* **7** 661

Stöhlker Th, Geissel H, Irnich H, Kandler T, Kozhuharov C, Mokler P H, Münzenberg G, Nickel F, Scheidenberger C, Suzuki T, Kucharski M, Warczak A, Rymuza P, Stachura Z, Kriessbach A, Dauvergne D, Dunford R, Eichler J, Ichihara A and Shirai T 1994 *Phys. Rev. Lett.* **73** 3520

Stöhlker Th, Kozhuharov C, Mokler P H, Warczak A, Bosch F, Giessel H, Moshammer R, Scheidenberger C, Eichler J, Ichihara A, Shirai T, Stachura Z and Rymuza P 1995 *Phys. Rev.* A **51** 2098

Stöhlker Th, Bosch F, Gallus A, Kozhuharov C, Menzel G, Mokler P H, Prinz H T, Eichler J, Ichihara A, Shirai T, Dunford R W, Ludziejewski T, Rymuza P, Stachura Z, Swiat P and Warczak A 1997 *Phys. Rev. Lett.* **79** 3270

Stöhlker Th 1999 *Phys. Scr.* **T80** 165

Stöhlker Th, Ludziejewski T, Bosch F, Dunford R W, Kozhuharov C, Mokler P H, Beyer H F, Brinzanescu O, Franzke B, Eichler J, Griegal A, Hagmann S, Ichihara A, Krämer A, Lekki J, Liesen D, Nolden F, Reich H, Rymuza P, Stachura Z, Steck M, Swiat P and Warczak A 1999 *Phys. Rev. Lett.* **82** 3232

Stöhlker Th, Mokler P H, Bosch F, Dunford R W, Klepper O, Kozhuharov C, Ludziejewski T, Franzke B, Nolden F, Reich H, Rymuza P, Stachura Z, Steck M, Swiat P and Warczak A 2000 *Phys. Rev. Lett.* **85** 3109

Stöhlker Th, Ma X, Ludziejewski T, Beyer H F, Bosch F, Brinzanescu O, Dunford R, Eichler J, Hagmann S, Ichihara A, Kozhuharov C, Krämer A, Liesen D, Mokler P H, Stachura Z, Swiat P and Warczak A 2001 *Phys. Rev. Lett.* **86** 983

Stöhlker Th, Banas D, Beyer H F, Gumberidze A, Kozhuharov C, Kanter E, Krings T, Lewoczko W, Ma X, Protic D, Sierpowski D, Spillmann U, Tachenov S and Warczak A 2003 *Nucl. Instruments and Methods* B **205** 210

Surzhykov A, Fritzsche S and Stöhlker Th 2001 *Phys. Lett.* A **289** 213

Surzhykov A, Fritzsche S, Gumberidze A and Stöhlker Th 2002a *Phys. Rev. Lett* **88** 153001

Surzhykov A, Fritzsche S and Stöhlker Th 2002b *J. Phys. B: At. Mol. Phys.* **35** 3713

Surzhykov A, Fritzsche S and Stöhlker Th 2003a *Nucl. Instruments and Methods* B **205** 496

Surzhykov A, Fritzsche S, Stöhlker Th and Tachenov S 2003b *Phys. Rev.* A **68** 022710

Surzhykov A, Fritzsche S and Stöhlker Th 2003c *Hyperfine Int.* in print

Tachenov S, Stöhlker Th, Banas D, Beyer H F, Bosch F, Gumberidze A, Hagmann S, Kozhuharov C, Krings Th, Ma X, Orsic Muthig A, Protic D, Sierpowski D, Spillmann U, Stachura Z and Warczak A 2002 *GSI Scientific Report* 113

Takacs E, Meyer E S, Gillaspy J D, Roberts J R, Chantler C T, Hudson L T, Deslattes R D, Brown C M, Laming J M, Dubau J and Inal M K 1996 *Phys. Rev.* A **54** 1342

Tanis J A and Shafroth S M 1978 *Phys. Rev. Lett* **40** 1174

Tawara H, Richard P and Kawatsura K 1982 *Phys. Rev.* A **26** 154

Trautmann D, Baur G and Rösel F 1983 *J. Phys.* B **16** 3005

Valluri S R, Becker U, Grün N and Scheid W 1984 *J. Phys. B: At. Mol. Phys.* **17** 4359

Varshalovich D A, Moskalev A N and Khersonskii V K 1988 *Quantum Theory of Angular Momentum* (Singapore: World Scientific)

von Neuman J 1927 *Göttinger Nachrichten* 245

Warczak A 2003 *Nucl. Instruments and Methods* B **205** 36

Yerokhin V A, Shabaev V M, Beier T and Eichler J 2000 *Phys. Rev.* A **62** 042712

Yerokhin V A and Shabaev V M 2001 *Phys. Rev.* A 062507

Yerokhin V A, Artemyev A N, Indelicato P and Shabaev V M 2003 *Nucl. Instruments and Methods* B **205** 47

Zare R 1988 *Angular Momentum: Understanding Spatial Aspects in Chemistry and Physics* (New York: John Wiley & Sons)

Chapter 8

Publications

The list of publications which have been prepared during period of my PhD study is presented below. In this Chapter, I include the full–text versions of the papers [1, 3, 4, 6, 8, 10], which are *directly* related to the the topic of the thesis work.

1. *Photon polarization in the radiative recombination of high–Z hydrogen–like ions*
   Surzhykov A, Fritzsche S and Stöhlker Th
   2001 *Phys. Lett.* A **289** 213

2. *Production of bare argon, manganese, iron and nickel nuclei in the Dresden EBIT*
   Kentsch U, Zschornack G, Grossmann F, Ovsyannikov V P, Ullmann F, Fritzsche S and Surzhykov A
   2002 *Nucl. Instruments and Methods* B **187** 238

3. *The Lyman–α₁ decay in hydrogen–like ions: Interference between the E1 and M2 transition amplitudes*
   Surzhykov A, Fritzsche S, Gumberidze A and Stöhlker Th
   2002 *Phys. Rev. Lett.* **88** 153001

4. *Photon–photon angular correlations in the radiative recombination of bare high–Z ions,*
   Surzhykov A, Fritzsche S and Stöhlker Th
   2002 *J. Phys. B: At. Mol. Phys.* **35** 3713

5. *Relativistic and retardation effects in the two–photon ionization of hydrogen–like ions*
   Koval P, Fritzsche S and Surzhykov A
   2003 *J. Phys. B: At. Mol. Phys.* **36** 873

6. *Two–step radiative recombination of polarized electrons into bare, high–Z ions*
   Surzhykov A, Fritzsche S and Stöhlker Th
   2003 *Nucl. Instruments and Methods* B **205** 391

7. *Wave packet approach to the ionization of high–Z, hydrogen–like ions*
   Fritzsche S, Surzhykov A and Stöhlker Th
   2003 *Nucl. Instruments and Methods* B **205** 496

8. *Polarization studies on the radiative recombination of highly charged ions*
   Surzhykov A, Fritzsche S, Stöhlker Th and Tachenov S
   2003 *Phys. Rev.* A **68** 0227101

9. *Structure and dynamics of high–Z ions studied at the ESR storage ring,*
   Stöhlker Th, Gumberidze A, Ma X, Beyer H F, Bednarz G, Bosch F, Cai X, Fritzsche S,
   Hagmann S, Kozhuharov C, Klepper O, Liesen D, Mokler P H, Sierpowski D, Stachura Z,
   Steck M, Surzhykov A, Toleikis S, Warczak A and Zhou Y
   2003 *Hyperfine Int.* **146–147** 97–102

10. *Polarization of the Lyman–α_1 emission following the radiative recombination of bare,
    high–Z ions*
    Surzhykov A, Fritzsche S and Stöhlker Th
    2003 *Hyperfine Int.* **146–147** 35–40

11. *Polarization and correlation studies on the electron capture into highly–charged ions*
    Fritzsche S, Surzhykov A and Stöhlker Th
    2003 *AIP: Conference Proceedings* in press

12. *Angular correlation and polarization studies for radiative electron capture into high–Z
    ions*
    Stöhlker Th, Banas D, Fritzsche S, Gumberidze A, Kozhuharov C, Ma X, Orsic–Muthig A,
    Spillmann U, Sierpowski D, Surzhykov A, Tachenov S and Warczak A
    2003 *AIP: Conference Proceedings* in press

13. *Electron angular distributions in the two–photon ionization of hydrogen–like ions: Rela-
    tivistic description*
    Koval P, Fritzsche S and Surzhykov A
    2003 *J. Phys. B: At. Mol. Phys.* submitted

8.1 Photon polarization in the radiative recombination of high–Z hydrogen–like ions

ELSEVIER

Photon polarization in the radiative recombination of high-Z, hydrogen-like ions

A. Surzhykov [a,*], S. Fritzsche [a], Th. Stöhlker [b]

[a] *Fachbereich Physik, Universität Kassel, D-34132 Kassel, Germany*
[b] *Gesellschaft für Schwerionenforschung, D-62491 Darmstadt, Germany*

Abstract

Density matrix theory is applied to re-investigate the radiative recombination and radiative electron capture of high-Z ions. Attention has been paid particularly to the polarization of the emitted photons. For the recombination of a free electron into the K-shell of Bi^{83+} projectiles, we calculated the angular-dependent Stokes parameters for the X-ray emission. We also discuss the importance of the choice of the quantization axis for understanding the polarization properties of the system both for the residual ion and the emitted light. © 2001 Elsevier Science B.V. All rights reserved.

PACS: 34.80.Lx; 34.80.Nz; 34.70.+e; 32.80.Fb

1. Introduction

The radiative recombination (RR) and radiative electron capture are two well-established processes from the study of electron–ion and atom–ion collisions. In these processes, a free or quasi-free electron is captured into a bound state of the ion, accompanied by the simultaneous emission of a photon. For bare, high-Z ions, for example, the radiative recombination has been explored in detail by Stöhlker and co-workers [1,2] at the GSI storage ring during recent years. So far, however, most experiments were focused on measuring the total and angle-differential recombination cross sections which are typically found in good agreement with theoretical predictions, based on Dirac's theory [2,3]. Much less attention, in con-

trast, has been paid previously to the polarization of the emitted radiation. A first step towards a polarization study was carried out by Eichler [4,5] a few years ago who calculated the alignment of the residual ions following the capture of an electron into the L- and M-shells of bare, high-Z ions. Experimentally evidence for an alignment of the ions in electron capture has been found recently in collisions of bare ions with light and medium targets atoms [6]. Till today, however, no polarization measurements have been performed for the emitted radiation, mainly because of the lack of efficient polarization detectors for hard X-rays. Only in the light of recent improvements in detector techniques, the observation of the photon polarization becomes more likely (for instance, at the GSI in Darmstadt) within the next few years.

A natural framework for studying the photon and ion polarization in the recombination of high-Z ions (following either a single or the subsequent capture of electrons) is given by the density matrix theory.

* Corresponding author.
  E-mail address: surz@physik.uni-kassel.de (A. Surzhykov).

For applications in atomic physics, and combined particularly with the concept of spherical tensors, this theory was originally developed by Fano [7] in the late fifties. Since then, the density matrix theory has been utilized successfully in a large number of case studies on the polarization properties and the "correlation" between emitted particles and light (see Refs. [8,9] for further examples). Today, this formalism provides us with a tool of a great elegance for our theoretical understanding of collision processes or, recently, in analyzing lifetime interferences in resonantly excited Auger cascades [10].

In this Letter, we apply the density matrix theory to the polarization of the photons in the radiative recombination of bare, high-Z ions. Relativistic calculations have been carried out in particular for the Stokes parameters of the photons, following the capture of a free electron into the K-shell of Bi^{83+} ions. In the next section, we first present a short outline of the density matrix formalism when applied to the recombination of ions. The basic relations between the polarization of the photons and the (final-state) density matrix are later derived in Section 3. In Section 4, we describe the computations and give a short discussion of the Stokes parameter while, finally, a brief summary is given in Section 5.

2. Application of density matrix theory to the radiative recombination of ions

In the radiative recombination of bare, high-Z ions, the initial state of the system (i.e., before the electron capture) is given by the ion and a free electron. Here, we may consider an electron with asymptotic momentum $\mathbf{p}$ and projection m_s, and an ion which is specified in term of its nuclear charge Z and its spin quantum numbers I_0 and projection M_0. In the density matrix approach [8,9] the initial state is represented by the density operator $\hat{\rho}_i$ which is then just the direct product of the operators of the bare ion and the incident electron $\hat{\rho}_i = \hat{\rho}_0 \otimes \hat{\rho}_e$ or, in terms of the density matrix (in the representation of the individual momenta),

$$\langle I_0 M_0, \mathbf{p} m_s | \hat{\rho}_i | I_0 M_0', \mathbf{p} m_s' \rangle$$
$$= \langle I_0 M_0 | \hat{\rho}_0 | I_0 M_0' \rangle \langle \mathbf{p} m_s | \hat{\rho}_e | \mathbf{p} m_s' \rangle. \tag{1}$$

Similarly, the final-state density matrix describes the recombined ion in some final-ionic state $|F, M_f\rangle$

as well as the emitted photon with wave vector $\mathbf{k}$ and helicity $\lambda = \pm 1$ (i.e., the spin projection of the photon onto the direction of $\mathbf{k}$). For bare ions, the bound-state $|F, M_f\rangle$ generally results from the coupling of the electron in the (one-particle) state $|j_b \mu_b\rangle$ with the nuclear spin: $\mathbf{F} = \mathbf{j_b} + \mathbf{I_0}$. As known from density matrix theory, the statistical operators of the initial and final states of the system are connected by the transition operator $\hat{R}$ which describes the interaction [8],

$$\hat{\rho}_f = \hat{R} \hat{\rho}_i \hat{R}^+, \tag{2}$$

i.e., the photon–ion interaction in the case of a radiative recombination. The particular form of $\hat{R}$, of course, depends on the framework in which we describe the coupling of the radiation field to the electronic motion in the ion. As appropriate for high-Z ions, below we always refer to a relativistic frame on the basis of the Dirac equation [3].

Making use of the initial state (1) and relation (2), we can easily find also the final-state density matrix in the representation of the angular momenta,

$$\langle FM_F, \mathbf{k}\lambda | \hat{\rho}_f | FM_F', \mathbf{k}\lambda' \rangle$$
$$= \sum_{M_0 M_0' m_s m_s'} M_{b,\mathbf{p}}^{RR}(m_s, M_0, \lambda, M_F)$$
$$\times M_{b,\mathbf{p}}^{RR*}(m_s', M_0', \lambda', M_F')$$
$$\times \langle I_0 M_0 | \hat{\rho}_0 | I_0 M_0' \rangle \langle \mathbf{p} m_s | \hat{\rho}_e | \mathbf{p} m_s' \rangle, \tag{3}$$

where we have used the abbreviation

$$M_{b,\mathbf{p}}^{RR}(m_s, M_0, \lambda, M_f) = \langle FM_F, \mathbf{k}\lambda | \hat{R} | \mathbf{p} m_s, I_0 M_0 \rangle \tag{4}$$

to represent the elements of the transition matrix. The final-state matrix (3) still contains the *complete* information about the system (i.e., about the ion "plus" photon) and can be used to derive the properties of the photon and the residual ion.

Obviously, the outcome of some given experiment depends on its particular set-up and on the capability of the detectors to *resolve* the individual properties of particles. In density matrix theory, this set-up of the experiment is typically described in terms of a projector operator $\hat{P}$ which characterizes the *detector systems* as a whole. Frankly speaking, this operator projects out all those quantum states of the final-state system which leads to a "count" at the detectors (or simultaneous counts in the case of coincidence

experiments). In the literature, the operator $\hat{P}$ is often called the *detector operator*; it gives us the probability to find an "event" at the detector simply by taking the trace of its product with the density matrix: $W = \text{Tr}(\hat{P}\hat{\rho})$. For example, in order to measure the angular distribution of the emitted photons in the RR, one often takes a photon detector in a given direction $\hat{n} = (\vartheta, \varphi)$, relative to the electron (or beam) direction which is neither sensitive to the polarization of the light nor to the spin state of the residual ion:

$$\hat{P}_{\mathbf{k}} = \sum_{\lambda F M_F} |\mathbf{k}\lambda\rangle |F M_F\rangle \langle F M_F| \langle \mathbf{k}\lambda|. \tag{5}$$

That is, in defining projector (5), we must sum over λ and the spin quantum numbers F, M_F. For the particular case of a zero nuclear spin ($I_0 = M_0 = 0$) and an unpolarized electron target, which gives rise to an additional summation over m_s, the trace over the product $(\hat{P}_{\mathbf{k}}\hat{\rho}_f)$ of matrix (3) leads immediately to the well-known angular distribution

$$W(\theta) = \frac{1}{2} \sum_{\lambda m_s \mu_b} \left| M_{b,\mathbf{p}}^{\text{RR}}(m_s, \lambda, \mu_b) \right|^2 \tag{6}$$

of the emitted photons [3]. Details about the calculation of these angular-differential cross section for a recombination into bare, high-Z ions have been discussed by Eichler in several papers [2,3] and confirmed in a number of experiments [1].

3. Photon polarization

Another set of detector operators $\{\hat{P}_x\}$ can be defined, of course, to "measure" the polarization properties of the emitted photons. Usually, however, it is more convenient to retain at the density matrix of the outgoing photons,

$$\langle \mathbf{k}\lambda | \hat{\rho}_\gamma | \mathbf{k}\lambda' \rangle_{\lambda, \lambda' = \pm 1}$$
$$= \frac{1}{2} \begin{pmatrix} 1 + P_3 & -P_1 + i P_2 \\ -P_1 - i P_2 & 1 - P_3 \end{pmatrix}, \tag{7}$$

since this matrix is directly related to the Stokes parameters of the light P_1, P_2, and P_3 [8,9]. In the theory of light, these parameters are usually used for characterizing the degrees of linear ($P_L = \sqrt{P_1^2 + P_2^2}$) and circular ($P_C \equiv P_3$) polarization.

The density matrix of photons (7) is obtained from the final-state density matrix (3) simply by taking the trace over all quantum numbers of the residual ion [8]:

$$\langle \mathbf{k}\lambda | \hat{\rho}_\gamma | \mathbf{k}\lambda' \rangle = \text{Tr}_{F M_F} (\hat{\rho}_f)$$
$$= \sum_{F M_F} \langle F M_F, \mathbf{k}\lambda | \hat{\rho}_f | F M_F, \mathbf{k}\lambda' \rangle. \tag{8}$$

In this general form, the photon matrix (8) still applies for any arbitrary spin of the nucleus. As indicated by its labels λ and λ', moreover, this matrix refers to the helicity representation of the photon states. Assuming a zero nuclear spin ($I_0 = M_0 = 0$), it simplifies to

$$\langle \mathbf{k}\lambda | \hat{\rho}_\gamma | \mathbf{k}\lambda' \rangle$$
$$= \sum_{\mu_b} \sum_{m_s m_s'} M_{b,\mathbf{p}}^{\text{RR}}(m_s, \lambda, \mu_b) M_{b,\mathbf{p}}^{\text{RR}*}(m_s', \lambda', \mu_b)$$
$$\times \langle \mathbf{p}m_s | \hat{\rho}_e | \mathbf{p}m_s' \rangle, \tag{9}$$

while the elements of the transition matrix $M_{b,\mathbf{p}}^{\text{RR}}$, which describes the interaction of the ion with the radiation field, takes the standard form

$$M_{b,\mathbf{p}}^{\text{RR}}(m_s, \lambda, \mu_b)$$
$$= \langle j_b \mu_b, \mathbf{k}\lambda | \hat{R} | \mathbf{p} m_s \rangle$$
$$= C \int d^3 r \, \psi_{j_b \mu_b}^+ (\mathbf{r}) \alpha \hat{\mathbf{u}}_\lambda^* e^{-i\mathbf{k}\mathbf{r}} \psi_{\mathbf{p}, m_s}(\mathbf{r}). \tag{10}$$

In recent years, this *relativistic* form of the transition matrix has been widely used for studying the radiative recombination of high-Z ions at intermediate and high collision energies [3]. For a capture into bare ions, $\psi_{j_b \mu_b}(\mathbf{r})$ and $\psi_{\mathbf{p}, m_s}(\mathbf{r})$ are the known solutions of the Dirac Hamiltonian for a bound or continuum electron, respectively. Moreover, the unit vector $\hat{u}_\lambda$ denotes the polarization of the photons. For the numerical calculations of the matrix element (10), we used the computer code DIRAC [11].

4. Calculations and discussion

The matrix element (10) presents the general form of the photon–electron interaction in a relativistic theory of one-electron ions. For its further simplification, one need to "fix" a quantization axis in order to make use of a well-defined representation of the wave functions. This issue has been discussed in detail by

Eichler [3,5]. In standard calculations, the quantization axis is typically chosen parallel to the photon direction since this facilitates the multipole expansion of the photon field and, hence, results in faster computations. However, the use of the *photon axis* for the quantization of the system is not appropriate if we need to consider some definite spin states of either the incident electron or the residual ion. For relativistic energies of the electron, moreover, a sharp spin projection only arises in parallel to its own propagation [3]. Therefore, in order to account for such definite spin projections of the electron and ion, the quantization axis must be chosen along the direction of the electron for the projectile, respectively). For evaluating the matrix element (10), this requires a transformation of the photon wave function and, eventually, increases the complexity of the computations.

In general, the polarization properties of the system in its final state (ion "plus" electron) will reflect also the spin state of the incident electron. If we first consider an unpolarized electron beam, we can still use the photon axis for quantization since a summation over all the projections m_s occurs. For using this *photon* axis, we can simply read off the Stokes parameters of the emitted radiation from the density matrix (8). Fig. 1 shows the degree of linear polarization $P_L = \sqrt{P_1^2 + P_2^2}$ of the RR photons as function of the photon angle, drawn for three typical energies of the projectile. Since, in experiment, the radiative recombination of ions is usually studied by collisions of bare, high-Z projectiles with (low-Z) target atoms, here we present the Stokes parameter for angles measured in the *laboratory system* (the rest frame of the target atoms). *No circular polarization occurs for the case of an unpolarized electron target.*

A circular polarization of the photons can be found only for an (at least partially) polarized electron target. This requires, however, to distinguish between different spin states of the electron and to use the beam axis for quantization (see above). To evaluate the matrix elements for this choice of quantization, we may start with a rotation of the photon field which is— most conveniently—expressed in terms of its (electric and magnetic) multipole components:

$$\mathcal{A}_{LM}^\lambda = A_{LM}(m) + i\lambda A_{LM}(e). \tag{11}$$

Then, a rotation of this field is achieved by

$$\hat{\mathbf{u}}_\lambda e^{i\mathbf{k}\mathbf{r}} = \sqrt{2\pi} \sum_{L=1}^{\infty} \sum_{M=-L}^{M=+L} i^L \sqrt{2L+1}\,\mathcal{A}_{LM}^\lambda \times D_{M\lambda}^L(\mathbf{k} \to \mathbf{z}), \tag{12}$$

where $D_{M\lambda}^L(\mathbf{k} \to \mathbf{z})$ denotes the Wigner rotation matrix. Now, inserting the right-hand side of Eq. (12) into (9) and by making use of the standard expansion for the product of two Wigner rotation matrices, we find a representation of the photon density matrix,

$$\langle \mathbf{k}\lambda | \hat{\rho}_\gamma | \mathbf{k}\lambda' \rangle$$
$$= C \sum_{\nu\mu} D_{0\mu}^\nu(\mathbf{k} \to \mathbf{z})$$
$$\times \sum_{m_s \mu_b LL'} i^{L'-L}(-1)^{m_s - \mu_b}$$
$$\times \sqrt{(2L+1)(2L'+1)} \langle \mathbf{p}m_s | \hat{\rho}_e | \mathbf{p}m_s \rangle$$
$$\times \langle L'm_s - \mu_b L\mu_b - m_s | \nu 0 \rangle \langle L'\lambda'L - \lambda | \nu\mu \rangle$$
$$\times \langle \mathbf{p}m_s | \alpha \mathcal{A}_{L'm_s - \mu_b}^{\lambda'} | \kappa_b \mu_b \rangle$$
$$\times \langle \mathbf{p}m_s | \alpha \mathcal{A}_{Lm_s - \mu_b}^{\lambda} | \kappa_b \mu_b \rangle^*, \tag{13}$$

where all momentum projections refer to the beam axis.
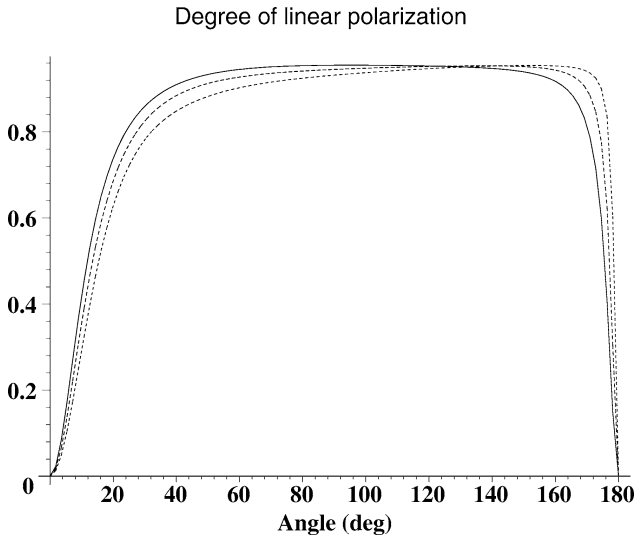
Degree of linear polarization

Fig. 1. Degree of linear polarization P_L of the emitted photon as a function of the *laboratory* photon angle for the K-shell RR of Bi^{83+} projectiles in collisions with unpolarized electrons. The linear polarization is shown for three different projectile energies: $T_p = 10$ MeV/u (—), $T_p = 50$ MeV/u (– –), and $T_p = 100$ MeV/u (- - -).
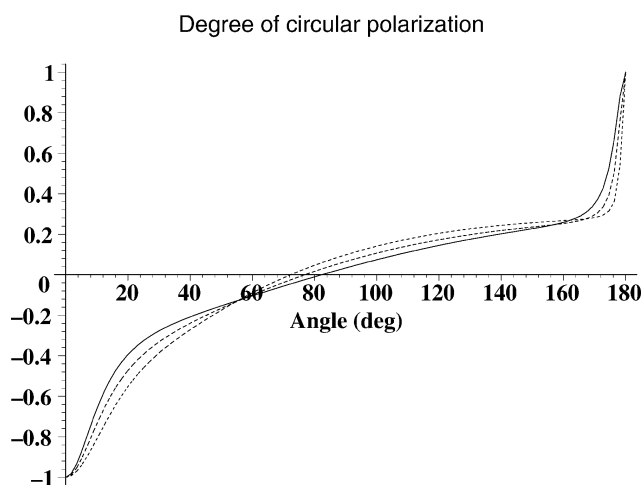
Degree of circular polarization

Fig. 2. Degree of the circular polarization $P_c = P_3$ as function of the *laboratory* photon angle for the K-shell RR of Bi^{83+} projectiles in collisions with completely polarized electrons ($m_s = 1/2$). Notations are the same as in Fig. 1.

The degree of the circular polarization $P_c = P_3$ of the photons for an initially (completely) polarized electron beam with $m_s = 1/2$ is shown in Fig. 2. A strong circular polarization will occur in particular in *forward* and *backward* emission of the photons. As expected from the φ-symmetry of the photon emission, the circular polarization must vanish for photons which are emitted perpendicular (or nearby) to the beam line.

Our present study of the photon polarization emphasizes the role of a proper choice of the quantization axis; a similar discussion was given before by Eichler and co-workers [5] who showed that, in order to determine the alignment of the residual ion, one also need to take the electron direction for quantization. The knowledge of the alignment is required, for instance, to understand both, the angular distribution and the polarization properties of subsequently emitted photons if the initial recombination leads to an excited state like the capture into one of the L-subshells.

5. Summary

In this Letter, we re-considered the radiative recombination of high-Z ions from the viewpoint of density matrix theory. This theory provides a consistent framework to investigate not only the total and angle-differential cross sections but also all the polarization

properties of the combined system, i.e., the residual ion and the photon. Here, we applied the theory to the calculation of the Stokes parameters of the emitted photons. The degree of linear and circular polarization has been shown for the recombination of a free electron into the K-shell of bare Bi^{83+} projectiles. Apart from the angle, the polarization depends on the spin state of both, the projectile and the electron target.

For studying the polarization of the light in the recombination of ions, both for single- and multi-step recombination processes, the role of the quantization axis has been pointed out. In present-day experiments with bare ions one can consider, for instance, the capture of an electron into any of the excited states which, then, will further decay by the emission of one or several subsequent photons. Although only a few of these multi-step processes have been analyzed so far in detail [5,6], they give rise to a large variety of possible polarization and correlation measurements in the (near) future. The density matrix approach, as discussed in this contribution, will certainly help to analyze such experiments. An extension of this formalism towards two-step RR processes is currently under work.

Acknowledgements

References

[1] Th. Stöhlker, C. Kozhuharov, P.H. Mokler, A. Warczak, F. Bosch, H. Geissel, R. Moshammer, C. Scheidenberger, J. Eichler, A. Ichihara, T. Shirai, Z. Stachura, P. Rymuza, Phys. Rev. A 51 (1995) 2098.
[2] A. Ichihara, T. Shirai, J. Eichler, Phys. Rev. A 49 (1994) 1875.
[3] J. Eichler, W. Meyerhof, Relativistic Atomic Collisions, Academic Press, San Diego, 1995, Chapter 9.
[4] J. Eichler, Nucl. Phys. A 572 (1994) 147.
[5] J. Eichler, A. Ichihara, T. Shirai, Phys. Rev. A 58 (1998) 2128.
[6] Th. Stöhlker, F. Bosch, A. Gallus, C. Kozhuharov, G. Menzel, P.H. Mokler, H.T. Prinz, J. Eichler, A. Ichihara, T. Shirai, R.W. Dunford, T. Ludziejewski, P. Rymuza, Z. Stachura, P. Swiat, A. Warczak, Phys. Rev. Lett. 79 (1997) 3270.
[7] U. Fano, G. Racah, Irreducible Tensorial Sets, Academic Press, New York, 1959.

[8] K. Blum, Density Matrix Theory and Applications, Plenum, New York, 1981.

[9] V.B. Berestetskii, E.M. Lifshitz, L.P. Pitaevskii, Relativistic Quantum Theory, Pergamon, Oxford, 1971.

[10] M. Kitajima, M. Okamoto, Y. Shimizu, H. Chiba, S. Fritzsche, N.M. Kabachnik, I.P. Sazhina, T. Hayaishi, H. Tanaka, Y. Sato, K. Ueda, J. Phys. B (2000), in press.

[11] A. Surzhykov, S. Fritzsche, unpublished (2001).

8.2 The Lyman–α_1 decay in hydrogen–like ions: Interference between the E1 and M2 transition amplitudes

PHYSICAL REVIEW LETTERS

Lyman-α_1 Decay in Hydrogenlike Ions: Interference between the $E1$ and $M2$ Transition Amplitudes

A. Surzhykov,[1] S. Fritzsche,[1] A. Gumberidze,[2,3,4] and Th. Stöhlker[2,3]

[1]*Universität Kassel, Heinrich-Plett-Strasse 40, 34132 Kassel, Germany*
[2]*Gesellschaft für Schwerionenforschung, 64291 Darmstadt, Germany*
[3]*Institut für Kernphysik, Universität Frankfurt, 60486 Frankfurt, Germany*
[4]*Tiblisi State University, 380028 Chavchavadze Avenue, Tiblisi, Georgia*
(Received 3 December 2001; published 28 March 2002)

For the Lyman-α_1 transition ($2p_{3/2} \rightarrow 1s_{1/2}$) in hydrogenlike ions an interference between the leading $E1$ decay channel and the much weaker $M2$ multipole transition gives rise to a remarkable modified angular distribution of the emitted photons from aligned ions. This effect is most pronounced for the heaviest elements but results in a still sizable correction for medium-Z ions. For the particular case of hydrogenlike uranium where the angular distribution of the Lyman-α_1 x rays following radiative electron capture has been measured, the former variance with theoretical findings is removed when this $E1$-$M2$ interference is taken into account.

Radiative transitions in high-Z heavy ions play a key role for our understanding of the effects of strong Coulomb fields on the electronic structure of atoms and ions [1]. At high-Z, transition rates and energies are strongly affected by relativistic corrections, and even quantum electrodynamical effects show up in a clear way [2]. One of the most prominent examples is the Lyman-α_1 transition ($2p_{3/2} \rightarrow 1s_{1/2}$) in hydrogen or one-electron ions which serves, e.g., as a precise measure for the $1s$ Lamb shift in hydrogenlike ions [3]. In the case of transitions rates, relativistic effects are manifested by the strongly enhanced importance of magnetic transitions; e.g., the $2s_{1/2}$ decay in high-Z one-electron ions is almost entirely governed by $M1$ transitions quite in contrast to the dominant $2E1$ decay at lower Z. In fact, the photon angular distribution of radiative transitions turns out to be more sensitive to magnetic and retardation effects than total decay rates. This was shown for the case of continuum-bound state transitions (radiative electron capture, REC) occurring in collisions of bare uranium ions with light atomic targets [4]. At high-Z and for not too high collision energies, the transition rates for REC and the corresponding cross sections are well described within the dipole approximation [2]. However, this approach fails to describe the associated photon angular distributions which are strongly modified by magnetic and retardation effects [5].

In this Letter we report on an interference between the $E1$ and $M2$ transition amplitudes in the decay of the $2p_{3/2}$ level in aligned hydrogenlike heavy ions which significantly alters the photon angular distribution of the Lyman-α_1 transition ($2p_{3/2} \rightarrow 1s_{1/2}$). Similar effects are well known for γ transitions between nuclear levels where the so-called *multipole mixing ratios,* e.g., for $E2$ and $M1$ transitions, provide detailed information about the nuclear states involved [6]. To the best of our knowledge such effects have not been reported yet for bound-bound transitions in highly charged ions. For L-shell vacancy pro-

duction following proton impact, however, evidence for multipole mixing has been observed [7]. As emphasized in this Letter, such interferences may have considerable impact also for the interpretation of experimental data. For the particular case of hydrogenlike uranium, where the angular distribution of the Lyman-α_1 x rays following radiative electron capture has been measured, the former disagreement with theoretical findings [8] is removed when taking this interference into account.

Because of parity and angular momentum conservation laws, the Lyman-α_1 ($2p_{3/2} \rightarrow 1s_{1/2}$) decay in hydrogenlike ions can proceed via either $E1$ or $M2$ transitions which reflect different properties of the electron distribution. While the electric dipole component describes the charge oscillations, the magnetic quadrupole reflects the non-spherical part of the electron motion, i.e., its current distribution [1]. However, for all hydrogenlike ions up to the heaviest elements, the magnetic interaction is much weaker than the electric one, although the decay rate for $M2$ transition ($\Gamma_{M2} \propto Z^8$) increases rapidly as a function of the nuclear charge Z when compared to the $E1$ rate ($\Gamma_{E1} \propto Z^4$). But even for hydrogenlike uranium ($Z = 92$) the $E1$ transition rate amounts to $\Gamma_{E1} = 3.92 \times 10^{16}$ s^{-1}, whereas the $M2$ rate $\Gamma_{M2} = 2.82 \times 10^{14}$ s^{-1} contributes less than 1% to the total decay rate. In the past this rather small contribution was one main reason why—till today—the $M2$ component of the radiation field has not been incorporated in computations on the $2p_{3/2}$ decay of hydrogenlike ions or similar $nl \rightarrow 1s$ transitions in the high-Z regime [9,10]. On the other hand, the Lyman-α_1 transition has been studied intensively both by theory and experiments during the last decades because the characteristics of this line, i.e., its polarization and angular distribution, may reveal subtle information on the population mechanisms and, thus, on the dynamical processes of high-Z ions. A number of detailed investigations have been carried out, for instance, for electron-impact excitation [11–13] as

well as for radiative electron capture in collisions of fast bare projectiles with light target ions [8,14,15].

To discuss the $E1$-$M2$ interference effects let us consider a hydrogenlike ion in the $2p_{3/2}$ level whose creation and decay occur as two independent steps, well separated in time (see, e.g., [8]). In the first step the excited level is just populated, for instance, by electron capture or excitation which may occur in ion-atom and ion-electron collisions. Because of the directionality of the collision, the population of magnetic sublevels is likely to deviate from a statistical distribution. In such cases the levels are aligned, thereby the pairs of atomic sublevels with the same magnetic quantum number (but with opposite signs) will be necessarily equally populated. Here we assume that neither the ions nor the target atoms are polarized in ion-atom collisions.

The alignment of an atomic level is commonly described in terms of one or several parameters $\mathcal{A}_k$ which are related to the population cross sections $\sigma(\mu_n)$ of the various sublevels μ_n. In the case of the $2p_{3/2}$ level only the alignment parameter $\mathcal{A}_2$ is nonzero (apart from $\mathcal{A}_0$), and it can be expressed as [16,17]

$$\mathcal{A}_2 = \frac{\sigma(\frac{3}{2}, \pm\frac{3}{2}) - \sigma(\frac{3}{2}, \pm\frac{1}{2})}{\sigma(\frac{3}{2}, \pm\frac{3}{2}) + \sigma(\frac{3}{2}, \pm\frac{1}{2})}, \qquad (1)$$

where $\sigma(3/2, \mu_n)$ describes the population of substate μ_n of the $2p_{3/2}$ level.

In the second step, this $2p_{3/2}$ level then decays into the ground state via the emission of a photon. But although this photon emission occurs independently of the particular creation of the level, it may exhibit an anisotropic emission pattern if the level has been aligned. The angular distribution of the photons in the emitter frame is related to the alignment parameter $\mathcal{A}_2$ by [11,15]

$$W(\theta) = A_0 + A_2 P_2(\cos\theta) \propto 1 + \beta_{20}(1 - \tfrac{3}{2}\sin^2\theta), \qquad (2)$$

where θ is the angle between the direction of the deexcitation photon and the beam direction while $P_2(\cos\theta)$

denotes the second-order Legendre polynomial. As seen from expression (2), the angular distribution is completely determined by the so-called *anisotropy* coefficient $\beta_{20} = \alpha\mathcal{A}_2$, while the coefficient α depends only on the total angular momenta of the initial and final ionic states, respectively. For the case of the $2p_{3/2} \rightarrow 1s_{1/2}$ transition $\alpha = 1/2$.

Expression (2) is well known from the literature (see, e.g., [18]). It includes the contribution from the electric-dipole ($E1$) transition, whereas the—weak—magnetic-quadrupole component ($M2$) is neglected. This $M2$ branch, however, can also be taken into account. For instance, by using the density matrix theory the angular distribution of radiation in its *general form* (i.e., including all allowed multipoles) was obtained by Fano and Racah [19] (see also [11]). Then, the consistent treatment of both decay modes in the Lyman-α_1 transition finally leads to the result that both the alignment and the anisotropy parameters have to be replaced by two corresponding *effective* parameters: $\mathcal{A}_2 \rightarrow \mathcal{A}_2^{(\text{eff})}$ and $\beta_2 \rightarrow \beta_2^{(\text{eff})}$. Note, the overall shape (2) of the angular distribution is preserved since it depends only on the quantum numbers of the initial and the final ionic states, respectively. The two effective parameters $\mathcal{A}_2^{(\text{eff})}$ and $\beta_2^{(\text{eff})}$ can be expressed as products of the original parameters with a *structure* function

$$\mathcal{A}_2^{(\text{eff})} = \mathcal{A}_2 \cdot f(E1, M2);$$
$$\beta_{20}^{(\text{eff})} = \beta_{20} \cdot f(E1, M2). \qquad (3)$$

The alignment parameter (1) depends only on the population mechanism of the excited level, i.e., on collisional parameters such as the projectile velocity or the charge of the target. In contrast, the *structure* function $f(E1, M2)$ is independent of the creation process and merely reflects the electronic structure of the ion. By applying the density matrix theory, this function $f(E1, M2)$ can be expressed for the $2p_{3/2} \rightarrow 1s_{1/2}$ transition as

$$f(E1, M2) = \left[\frac{\langle\|E1\|\rangle^2 - \langle\|M2\|\rangle^2 + 2\sqrt{3}\langle\|E1\|\rangle\langle\|M2\|\rangle^*}{\langle\|E1\|\rangle^2 + \langle\|M2\|\rangle^2}\right] \propto \left[1 + 2\sqrt{3}\frac{\langle\|M2\|\rangle}{\langle\|E1\|\rangle}\right], \qquad (4)$$

where $\langle\|E1\|\rangle = \langle 2p_{3/2}\|\alpha\mathbf{A}^{(\mathbf{e})}(L=1)\|1s_{1/2}\rangle$ and $\langle\|M2\|\rangle = \langle 2p_{3/2}\|\alpha\mathbf{A}^{(\mathbf{m})}(L=2)\|1s_{1/2}\rangle$ are the reduced matrix elements for the electric (magnetic) bound-bound multipole transitions of rank L [15,20].

In the dipole approximation, $\langle\|M2\|\rangle \approx 0$ is taken to be negligible and, thus, $f(E1, M2) \equiv 1$. As seen from Eq. (4), the main correction to this approximation arises from the term which is proportional to the ratio of the transition amplitudes $\langle\|M2\|\rangle/\langle\|E1\|\rangle$. For high-$Z$ ions this ratio is of the order ~ 0.1, leading to a 1% contribution of the $M2$ component to the total decay rate. Note that the $E1$-$M2$ interference term does not contribute to the transition probabilities (and, hence, the lifetimes) be-

cause the angular distribution [Eq. (2)] has to be integrated over all photon directions. From the properties of the Legendre polynomials, $\int P_2(\cos\theta)\,d\Omega = 0$, it is seen that the integral of the second term in Eq. (2), which contains the $E1$-$M2$ contribution, vanishes. For H-like uranium, this dimensionless function is as large as 1.28 due to the $E1$-$M2$ interference. Since this function basically depends on the ratio $\langle\|M2\|\rangle/\langle\|E1\|\rangle$ of the reduced matrix elements, a non-negligible effect of a few percent remains even for medium-Z ions. We finally note that this structure function scales approximately as $f(E1, M2) \propto Z^{2.24}$ for high-Z ions, while it is $f(E1, M2) \propto Z^{2.03}$ at lower

values of Z. Obviously, this is different from a Z^4 scaling as one might expect at a first glance from the corresponding decay rates.

In the following, we focus on REC in relativistic collisions of bare high-Z ions (e.g., U^{92+}) with low-Z target atoms [8,14,15]. In this process, the REC photon must carry away the excess energy and momentum when the electron is captured in any of the ionic bound states. Several theoretical [14,15] and experimental [8] studies were performed in the past to explore the capture into the ground and into the excited states. From a measurement of the anisotropic emission of the subsequent Lyman-α_1 photons, a rather significant alignment was deduced as confirmed by relativistic theory. However, when the theoretical and the observed angular distributions were compared in detail, a remarkable variance was found which could be attributed neither to additional cascade feeding processes (for the excited $2p_{3/2}$ level) nor to further corrections to the electron capture process. This deviation was surprising also in the sense that REC is otherwise one of the best studied processes for bare and few-electron high-Z ions in relativistic collisions for which an excellent agreement between theory and experiment is typically found [4].

As an example, the observed Ly-α_1 angular distribution (full squares) measured for 309 MeV/u $U^{92+} \rightarrow N_2$ collisions is given in Fig. 1 as a function of the laboratory observation angle θ_{lab}. The experimental anisotropy
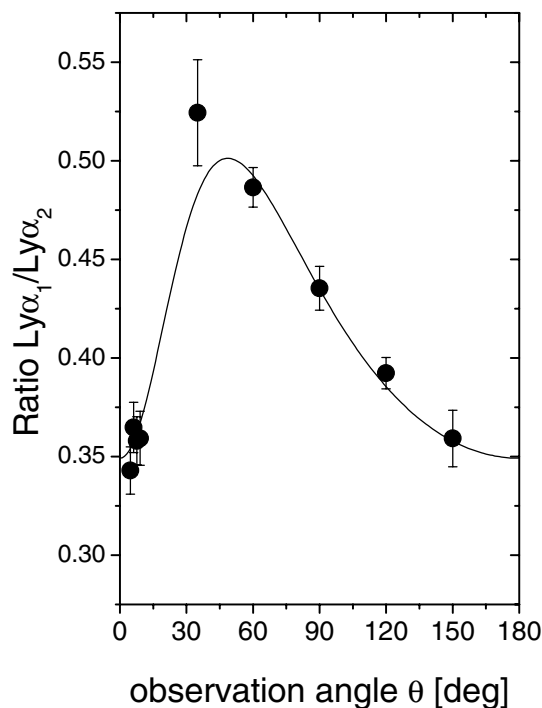
coefficient was determined by normalizing the intensity of the investigated Ly-α_1 transition to that of the Ly-α_2 ($+\mathbf{M1}$) radiation. Since the latter is isotropic in the projectile frame and energetically close to the Ly-α_1 line, this method allows us to strongly reduce the influence of possible systematic uncertainties. For the particular case displayed in Fig. 1, an effective anisotropy parameter β_{20}^{eff} of -0.23 ± 0.02 was deduced from a least-squares adjustment of Eq. (2) to the experimental Ly-α_1/Ly-α_2 intensity ratios by considering the correct relativistic angle and solid angle transformation (see, e.g., [8]). Following Eqs. (1) and (2), this means that REC favors the population of the magnetic substates $\mu_n = \pm 1/2$ [8].

For our present study we also evaluated the theoretical alignment parameters for the process of REC occurring in collisions of bare uranium with light gaseous targets. The actual computations were all carried out in the framework of Dirac's theory. The calculation of the alignment parameter $\mathcal{A}_2$ in Eq. (1) requires the evaluation of bound-free matrix elements for Dirac 4-spinors and was carried out already before [4,15]. Apart from the *impulse approximation* (see, e.g., [4]), no further approximation was made for the first step of the electron capture. As a result, the theoretical alignment parameters are the same as reported previously [15]. However, in order to compare with the experiments they need to be multiplied with the structure function $f(E1, M2)$.

In Fig. 2, we compare the experimental results (solid points) ([8]) for the effective anisotropy parameters β_{20}^{eff} with the corresponding theoretical findings (full line) as obtained from Eqs. (3) and (4). The dashed line, obtained assuming $f(E1, M2) \equiv 1$, i.e., neglecting the $E1$-$M2$ interference term, represents the theoretical treatment of the anisotropy parameter β_{20} as calculated by Eichler
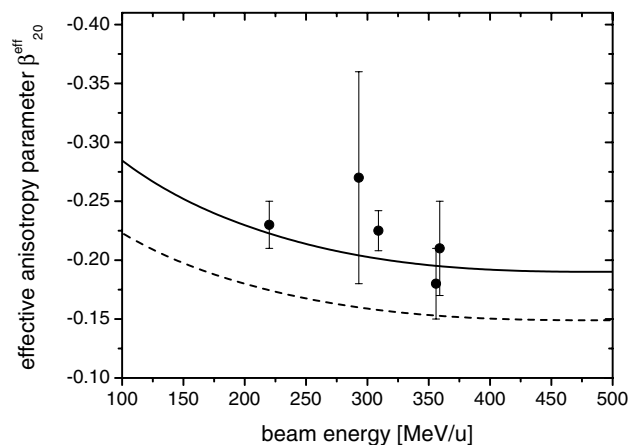

FIG. 1. Experimental Ly-α_1/Ly-α_2 intensity ratio (solid circles) measured for 309 MeV/u $U^{92+} \rightarrow N_2$ collisions (laboratory frame) [5]. The solid line depicts the result of the least-squares adjustment of Eq. (2) to the experimental data, considering the correct relativistic angle and solid angle transformation.

FIG. 2. The experimentally determined effective anisotropy parameters β_{20}^{eff} (solid points) for the Lyman-α_1 radiation of U^{91+} produced in $U^{92+} \rightarrow N_2$ collisions as a function of collision energy. The dashed line represents the theoretical predictions for $f(E1, M2) \equiv 1$, i.e., when the interference term is neglected. The solid line shows the theoretical β_{20}^{eff} parameter as defined by Eqs. (3) and (4).

et al. [15]. As seen from the figure, the former disagreement of the theoretical results from the experimental values [8] is removed when the interference term is taken into account.

In conclusion, an interference between the leading $E1$ decay channel and the—weak—$M2$ branch was studied for the case of the Lyman-α_1 transition in aligned hydrogenlike ions. This interference is found to affect considerably the angular distribution of the emitted photons. Similarly, it also affects the linear polarization of the Lyman-α_1 radiation, a topic which will be discussed in a forthcoming publication [21]. For the particular case of the Lyman-α_1 transition in the hydrogenlike uranium following electron capture, the former deviation between the experimental and theoretical findings for the alignment of the excited ion state [8] is removed when the interference correction is taken into account. Also, we have to add that one may expect similar sizable corrections for any other atomic transitions in the high-Z regime where beside the leading **E1** term, higher multipole contributions are small but allowed. Here, e.g., doubly excited states in He-like ions such as produced by dielectronic recombination must be mentioned [9,10]. More general, the study of decay rates and transition matrix elements of atomic transitions are of great importance to test and advance our basic knowledge about the physics of strong Coulomb fields as they are present at high-Z. However, at high-Z, most of these transitions exhibit such fast decay rates that lifetime measurements are excluded. Because of the sensitivity of the effective alignment parameter on the reduced matrix elements of the multipole transitions involved, the latter can be addressed by measuring precisely the associated photon angular distributions. It represents therefore an experimental tool to study the decay properties of atomic states in the realm of high-Z ions.

Helpful discussions and the long-standing close collaboration with Jörg Eichler are gratefully acknowledged. We also thank R. W. Dunford and N. M. Kabachnik for helpful comments on the manuscript.

[1] V. B. Berestetskii, E. M. Lifshitz, and L. P. Pitaevskii, *Relativistic Quantum Theory* (Pergamon, Oxford, 1971).

[2] P. H. Mokler and Th. Stöhlker, Adv. At. Mol. Opt. Phys. **37**, 297 (1996).

[3] Th. Stöhlker, P. H. Mokler, F. Bosch, R. W. Dunford, O. Klepper, C. Kozhuharov, T. Ludziejewski, B. Franzke, F. Nolden, H. Reich, P. Rymuza, Z. Stachura, M. Steck, P. Swiat, and A. Warczak, Phys. Rev. Lett. **85**, 3109 (2000).

[4] For a review of relativistic ion-atom collisions see, e.g., J. Eichler and W. E. Meyerhof, *Relativistic Atomic Collisions* (Academic Press, San Diego, 1995).

[5] Th. Stöhlker, X. Ma, T. Ludziejewski, H. F. Beyer, F. Bosch, O. Brinzanescu, R. W. Dunford, J. Eichler, S. Hagmann, A. Ichihara, C. Kozhuharov, A. Krämer, D. Liesen, P. H. Mokler, Z. Stachura, P. Swiat, and A. Warczak, Phys. Rev. Lett. **86**, 983 (2001).

[6] M. K. Kabadiyski, K. P. Lieb, and D. Rudolph, Nucl. Phys. **A563**, 301 (1993).

[7] T. Papp, Y. Awaya, H. Hitachi, T. Kambara, Y. Kanai, T. Mizogawa, and I. Török, J. Phys. B **24**, 3797 (1991).

[8] Th. Stöhlker, F. Bosch, A. Gallus, C. Kozhuharov, G. Menzel, P. H. Mokler, H. T. Prinz, J. Eichler, A. Ichihara, T. Shirai, R. W. Dunford, T. Ludziejewski, P. Rymuza, Z. Stachura, P. Swiat, and A. Warczak, Phys. Rev. Lett. **79**, 3270 (1997).

[9] M. H. Chen and J. H. Scofield, Phys. Rev. A **52**, 2057 (1995).

[10] M. Gail, N. Grün, and W. Scheid, J. Phys. B **31**, 4645 (1998).

[11] E. G. Berezhko and N. M. Kabachnik, J. Phys. B **10**, 2467 (1977).

[12] K. J. Reed and M. H. Chen, Phys. Rev. A **48**, 3644 (1993).

[13] G. K. James, J. A. Slevin, D. Dziczek, J. W. McConkey, and I. Bray, Phys. Rev. A **57**, 1787 (1998).

[14] J. Eichler, Nucl. Phys. **A572**, 147 (1994).

[15] J. Eichler, A. Ichihara, and T. Shirai, Phys. Rev. A **58**, 2128 (1998).

[16] V. V. Balashov, A. N. Grum-Grzhimailo, and N. M. Kabachnik, *Polarization and Correlation Phenomena in Atomic Collisions* (Kluwer Academic, Plenum Publishers, New York, 2000).

[17] K. Blum, *Density Matrix Theory and Applications* (Plenum, New York, 1981).

[18] K. Siegbahn, *Alpha-, Beta-, and Gamma-Ray Spectroscopy* (North-Holland Publishing Company, New York, 1965).

[19] U. Fano and G. Racah, *Irreducible Tensorial Sets* (Academic Press, New York, 1959).

[20] G. Drake, in *The Spectrum of Atomic Hydrogen: Advances,* edited by G. W. Series (World Scientific, Singapore, 1988).

[21] A. Surzhykov *et al.* (to be published).

8.3 Photon–photon angular correlations in the radiative recombination of bare high–Z ions

Photon–photon angular correlations in the radiative recombination of bare high-Z ions

Andrey Surzhykov[1,3]**, Stephan Fritzsche**[1] **and Thomas Stöhlker**[2]

[1] Fachbereich Physik, Universität Kassel, D-34132 Kassel, Germany
[2] Gesellschaft für Schwerionenforschung, D-62491 Darmstadt, Germany

E-mail: surz@physik.uni-kassel.de

Abstract

The radiative recombination of a free electron into excited states of bare, high-Z ions and the subsequent photon decay are studied in the framework of the density matrix theory. Emphasis is placed, in particular, on the angular correlation between the recombination and the decay photons. The general expression for the photon–photon angular correlation function is derived, based on Dirac's equation as appropriate for high-Z ions. Computations for the dependence of the photon–photon correlation function on the nuclear charge and the projectile energies are carried out for the capture into the $2p_{3/2}$ level and the subsequent *Lyman*-α_1 ($2p_{3/2} \to 1s_{1/2}$) radiation.

1. Introduction

In the radiative recombination of ions, a free (or quasi-free) electron is captured into a bound state under the simultaneous emission of a photon, which carries away the excess energy and momentum. This process occurs frequently not only in many stellar and laboratory plasmas, but also in the collision of heavy ions with target electrons at ion storage rings. For fast ions, for example, the radiative recombination is the dominant (loss) process for the ions in the ring. In the past, therefore, many experiments have been carried out on the radiative recombination which first focused on the capture into the $1s_{1/2}$ (hydrogen-like) ground state. For this capture, total and angle-differential cross sections have been measured by Stöhlker *et al* (1995) in a series of experiments and were found in good agreement with computations which are based on Dirac's equation. If, instead of the ground state, the electron is however captured into any of the excited states of the ion, the subsequent radiative decay of the excited ions leads to the emission of one or several *characteristic* photons until the ground state is reached. During the last few years, a number of experiments have been performed also for such *decay cascades* (Stöhlker 1999) since the angular distribution of the characteristic radiation may provide information

---

[3] Author to whom any correspondence should be addressed.

about the population dynamics in the radiative capture. For the capture of an electron into the
L shell of a bare uranium ion, for instance, a strong alignment was found for the residual ions,
both by experiment (Stöhlker *et al* 1997) and in computations (Eichler *et al* 1998).

So far, however, the angular distributions of the photons have been measured *separately*
in all experiments, either for the *recombination* or for the subsequent *decay* photons. More
information about the incident particles and the capture process can be obtained, if both photons
are measured in an (e, 2γ) coincidence experiment. Apart from studying the dynamics, photon–
photon coincidences may provide information about the polarization of the incident particles
as the *axial symmetry* of the collision process is broken. Moreover, coincidence measurements
help distinguish between different population mechanisms of the excited states, following
either the (direct) capture of the electron in this level or a cascade feeding from the upper
levels. Owing to recent improvements in the available x-ray detectors, such coincidence
experiments are likely to be carried out at the GSI storage ring in Darmstadt within the next
few years.

In this contribution, we study the angular correlation between the *recombination* and *decay*
photons in the (e, 2γ) capture of an electron into bare, high-Z ions. Such *particle–particle*
correlation phenomena can be described most easily in the framework of the density matrix
theory. However, before we present details from this theory, we first summarize the *geometry*
under which the photon–photon correlations are to be considered. In section 3, then, the general
expressions for the statistical tensors of the ion following electron capture and the two-photon
angular correlation function $W(n, n_{RR})$ are derived. While, of course, these expressions can
be applied to all hydrogen-like ions, detailed computations on the basis of the Dirac equation
have been carried out for the electron capture into the bare uranium ion U^{92+}. Special attention
was paid to the radiative recombination of a free electron into the $2p_{3/2}$ state of such an ion. In
section 4 we discuss how the population of the $2p_{3/2}$ state and, then, the angular distribution of
subsequent *Lyman-α_1* photons depend on the projectile ion energy as well as on the emission
angle of the *recombination* photon.

2. Geometry of two-photon coincidence experiments

In order to describe (e, 2γ) coincidence experiments, we shall first agree about the *geometry
and coordinates* under which the electron–ion collision and the emission of the two photons
are considered. Apart from the direction of the incident beam which, usually, is taken parallel
to the z-axis, we may define the (polar) angles of the recombination and decay photons with
respect to the beam as shown in figure 1. Since, moreover, all results will be presented
within the *projectile* frame in this paper, i.e. the rest frame of the projectile ion, we adopt the
incident electron momentum $p \parallel e_z$ as the quantization axis. Together with the direction of
the recombination photon k_{RR}, this axis defines the *reaction* plane (x–z plane) so that only one
(polar) angle θ_{RR} is needed to characterize the recombination photon, while the two angles
$\hat{n} = (\theta, \phi)$ are used to describe the subsequent emission of the decay photon (cf figure 1).

Obviously, the 'electron + ion' collision system obeys an axial symmetry which leads
to the angular distribution of the *recombination* photon, independent of the axial angle ϕ_{RR}.
Hence, if only the *recombination* photon is detected explicitly, this symmetry is broken for the
subsequent emission of the characteristic decay photon and may result in an angular distribution
which depends on both the directions of the photons relative to each other and with regard
to the quantization axis. This dependence is eventually described by the two-photon angular
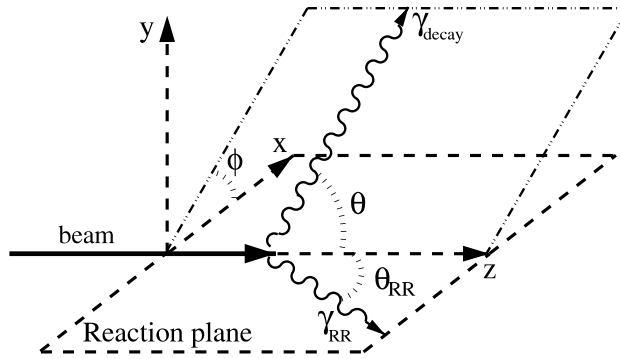correlation function.

Figure 1. Geometry for the radiative recombination of a free electron into an excited state of a projectile ion followed by the subsequent photon decay.

3. Density matrix approach to the two-step electron capture

In density matrix theory, the state of a physical system is usually described in terms of the *so-called* statistical operators (Blum 1981). These operators can be considered to represent, for instance, an ensemble of (equally prepared) systems which are—altogether—in either a *pure* quantum state or in a *mixture* of different states with any degree of coherence. The basic idea of the density matrix formalism is to *accompany* such an ensemble through the collision process, starting from a well defined 'initial' state and by passing through one or, possibly, several intermediate states until the final state of the collision and/or decay process is attained. Hereby, a physical characterization of the process is achieved simply by making use of a proper set of detectors which 'measure' (some or all of) the properties of the involved particles.

In the following, we apply this general concept to the description of a *two-step radiative recombination process*. To this end, let us first consider the capture of an electron into an intermediate ionic state, accompanied by the emission of the *recombination* photon. For this capture process, we can derive the density matrix of the intermediate state as well as the angular distribution of the *recombination* photons. The relation between the density matrix (and, then, statistical tensors) of the residual ion and 'experimental' set-up is discussed in sections 3.1 and 3.2. It is shown, for instance, that the statistical tensors of the intermediate ion state, as they arise from the electron capture, are directly related to the *recombination* photon emission angle $\hat{n}_{RR} = (\theta_{RR}, \phi_{RR})$. From the intermediate state density matrix, we may continue to derive the final-state tensors, following the decay of the excited state, and again the angular distribution of the *decay* photons as well as the photon–photon correlation function in section 3.3. Finally, to provide an example of this theory, we consider the *Lyman*-α_1 decay following the capture of an electron into the $2p_{3/2}$ substates of the ions.

3.1. Radiative recombination

In the first step of a radiative recombination process, the 'initial' state of the (combined) system is given by the ion *plus* a free electron. For the sake of simplicity, here we consider an electron with well defined asymptotic momentum p and projection m_s as well as a (bare) ion which is just specified by its nuclear charge Z. That is, in all formulae and discussions below we consider a *zero nuclear spin*. In this case, the initial spin state $\hat{\rho}_i$ of the combined 'electron + ion' system is just equivalent to the statistical operators of a free electron $\hat{\rho}_i \equiv \hat{\rho}_e$.

In the 'intermediate' state, following the capture of the electron, the statistical operators must describe both the recombined excited ion in some bound substate $|j_b\mu_b\rangle$ as well as

the recombination photon with wavevector $\boldsymbol{k}_{RR}$ and helicity $\lambda = \pm 1$ (i.e. with definite spin projection of the photon along the direction of $\boldsymbol{k}_{RR}$). As known from density matrix theory, the statistical operators of the initial and the (subsequent) intermediate states of the system are simply connected by Blum (1981)

$$\hat{\rho}_b = \hat{R}\hat{\rho}_e\hat{R}^+, \tag{1}$$

where $\hat{R}$ represents the *transition operator* which describes the photon–ion interaction in the case of the radiative recombination. The particular form of this interaction operator $\hat{R}$, of course, depends on the framework in which the coupling of the radiation field with the electronic motion is described. As appropriate for high-Z ions, below we always refer to a relativistic description of the electron–photon interaction, based on Dirac's equation and the *minimal* coupling of the radiation field (Eichler and Meyerhof 1995).

By means of the free-electron operator $\hat{\rho}_e$ and relation (1), we may obtain the intermediate-state density matrix in the representation of the angular momenta

$$\langle j_b\mu_b, \boldsymbol{k}_{RR}\lambda|\hat{\rho}_b|j_b'\mu_b', \boldsymbol{k}_{RR}\lambda'\rangle = \sum_{m_s m_s'} \langle j_b\mu_b, \boldsymbol{k}_{RR}\lambda|\hat{R}|\boldsymbol{p}m_s\rangle$$

$$\times \langle \boldsymbol{p}m_s|\hat{\rho}_e|\boldsymbol{p}m_s'\rangle\langle\boldsymbol{p}m_s'|\hat{R}^+|j_b\mu_b', \boldsymbol{k}_{RR}\lambda'\rangle \tag{2}$$

where $\langle j_b\mu_b, \boldsymbol{k}_{RR}\lambda|\hat{R}|\boldsymbol{p}m_s\rangle$ is the transition matrix element for the capture of a free electron into a bound state under the emission of a photon. This intermediate-state density matrix (2) still contains the *complete* information about the system (i.e. about the ion *plus* photon) and, hence, can be used to derive the properties of both the photons and the residual ions. Obviously, however, the outcome of a particular experiment will depend on the set-up and efficiency of the detectors which are used to *record* the properties of the particles. In density matrix theory, this experimental *set-up* is typically described in terms of a projection operator $\hat{P}$ which characterizes the whole *detector system*. Frankly speaking, this operator simply *projects out* all those quantum states of the overall system which lead to a 'click' at the detectors (or to a simultaneous event in the case of coincidence experiments). In the literature, the projection operator $\hat{P}$ is often called the *detector operator*; it helps determine the probability for a 'count' at the detectors simply by taking the trace of its product $W = \text{Tr}(\hat{P}\hat{\rho})$ with the density matrix.

To *measure*, for instance, the angular distribution of the emitted recombination photons, one often uses a photon detector in a given direction $\hat{n}_{RR} = (\theta_{RR}, \phi_{RR})$ relative to the electron (or beam) direction, which is sensitive neither to the polarization of the light nor to the spin state of the residual ion

$$\hat{P}_{\boldsymbol{k}_{RR}}^b = \sum_{\lambda\mu_b} |\boldsymbol{k}_{RR}\lambda\rangle|j_b\mu_b\rangle\langle j_b\mu_b|\langle\boldsymbol{k}_{RR}\lambda|, \tag{3}$$

that is, we need to sum over λ and the magnetic quantum numbers μ_b of the ions in order to define a proper projector (3). From this projector operator, taking the trace $\text{Tr}(\hat{P}_{\boldsymbol{k}_{RR}}^b\hat{\rho}_b)$ over its product with the density matrix (2), we immediately obtain the well known angular distribution of the recombination photons

$$\frac{\text{d}\sigma_{j_b}^{RR}}{\text{d}\Omega_{RR}}(\theta_{RR}, \phi_{RR}) = \sum_{\lambda m_s m_s'\mu_b} \langle j_b\mu_b, \boldsymbol{k}_{RR}\lambda|\hat{R}|\boldsymbol{p}m_s\rangle\langle\boldsymbol{p}m_s|\hat{\rho}_e|\boldsymbol{p}m_s'\rangle\langle\boldsymbol{p}m_s'|\hat{R}^+|j_b\mu_b, \boldsymbol{k}_{RR}\lambda\rangle \tag{4}$$

following an electron capture into a bound-state level with total angular momentum j_b.

However, apart from deriving the *observable* quantities of the emitted photons (such as their angular distribution or the total cross section), we can also use the intermediate-state density matrix (2) to *separate* the density matrices of the individual sub-systems from one another and to obtain two independent matrices for the recombination photons and the residual

ions, respectively. For example, the density matrix of only the excited ions just follows from taking the trace over all unobserved quantum numbers of the emitted photon in (2). If we suppose that the photon detectors are not sensitive to the polarization of the emitted light, the density matrix of the ion simply reads

$$\langle j_b\mu_b|\hat{\rho}_b(\theta_{RR}, \phi_{RR})|j_b\mu_b'\rangle = \sum_\lambda \sum_{m_s m_s'} \langle j_b\mu_b, \boldsymbol{k}_{RR}\lambda|\hat{R}|\boldsymbol{p}m_s\rangle\langle \boldsymbol{p}m_s|\hat{\rho}_e|\boldsymbol{p}m_s'\rangle$$

$$\times \langle \boldsymbol{p}m_s'|\hat{R}^+|j_b\mu_b', \boldsymbol{k}_{RR}\lambda\rangle. \tag{5}$$

Moreover, when we compare equations (4) and (5), we see that the density matrix of the intermediate ion state is normalized in such a way that its trace is equal to the angle-differential cross section for the emission of the recombination photons

$$\mathrm{Tr}\,\hat{\rho}_b(\theta_{RR}, \phi_{RR}) = \frac{\mathrm{d}\sigma_{j_b}^{RR}}{\mathrm{d}\Omega_{RR}}(\theta_{RR}, \phi_{RR}). \tag{6}$$

3.2. Statistical tensors of the excited ion states

The density matrix (5) describes the intermediate ion state following the radiative capture of an electron and the emission of the photon in direction $\hat{n}_{RR} = (\theta_{RR}, \phi_{RR})$, while the polarization of the photon remains unobserved. Instead of using this density matrix, however, it is often more convenient to represent the intermediate state of the ions in terms of the so-called *statistical tensors* $\hat{\rho}_{kq}^b(\theta_{RR}, \phi_{RR})$. Although, from a mathematical viewpoint, these statistical tensors are equivalent to the density matrix, they are constructed to represent the spherical tensors of rank k and component q. Hence, the statistical tensors can be expressed as a linear combination of the density matrix elements (Blum 1981)

$$\hat{\rho}_{kq}^b(\theta_{RR}, \phi_{RR}) = \sum_{\mu_b\mu_b'} (-1)^{j_b-\mu_b'}\langle j_b\mu_b j_b - \mu_b'|kq\rangle\langle j_b\mu_b|\hat{\rho}_b(\theta_{RR}, \phi_{RR})|j_b\mu_b'\rangle \tag{7}$$

following the standard procedure for the coupling of angular momenta. Owing to the properties of the Clebsch–Gordan coefficients, nonzero tensor components arise only for integer indices k, q with $0 \leqslant k \leqslant 2j_b$ and $q = -k, -k+1, \ldots, k$, respectively.

Of course, both the density matrix (5) and the statistical tensors (7) of the intermediate ion states depend on the electron–photon transition matrix. Within the framework of Dirac's theory, the elements of this transition matrix are given by

$$\langle j_b\mu_b, \boldsymbol{k}_{RR}\lambda|\hat{R}|\boldsymbol{p}m_s\rangle = C \int \mathrm{d}^3r\,\psi_{j_b\mu_b}^+(\boldsymbol{r})\alpha\hat{\boldsymbol{u}}_\lambda^* \mathrm{e}^{-\mathrm{i}\boldsymbol{k}_{RR}\boldsymbol{r}}\psi_{\boldsymbol{p},m_s}(\boldsymbol{r}) \tag{8}$$

where $\psi_{j_b\mu_b}(\boldsymbol{r})$ and $\psi_{\boldsymbol{p},m_s}(\boldsymbol{r})$ denote Dirac's wavefunctions for a bound and a free electron, respectively; moreover, the unit vector $\hat{\boldsymbol{u}}_\lambda$ is used to specify the polarization of the photons. Matrix elements of the type (8) were first implemented by Pratt *et al* (1973) in studying the atomic photoeffect for the relativistic energies.

To further simplify the electron–photon transition matrix (8) for practical computations, we may decompose both the photon as well as continuum wavefunctions into partial waves. As discussed previously (Surzhykov *et al* 2001), however, attention has to be paid in this case to the particular choice of the quantization axis, in dependence on the properties to be considered. For instance, in using the beam direction as the quantization axis, as outlined in section 2, we shall start from a rotation of the photon field which is—most conveniently—expressed in terms of its (electric and magnetic) multipole components

$$\mathcal{A}_{LM}^\lambda = \boldsymbol{A}_{LM}^{(m)} + \mathrm{i}\lambda\boldsymbol{A}_{LM}^{(e)}. \tag{9}$$

A rotation of the photon field is achieved by

$$\hat{u}_\lambda e^{ik r_{RR}} = \sqrt{2\pi} \sum_{L=1}^{\infty} \sum_{M=-L}^{M=+L} i^L \sqrt{2L+1} \mathcal{A}_{LM}^\lambda D_{M\lambda}^L (k_{RR} \rightarrow z), \tag{10}$$

where $D_{M\lambda}^L (k \rightarrow z)$ denotes the Wigner rotation matrix. Using the expansion (10) of the photon field in the matrix element (8), we can now represent the electron–photon transition matrix

$$\langle j_b \mu_b, k_{RR} \lambda | \hat{R} | p m_s \rangle = C \sum_{L=1}^{\infty} \sum_{M=-L}^{M=+L} i^{-L} \sqrt{2L+1} D_{M\lambda}^{L*} (k_{RR} \rightarrow z) \langle j_b \mu_b | \alpha \mathcal{A}_{LM}^{\lambda*} | p m_s \rangle \tag{11}$$

in terms of its multipole matrix elements which, however, still include a free-electron wave with definite momentum p and helicity m_s. In a second expansion, therefore, we also decompose these continuum wavefunctions into partial waves (Eichler and Meyerhof 1995)

$$|p m_s\rangle = \sum_{\kappa} i^l e^{-i\Delta_\kappa} \sqrt{4\pi (2l+1)} \langle l0 1/2 m_s | j m_s \rangle | E \kappa j \rangle \tag{12}$$

where the summation runs over Dirac's angular momentum quantum number

$$\kappa \equiv \kappa(j, l) = \pm(j + 1/2) \qquad \text{for } l = j \pm 1/2$$

with l representing the parity of the partial waves $|E\kappa j\rangle$. In expansion (12), moreover, Δ_κ is called the Coulomb phase shift which arises due to the $-Z/r$ nuclear potential of a pointlike charge. Of course, the partial waves

$$\langle r | E \kappa j \rangle = \frac{1}{r} \begin{pmatrix} P_{E\kappa}(r) \chi_\kappa^{m_s} \\ i Q_{E\kappa}(r) \chi_{-\kappa}^{m_s} \end{pmatrix} \tag{13}$$

separate into a radial and an angular part and, thus, help carry out the integration over all angles in the transition matrix elements (11) analytically. In (13), the two functions of the radial part, $P_{E\kappa}(r)$ and $Q_{E\kappa}(r)$, are often called the *large* and *small* components of the partial wave, while $\chi_\kappa^{m_s}$ denotes a standard Dirac spin-angular function.

Combining the two expansions (11) and (12) with the density matrix (5) and the definition of the statistical tensors (7), and by making use of the standard expansion for products of two Wigner rotation matrices, the statistical tensors of the ion in its intermediate state can be expressed as

$$\hat{\rho}_{kq}^b (\theta_{RR}, \phi_{RR}) = C \sum_\nu Y_{\nu-q}(\theta_{RR}, \phi_{RR}) B_\nu^{kq}(j_b, j_b) \tag{14}$$

with

$$\begin{aligned}
B_\nu^{kq}(j_b, j_b) = &\sum_{LL'} \sum_{\kappa\kappa'\lambda} i^{L'-L} i^{l-l'} (-1)^{-j'+L-\nu+1/2} e^{i(\Delta_{\kappa'}-\Delta_\kappa)} [L, L', j, j', l, l', k]^{1/2} \\
&\times \langle L - \lambda L' \lambda | \nu 0 \rangle \langle E\kappa j \| \alpha \mathcal{A}_L^\lambda \| n_b j_b \rangle^* \langle E\kappa' j' \| \alpha \mathcal{A}_{L'}^\lambda \| n_b j_b \rangle \\
&\times \sum_t \langle kq \nu - q | t0 \rangle \langle l'0 l0 | t0 \rangle \begin{Bmatrix} j & j' & t \\ l' & l & 1/2 \end{Bmatrix} \begin{Bmatrix} L' & j_b & j' \\ L & j_b & j \\ \nu & k & t \end{Bmatrix}.
\end{aligned} \tag{15}$$

The statistical tensor $\hat{\rho}_{00}(\theta_{RR}, \phi_{RR})$ has a particular meaning. If, namely, the density matrix is normalized due to relation (6), this *rank-zero* tensor, again, represents (up to the factor $1/\sqrt{2j_b+1}$) the differential cross section for the capture of an electron into the level $|n_b \kappa_b\rangle$

$$\hat{\rho}_{00}^b (\theta_{RR}, \phi_{RR}) = \frac{1}{\sqrt{2j_b+1}} \frac{d\sigma_{j_b}^{RR}}{d\Omega_{RR}} (\theta_{RR}, \phi_{RR}). \tag{16}$$

The tensors with *non-zero* ranks, in contrast, are related to the population of the individual substates of $|n_b\kappa_b\mu_b\rangle$, relative to each other. Instead of using the statistical tensors (14), however, it is often more convenient to describe this relative population in terms of the so-called *reduced statistical tensors* (Balashov *et al* 2000):

$$\mathcal{A}_{kq}(\theta_{RR}, \phi_{RR}) = \frac{\hat{\rho}^b_{kq}(\theta_{RR}, \phi_{RR})}{\hat{\rho}^b_{00}(\theta_{RR}, \phi_{RR})} \tag{17}$$

which are independent of the particular normalization of the density matrix.

3.3. Subsequent photon emission

The density matrix (5) and the statistical tensors (14) are two different but theoretically *equivalent* representations to describe the intermediate state $|j_b\mu_b\rangle$ of the ions following the capture of a free electron. To accommodate the system also *through* the subsequent characteristic photon emission, which results in the (final-ionic) state $|j_0\mu_0\rangle$, it is useful to return to the density matrix representation (5) and to utilize, once more, the relation $\hat{\rho}_0 = \hat{R}\hat{\rho}_b\hat{R}^+$ (cf equation (1)). Similarly to before, the statistical operator $\hat{\rho}_0$ describes both the ion in its final state $|j_0\mu_0\rangle$ as well as the characteristic (decay) photon with wavevector $\boldsymbol{k}$ and helicity λ; in the representation of the individual momenta this operator takes the form

$$\langle j_0\mu_0, \boldsymbol{k}\lambda|\hat{\rho}_0|j_0\mu_0', \boldsymbol{k}\lambda'\rangle = \sum_{\mu_b\mu_b'} \langle j_0\mu_0, \boldsymbol{k}\lambda|\hat{R}|j_b\mu_b\rangle\langle j_b\mu_b|\hat{\rho}_b(\theta_{RR}, \phi_{RR})|j_b\mu_b'\rangle$$

$$\times \langle j_b\mu_b'|\hat{R}^+|j_0\mu_0', \boldsymbol{k}\lambda'\rangle \tag{18}$$

where $\langle j_0\mu_0, \boldsymbol{k}\lambda|\hat{R}|j_b\mu_b\rangle$ represents the transition matrix for the *bound–bound* transition $|j_b\mu_b\rangle \longrightarrow |j_0\mu_0\rangle$. From expression (18) of the final-state density matrix, the angular distribution of the de-excitation photons is obtained by applying the projection operator $\hat{P}^0_{\boldsymbol{k}} = \sum_{\lambda\mu_0} |\boldsymbol{k}\lambda\rangle|j_0\mu_0\rangle\langle j_0\mu_0|\langle\boldsymbol{k}\lambda|$:

$$W_\gamma(\theta, \phi; \theta_{RR}, \phi_{RR}) = \mathrm{Tr}(\hat{P}^0_k\hat{\rho}_0) = \sum_{\lambda\mu_0} \langle j_0\mu_0, \boldsymbol{k}\lambda|\hat{\rho}_0|j_0\mu_0, \boldsymbol{k}\lambda\rangle$$

$$= \sum_{\mu_b\mu_b'kq} \sum_{\lambda\mu_0} (-1)^{j_b-\mu_b'} \langle j_b\mu_b j_b - \mu_b'|kq\rangle\langle j_0\mu_0, \boldsymbol{k}\lambda|\hat{R}|j_b\mu_b\rangle$$

$$\times \langle j_0\mu_0, \boldsymbol{k}\lambda|\hat{R}|j_b\mu_b'\rangle^* \hat{\rho}^b_{kq}(\theta_{RR}, \phi_{RR}), \tag{19}$$

analogous to equation (3) in the first step. In the second and third line of (19), we only replaced the intermediate-state density matrix by its statistical tensors (14).

The angular distribution (19) is often called the *photon–photon angular correlation function*. In this function, the dependence on the angles (θ_{RR}, ϕ_{RR}) of the *recombination* photon results from the intermediate-state statistical tensors (14), while the angular dependence (θ, ϕ) of the decay photon arises from the bound–bound transition matrix

$$\langle j_0\mu_0, \boldsymbol{k}\lambda|\hat{R}|j_b\mu_b\rangle = C \int \mathrm{d}^3r\, \psi^+_{j_0\mu_0}(\boldsymbol{r})\alpha\hat{\boldsymbol{u}}^*_\lambda \mathrm{e}^{-\mathrm{i}\boldsymbol{k}\boldsymbol{r}} \psi_{j_b\mu_b}(\boldsymbol{r}), \tag{20}$$

which is very similar to the bound–free transition matrix element (8). The only difference in (20) is that both (one-electron) wavefunctions represent bound states and, hence, only the photon field needs to be expanded into its multipole components (9). Inserting this expansion of the photon wave into the matrix element (20) and by making use of (10), we can re-write the photon–photon correlation function as

$$W_\gamma(\theta, \phi; \theta_{RR}, \phi_{RR}) = C \sum_{kq} \hat{\rho}^b_{kq}(\theta_{RR}, \phi_{RR}) Y_{kq}(\theta, \phi) \frac{1}{\sqrt{2k+1}} \sum_{LL'\lambda} \mathrm{i}^{L'-L}(-1)^{1+j_b+k+j_0}$$

$$\times (2j_b + 1)\sqrt{2L+1}\sqrt{2L'+1}\langle L'\lambda L - \lambda|k0\rangle \begin{Bmatrix} j_b & j_b & k \\ L & L' & j_0 \end{Bmatrix}$$

$$\times \langle n_b j_b||\alpha \mathcal{A}_L^\lambda||n_0 j_0\rangle^* \langle n_b j_b||\alpha \mathcal{A}_{L'}^\lambda||n_0 j_0\rangle. \tag{21}$$

Again, the term with $k = q = 0$ represents the total intensity and is often separated from the rest; with this separation, the *common form* of the angular correlation function finally reads (cf Balashov *et al* (2000))

$$W_\gamma(\theta, \phi; \theta_{RR}, \phi_{RR}) = \frac{W_\gamma^0}{4\pi}\left(1 + \frac{1}{2}\sum_{k=1}^{2j_b}\sum_{q=-k}^{k}\sqrt{\frac{4\pi}{2k+1}}Y_{kq}(\theta, \phi)\mathcal{A}_{kq}(\theta_{RR}, \phi_{RR})f_k^{(j_b, j_0)}\right) \tag{22}$$

where the $\mathcal{A}_{kq}(\theta_{RR}, \phi_{RR})$ are the reduced statistical tensors (17) and the *structure* function

$$f_k^{(j_b, j_0)} = (-1)^{j_0+j_b+k+1}2\sqrt{2j_b+1}\sum_{LL'\lambda}\sqrt{2L+1}\sqrt{2L'+1}\langle L'\lambda L - \lambda|k0\rangle$$

$$\times (-1)^{L'-L}\begin{Bmatrix} j_b & j_b & k \\ L & L' & j_0 \end{Bmatrix}\langle n_b j_b||\alpha \mathcal{A}_L^\lambda||n_0 j_0\rangle^* \langle n_b j_b||\alpha \mathcal{A}_{L'}^\lambda||n_0 j_0\rangle$$

$$\times \left(\sum_{L\lambda}|\langle n_b j_b||\alpha \mathcal{A}_L^\lambda||n_0 j_0\rangle|^2\right)^{-1} \tag{23}$$

arises entirely from the bound-state structure of the ion.

Equation (22), together with the expressions (14)–(15) and (23), represents the general form of the angular correlation function for a *two-step electron capture* into bare (high-Z) ions. In the following, we make use of these relations to analyse both the capture into the $2p_{3/2}$ level as well as the subsequent *Lyman-α_1* decay into the $1s_{1/2}$ ground state. As mentioned before, these *two steps* of such a cascade have been investigated at the GSI in Darmstadt: so far, however, always independently of each other. In coincidence measurements at the GSI storage ring, they are likely to be studied first in order to also explore the *correlated emission* of both photons.

4. Angular distribution of the Lyman-α_1 radiation

The structure function $f_k^{(j_b, j_0)}$ is non-zero only if k is *even* and $1 \leqslant k \leqslant 2j_b$. For a *Lyman-$\alpha_1$* ($2p_{3/2} \to 1s_{1/2}$) transition with $2j_b = 3$, therefore, the angular distribution of the emitted photons just contains the reduced tensors of rank $k = 2$,

$$W_\gamma(\theta, \phi; \theta_{RR}, \phi_{RR}) = \frac{W_\gamma^0}{4\pi}\left(1 + \sqrt{\frac{4\pi}{5}}\sum_{q=-2}^{2}Y_{2q}(\theta, \phi)\frac{\mathcal{A}_{2q}(\theta_{RR}, \phi_{RR})}{2}f_2^{(3/2, 1/2)}\right). \tag{24}$$

In this case, moreover, the structure function $f_2^{(3/2, 1/2)}$ can be easily expressed in terms of the reduced matrix elements for the electric and magnetic bound–bound multipole transitions (Surzhykov *et al* 2002)

$$f_2^{(3/2, 1/2)} = \left[\frac{|\langle ||E1||\rangle|^2 - |\langle ||M2||\rangle|^2 + 2\sqrt{3}\langle ||E1||\rangle\langle ||M2||\rangle^*}{|\langle ||E1||\rangle|^2 + |\langle ||M2||\rangle|^2}\right] \propto 1 + 2\sqrt{3}\frac{\langle ||M2||\rangle}{\langle ||E1||\rangle} \tag{25}$$

where we have introduced the two short-hand notations

$$\langle ||E1||\rangle = \langle 2p_{3/2}||\alpha A_{L=1}^{(e)}||1s_{1/2}\rangle \qquad \text{and} \qquad \langle ||M2||\rangle = \langle 2p_{3/2}||\alpha A_{L=2}^{(m)}||1s_{1/2}\rangle.$$

Obviously, the structure function becomes $f_2^{(3/2, 1/2)} = 1$ in the *electric dipole approximation*, i.e. if only the E1 term is considered to contribute the *Lyman-α_1* transition. The function (25) therefore describes the deviation from the dipole approximation for the subsequent photon

emission due to the *interference* between the leading E1 and the—much weaker—M2 components. For high-Z ions, the ratio $\langle||M2||\rangle/\langle||E1||\rangle$ of the two amplitudes is of the order of $\propto 0.1$, leading to 20–30% magnetic quadrupole correction over the dipole approximation. For hydrogen-like uranium U^{91+}, for instance, the structure function contributes as much as $f_2^{(3/2,1/2)} = 1.28$ to the angular distribution of the characteristic photon emission (Surzhykov *et al* 2002).

As seen from equation (24), there are five parameters in general which characterize the polarization state of the excited ion. These parameters are given in terms of the (five) tensor components $\mathcal{A}_{2q}(\theta_{RR}, \phi_{RR})$, $q = -2, \dots, 2$. For the case of *initially unpolarized electrons and projectile ions* all these components are real and only three of these parameters are independent due to the relations $\mathcal{A}_{22}(\theta_{RR}, \phi_{RR}) = \mathcal{A}_{2-2}(\theta_{RR}, \phi_{RR})$ and $\mathcal{A}_{21}(\theta_{RR}, \phi_{RR}) = -\mathcal{A}_{2-1}(\theta_{RR}, \phi_{RR})$. The component with zero projection $\mathcal{A}_{20}(\theta_{RR}, \phi_{RR})$ is called the *differential alignment parameter* and can be expressed in terms of the differential cross sections $\frac{d\sigma_{j_b\mu_b}^{RR}}{d\Omega}(\theta_{RR}, \phi_{RR})$ for the capture of the electron into the magnetic substates $|j_b\mu_b\rangle$

$$\mathcal{A}_{20}(\theta_{RR}, \phi_{RR}) = \frac{\frac{d\sigma_{j_b\mu_b=\pm3/2}^{RR}}{d\Omega}(\theta_{RR}, \phi_{RR}) - \frac{d\sigma_{j_b\mu_b=\pm1/2}^{RR}}{d\Omega}(\theta_{RR}, \phi_{RR})}{\frac{d\sigma_{j_b\mu_b=\pm3/2}^{RR}}{d\Omega}(\theta_{RR}, \phi_{RR}) + \frac{d\sigma_{j_b\mu_b=\pm1/2}^{RR}}{d\Omega}(\theta_{RR}, \phi_{RR})}, \tag{26}$$

i.e. the alignment of the residual ion state generally depends on the angle at which the recombination photon is observed. Only if this RR photon remains *unobserved*, the (averaged) alignment of the ions is described by a single parameter A_2 which, in terms of the *total* population cross sections, is given by Berezhko and Kabachnik (1977)

$$A_2 = \frac{\sigma_{j_b\mu_b=\pm3/2}^{RR} - \sigma_{j_b\mu_b=\pm1/2}^{RR}}{\sigma_{j_b\mu_b=\pm3/2}^{RR} + \sigma_{j_b\mu_b=\pm1/2}^{RR}}. \tag{27}$$

The angular distribution of the subsequent photon emission simplifies then to the well known formula

$$W_{Ly-\alpha_1}(\theta) = \frac{W_{Ly-\alpha_1}^0}{4\pi}(1 + \beta_2 P_2(\cos\theta) f_2^{(3/2,1/2)}), \tag{28}$$

where the parameter $\beta_2 = A_2/2$ is the so-called *anisotropy* coefficient.

5. Calculations

As seen from expressions (14)–(15) and (22)–(23), the analysis of both the statistical tensors of the intermediate ion state as well as the photon–photon angular correlation function $W_\gamma(\theta, \phi; \theta_{RR}, \phi_{RR})$ can be traced back to the evaluation of the reduced matrix elements $\langle E\kappa j||\alpha \mathcal{A}_L^\lambda||n_b j_b\rangle$ and $\langle n_b j_b||\alpha \mathcal{A}_L^\lambda||n_0 j_0\rangle$, respectively. These matrix elements describe the interaction of an electron with the radiation field for a *free–bound* and *bound–bound* electron transition. Since they arise from the same transition operator (9), all these reduced matrix elements can be evaluated in a similar way using the calculus of the irreducible tensor operators (cf Balashov *et al* (2000)). An explicit expression in terms of (geometrical) spin–angular coefficients and radial integrals are given in the appendix; for a pointlike nucleus and the use of exact Coulomb bound-state and continuum wavefunctions, all radial integrals can be expressed by means of the hypergeometric function $_2F_1(a, b; c; z)$ (Trautmann *et al* 1983). All computations of the reduced matrix elements and angular coefficients have been carried out by using the two computer-algebraic packages RACAH (Fritzsche 1997, Fritzsche *et al* 2001) and DIRAC, where the latter one, in particular, represents a toolbox of Maple procedures for studying the properties and the dynamical behaviour of hydrogen-like ions. The DIRAC
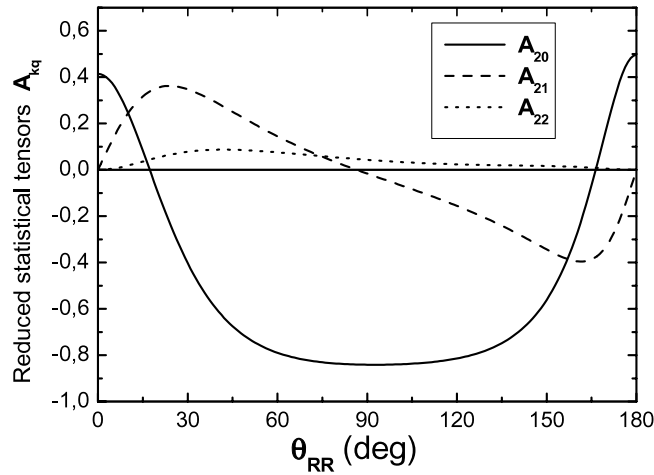
Figure 2. Components of the reduced statistical tensor $\mathcal{A}_{kq}(\theta_{RR}, \phi_{RR})$ as functions of the photon emission angle. The three tensor components $\mathcal{A}_{2q}, q = 0, 1$ and 2 are displayed for the capture of an electron into the $2p_{3/2}$ level in collisions of the bare uranium ion U^{92+} at an energy of $T_p = 1$ MeV u^{-1}, given in the projectile frame.

program has been developed in our group over the last few years and now supports both symbolic *and* numerical computations for quite a variety of different atomic properties.

To calculate the statistical tensors (14) and (15) of the ion following the capture of an electron with well defined momentum p, a sufficiently large number of the partial waves $|\kappa m_s\rangle$ needs to be taken into account in the expansion (12) of the free-electron wave. As discussed by Eichler and Meyerhof (1995), the required number of partial waves depends on the ion projectile energy. For the electron capture into a bound state of 220 MeV u^{-1} U^{92+} projectile ions, we included all partial waves with $|\kappa| \leqslant 15$.

6. Results and discussion

Several experiments have been carried out during recent years to explore the angular emission of the photons in the radiative recombination of free (or quasi-free) electrons into the $2p_{3/2}$ level of bare *uranium* ions and their subsequent decay. So far, however, these angular distributions were measured only *either* for the recombination *or* the decay photons (Stöhlker *et al* 1997) but not for both photons *in coincidence*. Coincidence measurements are planned to be carried out at the GSI storage ring in Darmstadt later this year.

In the following, we analyse the reduced statistical tensors (17) of the second rank and the photon–photon angular correlation function (22) for the recombination of an electron into the $2p_{3/2}$ level of high-Z ions. Detailed computations have been carried out, in particular, for the capture into bare uranium for several projectile energies in the range $1 \leqslant T_p \leqslant 220$ MeV u^{-1}. After the emission of the recombination photon, the residual ion is left in an aligned state which generally depends on the emission angles θ_{RR}. Figure 2 displays the three components of the reduced statistical tensor $\mathcal{A}_{2q}(\theta_{RR}, \phi_{RR})$ for the capture of an electron at a projectile energy of $T_p = 1$ MeV u^{-1}; for such energy, the *differential* alignment parameter $\mathcal{A}_{20}$ is *positive* in the forward and backward directions, referring to a preferred population of the two $\mu_n = \pm 3/2$ substates. In contrast, the emission of the recombination photon perpendicular to the beam mainly results—more than 80%—in the population of the $\mu_n = \pm 1/2$ substates.
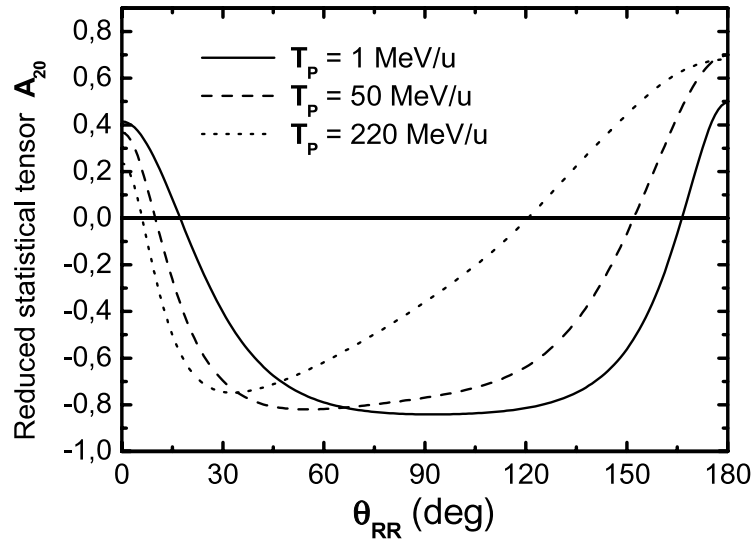
Figure 3. The reduced statistical tensor $\mathcal{A}_{20}(\theta_{RR}, \phi_{RR})$ of the $2p_{3/2}$ state following the radiative recombination of a free electron into bare uranium ions U^{92+} with energies $T_p = 1$, 50 and 220 MeV u^{-1}. All results are presented for the projectile frame.

If the *recombination* photon remains undetected, as is typical for present-day experiments, the alignment of the excited ion state is described only by the *integral* parameter A_2 from equation (27). This *integral* alignment parameter A_2 characterizes the average over all emission angles of the *recombination* photon and, hence, can only depend on the projectile energy. For the capture into bare uranium at a projectile energy of $T_p = 1$ MeV u^{-1}, for instance, the overall alignment of the residual ions is $A_2 = -0.768$. This alignment parameter decreases for higher projectile energies in the range of $T_p = 1$–300 MeV u^{-1} as first pointed out by Stöhlker *et al* (1997). This behaviour of the *integral* alignment can be easily seen also from the energy dependence of the *differential* alignment parameter $\mathcal{A}_{20}(\theta_{RR}, \phi_{RR})$ as displayed in figure 3. For higher projectile energies, the differential alignment increases in the backward direction, thus leading to a overall decrease in A_2.

Beside of the reduced statistical tensor $\mathcal{A}_{20}(\theta_{RR}, \phi_{RR})$, which refers to the *differential* alignment, the spin state of the excited ions in the $2p_{3/2}$ level is also described by the parameters $\mathcal{A}_{2\pm1}(\theta_{RR}, \phi_{RR})$ and $\mathcal{A}_{2\pm2}(\theta_{RR}, \phi_{RR})$, i.e. by the non-diagonal elements of the density matrix. These (additional) parameters also depend on the projectile energy as well as on the emission angle of the *recombination* photon, cf figure 2. They *must* be zero, however, for $\theta_{RR} = 0°$ and $\theta_{RR} = 180°$ since a photon emission either in *forward* or *backward* directions does not break the axial symmetry for the intermediate 'ion plus photon' system and, hence, cannot lead to a *non-diagonal* density matrix in this case. For the same arguments, moreover, the *integral* parameters $A_{2\pm1}$ and $A_{2\pm2}$ are always *zero* because the integration over the photon angles θ_{RR} also 'restores' the axial symmetry again.

As seen from equation (24), the angular distribution of the subsequent *Lyman-α_1* radiation is closely related to the reduced statistical tensors $\mathcal{A}_{2\pm q}(\theta_{RR}, \phi_{RR})$. In coincidence measurements, therefore, the distribution of these photons will depend on both the projectile energy as well as the angle under which the recombination photon is observed. In figure 4, we display this *Lyman-α_1* angular distribution for different angles $\theta_{RR} = 0°$, $15°$, $30°$ and $90°$ of the recombination photon with respect to the beam direction. Moreover, these angular
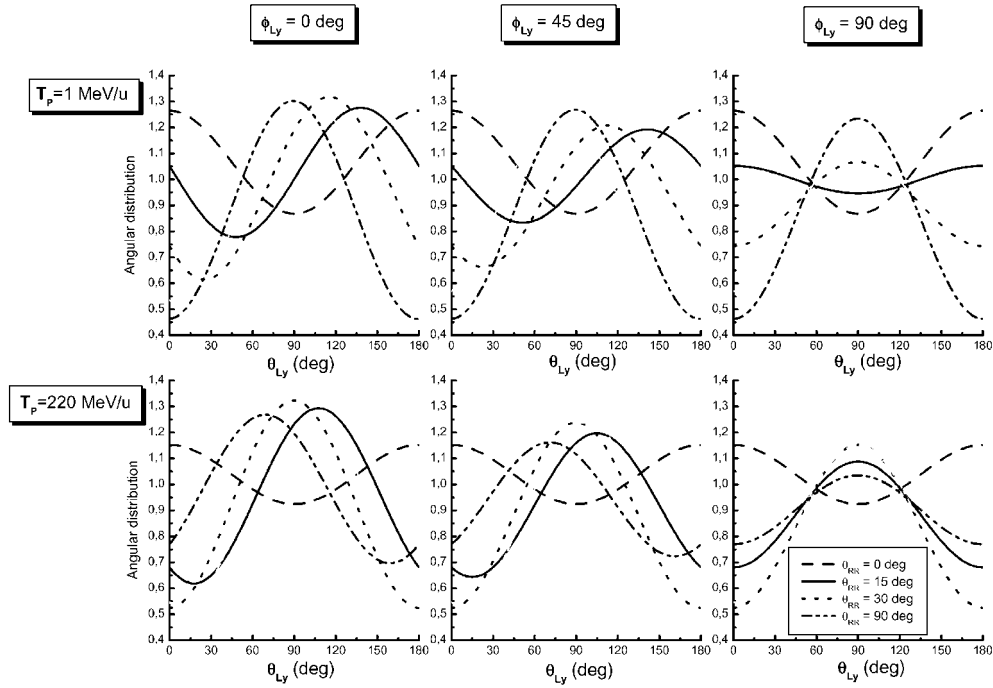
Figure 4. Angular distribution of the *Lyman-*α_1 radiation following the radiative recombination of a free electron into the $2p_{3/2}$ level of the bare uranium projectiles with energies $T_p = 1$ and 220 MeV u^{-1}. Distributions are shown for the angles $\phi_{Ly} = 0°$, $45°$ and $90°$ with respect to the reaction plane.

distributions are presented in the planes, tilted by the angles $\phi_{Ly} = 0°, 45°$ and $90°$ with respect to the reaction plane, and for the two projectile energies $T_p = 1$ (upper part) and 220 MeV u^{-1} (lower part). The angular distributions for both projectile energies are normalized in such a way that the normalization constant is $W^0_{Ly-\alpha_1} = 4\pi$. As expected for a *forward* emission of the recombination photon ($\theta_{RR} = 0$), the *Lyman-*α_1 distribution is symmetric around $\theta_{Ly} = 90°$ and also has its minimum at this value since, in this case, the differential alignment $\mathcal{A}_{20}(\theta_{RR}, \phi_{RR})$ is positive and the reduced tensor components $\mathcal{A}_{2\pm1}(\theta_{RR}, \phi_{RR})$ and $\mathcal{A}_{2\pm2}(\theta_{RR}, \phi_{RR})$ are all *zero*. For all other angles ($\theta_{RR} \neq 0°$ and $180°$), these statistical tensors are generally non-zero, giving rise to an asymmetric distribution of the *Lyman-*α_1 photons in coincidence measurements.

As the initial axial symmetry is broken for most coincidence experiments (apart from an observation of the recombination photon in forward or backward direction), the *Lyman-*α_1 angular distribution also depends on the axial angles ϕ_{Ly}. Only if these photons are measured perpendicular to the reaction plane ($\phi_{Ly} = 90°$), a symmetric distribution around $\theta_{Ly} = 90°$ is always obtained as also becomes clear from expression (24). Furthermore, the alignment effects from the intermediate-state ions can appear either pronounced or suppressed in dependence on the angles under which the coincidence experiments are carried out.

Until now, we have considered the photon–photon angular correlations for the capture of an electron into bare uranium ions U^{92+}. Apart from the projectile energies, of course, these angular correlations will also depend on the charge of the projectiles. Figure 5 shows the dependence of the *Lyman-*α_1 angular distribution on the nuclear charge of the (bare) ions,
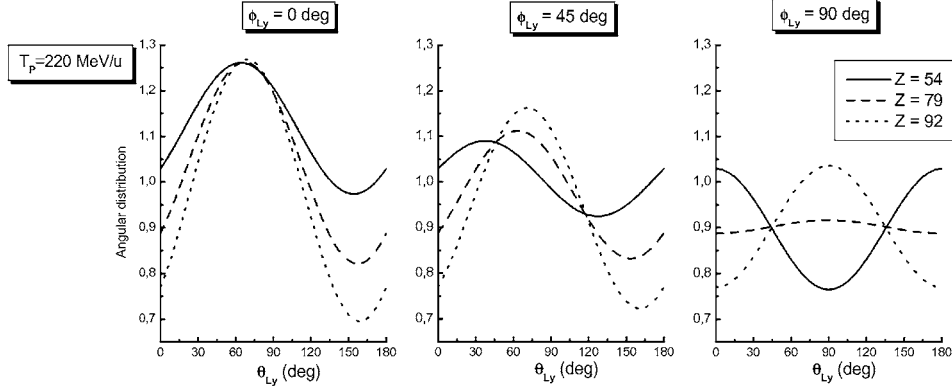
Figure 5. Charge dependence of the angular distribution of the *Lyman*-α_1 radiation following radiative recombination of a free electron into the $2p_{3/2}$ state of the bare uranium projectile with energy $T_p = 220$ MeV u^{-1}. Results are shown for the three nuclear charges $Z = 54, 79$ and 92.

taken for a emission of the recombination photon perpendicular to the beam ($\theta_{RR} = 90°$). Again, angular distributions are shown for different axial angles $\phi_{Ly} = 0°, 45°$ and $90°$ of the *Lyman*-α_1 emission. As seen from this figure, the strongest Z-dependence of the *Lyman*-α_1 distribution will arise for a measurement perpendicular to the reaction plane.

7. Summary

In this paper, we have considered the radiative capture of a free electron into an excited state of a bare, high-Z ion and its subsequent photon decay in the framework of the density matrix theory. This theory provides a consistent *ground* not only to investigate the total and angle-differential cross sections of the *recombination* and the *decay* photons separately but also for their 'angular correlation' in coincidence measurements. Here, we have applied this theory to the capture into the $2p_{3/2}$ level and the study of the subsequent *Lyman*-α_1 ($2p_{3/2} \rightarrow 1s_{1/2}$) angular distributions, where we have assumed that the *recombination* photon is to be detected in coincidence. As shown above, the emission pattern of the subsequent radiation usually depends strongly on the particular angle at which the recombination photon is observed. Apart from the coplanar geometry, which might first be utilized by experiment, detailed angular distributions are presented also for a *non-coplanar* set-up of the detectors.

In the future, photon–photon angular correlation measurements may serve as a tool for determining the polarization of either the electron target or the ion beam. Similarly, as in the present contribution, the density matrix theory may then help analyse different experimental *scenarios* and predict the effects of a polarization of the particles. A more detailed analysis of such *polarization effects* is currently underway.

Appendix. Evaluation of the transition matrix element

The reduced matrix element $\langle n_a \kappa_a || \alpha \mathcal{A}_L^\lambda || n_b \kappa_b \rangle$, which describes the radiative bound–bound as well as bound–free (in this case the $|n_a \kappa_a \rangle$ vector should be substituted by the partial wave $|E\kappa \rangle$) electron transitions, can be decomposed, according to equation (9):

$$\langle n_a \kappa_a || \alpha \mathcal{A}_L^\lambda || n_b \kappa_b \rangle = \langle n_a \kappa_a || A_L^{(m)} || n_b \kappa_b \rangle + i\lambda \langle n_a \kappa_a || A_L^{(e)} || n_b \kappa_b \rangle. \tag{A.1}$$

The magnetic and electric multipole fields can be expressed, respectively, as (Rose 1957)

$$A_{LM}^{(m)} = j_L(kr) T_{L,L}^M, \tag{A.2}$$

$$A_{LM}^{(e)} = j_{L-1}(kr)\sqrt{\frac{L+1}{2L+1}} T_{L,L-1}^M - j_{L+1}(kr)\sqrt{\frac{L}{2L+1}} T_{L,L+1}^M, \tag{A.3}$$

where $j_L(kr)$ is a spherical Bessel function and the vector spherical harmonics $T_{L,L}^M$ are the spherical tensors of rank L, resulting from the coupling of the spherical unit vector $\xi_m, m = 0, \pm 1$ with the spherical harmonics Y_{lm}:

$$T_{L,\Lambda}^M = \sum_m \langle \Lambda M - m 1 m | L M \rangle Y_{\Lambda M - m} \xi_m. \tag{A.4}$$

By making use of the equations (A.2) and (A.3) one can evaluate the reduced magnetic and electric multipole matrix elements as (Grant 1974)

$$\langle n_a \kappa_a || A_L^{(m)} || n_b \kappa_b \rangle = \frac{1 - (-1)^{l_a + l_b + L}}{2} \langle j_a || C^{(L)} || j_b \rangle \bar{M}_{ab}^{(m)}(L), \tag{A.5}$$

$$\langle n_a \kappa_a || A_L^{(e)} || n_b \kappa_b \rangle = \frac{1 + (-1)^{l_a + l_b + L}}{2} \langle j_a || C^{(L)} || j_b \rangle \bar{M}_{ab}^{(e)}(L), \tag{A.6}$$

where the irreducible tensors $C^{(L)}$ can be written in terms of spherical harmonics:

$$C^{(L)}(\theta, \phi) = \sqrt{\frac{4\pi}{2L+1}} Y_L(\theta, \phi). \tag{A.7}$$

One can evaluate the reduced matrix element of the irreducible tensor $C^{(L)}$ by using the irreducible operator technique as

$$\langle j_a || C^{(L)} || j_b \rangle = (-1)^{(L)} \sqrt{2 j_a + 1} \langle j_a 1/2\, L 0 | j_b 1/2 \rangle. \tag{A.8}$$

The $\bar{M}_{ab}^{(e,m)}(L)$ involve only the radial integrals: explicitly, for magnetic type multipoles,

$$\bar{M}_{ab}^{(m)}(L) = \frac{-\mathrm{i}}{\sqrt{4\pi}} \sqrt{\frac{2L+1}{L(L+1)}} (\kappa_a + \kappa_b) I_L^+(k; ab), \tag{A.9}$$

and for electric type multipoles, written in the velocity gauge (Grant 1974),

$$\bar{M}_{ab}^{(e)}(L) = \frac{\mathrm{i}}{\sqrt{4\pi}} \left(\sqrt{\frac{L}{(L+1)(2L+1)}} [(\kappa_a - \kappa_b) I_{L+1}^+(k; ab) + (L+1) I_{L+1}^-(k; ab)] \right.$$
$$\left. - \sqrt{\frac{L+1}{L(2L+1)}} [(\kappa_a - \kappa_b) I_{L-1}^+(k; ab) - L I_{L-1}^-(k; ab)] \right), \tag{A.10}$$

where the radial integrals are

$$I_\Lambda^\pm(k; ab) = \int_0^\infty (P_a(r) Q_b(r) \pm P_b(r) Q_a(r)) j_\Lambda(kr)\, \mathrm{d}r. \tag{A.11}$$

References

Balashov V V, Grum-Grzhimailo A N and Kabachnik N M 2000 *Polarization and Correlation Phenomena in Atomic Collisions* (New York: Kluwer Academic)
Berezhko E G and Kabachnik N M 1977 *J. Phys. B: At. Mol. Phys.* **10** 2467
Blum K 1981 *Density Matrix Theory and Applications* (New York: Plenum)
Eichler J, Ichihara A and Shirai T 1998 *Phys. Rev.* A **58** 2128
Eichler J and Meyerhof W 1995 *Relativistic Atomic Collisions* (San Diego, CA: Academic)
Fano U and Racah G 1959 *Irreducible Tensorial Sets* (New York: Academic)

Fritzsche S 1997 *Comput. Phys. Commun.* **103** 51
Fritzsche S, Inghoff T, Bastug T and Tomaselli M 2001 *Comput. Phys. Commun.* **139** 314
Grant I 1974 *J. Phys. B: At. Mol. Phys.* **7** 1458
Pratt R H, Akiva R and Tseng H K 1973 *Rev. Mod. Phys.* **45** 273
Rose M E 1957 *Elementary Theory of Angular Momentum* (New York: Wiley)
Stöhlker Th *et al* 1995 *Phys. Rev.* A **51** 2098
Stöhlker Th *et al* 1997 *Phys. Rev. Lett.* **79** 3270
Stöhlker Th 1999 *Phys. Scr.* T **80** 165
Surzhykov A, Fritzsche S and Stöhlker Th 2001 *Phys. Lett.* A **289** 213
Surzhykov A, Fritzsche S, Gumberidze A and Stöhlker Th 2002 *Phys. Rev. Lett.* **88** 153001
Trautmann D, Baur G and Rösel F 1983 *J. Phys. B: At. Mol. Phys.* **16** 3005

8.4 Two–step radiative recombination of polarized electrons into bare, high–Z ions

ELSEVIER

Two-step radiative recombination of polarized electrons into bare, high-Z ions

A. Surzhykov [a,*], S. Fritzsche [a], Th. Stöhlker [b]

[a] *Fachbereich Physik, Universität Kassel, Heinrich-Plett-Str. 40, D-34132 Kassel, Germany*
[b] *Gesellschaft für Schwerionenforschung, Planckstr. 1, 64291 Darmstadt, Germany*

Abstract

The radiative recombination of *polarized* electrons into the excited states of bare, high-Z ions and the subsequent photon decay are studied in the framework of the density matrix theory. The two-photon angular correlation function is analyzed for the electron capture into the $2p_{3/2}$ state of bare uranium projectile and following Lyman-α_1 ($2p_{3/2} \to 1s_{1/2}$) transition. It is shown that the two-photon angular correlation function is sensitive to the incident electron polarization and, therefore, can be used to determine either the polarization of the electron target and/or the projectile ions.
© 2003 Elsevier Science B.V. All rights reserved.

1. Introduction

During recent years, a large number of experiments have been carried out at the GSI storage ring in Darmstadt in order to explore the radiative recombination (RR) of free (or quasi-free) electrons into the bound states of highly charged ions. At the beginning, most of the measurements concerned the electron capture into the K-shell of *bare* projectile ions. For such capture process, the total and angle-differential cross sections of the recombination photons have been analyzed in detail by Stöhlker and co-workers [1] in the middle of

nineties. In later years, several experiments focused on the RR into the *excited* states of the projectile ions, including their subsequent photon decay, since the angular distribution of the characteristic photons may provide useful information about the population of the ionic sublevels following electron capture. From the measurement of the anisotropic emission of the Lyman-α_1 radiation, for instance, a significant alignment of the $2p_{3/2}$ state of hydrogen-like uranium was recently deduced [2].

So far, however, the angular distributions of the *recombination* and subsequent *decay* photons have always been measured *separately*. These – individual – angular distributions are, in fact, not much sensitive to the incident particle polarization. In most theoretical studies of the RR into high-Z ions [3,4], therefore, it is assumed that neither the

projectile ions nor the target electrons are polarized. This assumption, however, has to be examined if both, the recombination and decay photons are measured in *coincidence*. The simultaneous detection of both photons, namely, brakes the axial symmetry of any independent measurement (with respect to the beam direction) and, therefore, is expected to be sensitive to the incident particle polarization. Owing to the recent improvements in the X-ray detector technique, such (e, 2γ) coincidence measurements are likely to be carried out at the GSI storage ring within the next few years.

2. Theoretical description

In this contribution, we study the angular correlations between the recombination and decay photons in the capture of a (free) *polarized* electron $|\mathbf{p}m_s\rangle$ into the excited state $|n_b j_b\rangle$ of a bare projectile ion. The theoretical background of such two-photon coincidence studies has been developed recently by us in the framework of the density matrix theory [5], where we derived the two-photon angular correlation function both for an *unpolarized* projectile ion and target electron. Of course, this correlation function needs to be modified in order to describe the capture of an electron with a well-defined spin projection. For *relativistic* energies, the spin projection of the electron has a sharp value only along its direction of propagation $\mathbf{p}$ [3], which we will choose as the quantization axis (z-axis). For such choice of the quantization axis the spin density matrix of the electron is given by [6]:

$$\hat{\rho}_e = \tfrac{1}{2}(\hat{I} + P\hat{\sigma}_z), \tag{1}$$

where $\hat{I}$ is the 2×2 unit matrix and $\hat{\sigma}_z$ is the Pauli matrix. As seen from Eq. (1), the polarization of the electron can be described by the single real parameter P which is called the *degree of polarization* and which takes values in the range $-1 \leqslant P \leqslant +1$. Obviously, the degree of polarization $P = 0$ corresponds an unpolarized electron while, in the case of $P = \pm 1$, Eq. (1) describes a completely polarized electron with spin projections along the quantization axis of $m_s = \pm 1/2$.

The capture of an unpolarized electron ($P = 0$) into an ionic bound state leads to an equal population of all pairs of sublevels with the same modulus of the magnetic quantum numbers $|\mu_b|$. Moreover, an ion is said to be *aligned* if, for $j_b > 1/2$, different pairs of such magnetic substates are unequally populated. For a capture of polarized electron, in contrast, one may expect also a *polarization* of the residual ion, which means that the magnetic sublevels can be *all* populated unequally. In the framework of the density matrix theory the population of the ionic substates is described in terms of so-called *statistical tensors* $\hat{\rho}_{kq}(\theta_{RR}, \phi_{RR})$. In general, these tensors depend on the collisional parameters such as the projectile ion energy and the nuclear charge as well as on the angle $\hat{n}_{RR} = (\theta_{RR}, \phi_{RR})$ with respect to the ion beam, under which the recombination photon is detected. Moreover, these statistical tensors also reflect the polarization properties of the electron target. Following Eq. (1), the statistical tensors can generally be written as a sum of two parts, the unpolarized tensor as well as the polarized part which is weighted by the degree of polarization P:

$$\hat{\rho}_{kq}(\theta_{RR}, \phi_{RR}) = \hat{\rho}_{kq}^{unp}(\theta_{RR}, \phi_{RR}) + P \cdot \hat{\rho}_{kq}^{pol}(\theta_{RR}, \phi_{RR}). \tag{2}$$

In this decomposition, the unpolarized tensor $\hat{\rho}_{kq}^{unp}(\theta_{RR}, \phi_{RR})$ refers to the capture of an unpolarized electron ($P = 0$):

$$\hat{\rho}_{kq}^{unp}(\theta_{RR}, \phi_{RR}) = C \sum_{v} Y_{v-q}(\theta_{RR}, \phi_{RR}) B_v^{kq}(j_b, j_b) \tag{3}$$

and was derived earlier in [5], cf. Eqs. (14) and (15). A similar expansion also applies for the polarized part $\hat{\rho}_{kq}^{pol}(\theta_{RR}, \phi_{RR})$ of the statistical tensor in Eq. (2) which arises due to a capture of a polarized electron:

$$\hat{\rho}_{kq}^{pol}(\theta_{RR}, \phi_{RR}) = i \cdot C \sum_{v} Y_{v-q}(\theta_{RR}, \phi_{RR}) \tilde{B}_v^{kq}(j_b, j_b) \tag{4}$$

and where the expansion coefficients take the form:

$$\tilde{B}_\nu^{kq}(j_b, j_b) = -2 \sum_{\lambda t m_s} \sum_{LL'} (-1)^{L-\nu-j'} i^{L'-L+l-l'} e^{i(\Delta_\kappa - \Delta_{\kappa'})}$$

$$\times [L, L', l, l', k]^{1/2}$$

$$\times \langle kq\nu - q|t0\rangle \langle L - \lambda L'\lambda|\nu 0\rangle$$

$$\times \langle jm_s j' - m_s|t0\rangle \langle l01/2m_s|jm_s\rangle$$

$$\times \langle l'01/2m_s|j'm_s\rangle \langle \kappa j\|\alpha \mathscr{A}_L^\lambda\|n_b j_b\rangle^*$$

$$\times \langle \kappa' j'\|\alpha \mathscr{A}_{L'}^\lambda\|n_b j_b\rangle \begin{Bmatrix} L' & j_b & j' \\ L & j_b & j \\ \nu & k & t \end{Bmatrix}. \tag{5}$$

In these coefficients, moreover, Δ_κ is the Coulomb phase [3], $[L] = (2L+1)$ and the reduced matrix element $\langle \kappa j\|\alpha \mathscr{A}_L^\lambda\|n_b j_b\rangle$ describes the RR of a free electron into a bound state $|n_b j_b\rangle$ of the bare ion. A possible route to evaluate this reduced matrix element in the framework of Dirac's theory has been discussed previously [5].

Instead of using the statistical tensors (2), it is often more convenient to describe the relative population of the ion in terms of the (so-called) *reduced statistical tensors* [6] which are normalized by means of *zero*-rank tensor:

$$\mathscr{A}_{kq}(\theta_{RR}, \phi_{RR}) = \frac{\hat{\rho}_{kq}(\theta_{RR}, \phi_{RR})}{\hat{\rho}_{00}(\theta_{RR}, \phi_{RR})}. \tag{6}$$

In general, the (reduced) statistical tensors obey several properties. For instance, since for $k = q = 0$ the expansion coefficients (5) vanish for all ν, the zero-rank statistical tensor does not depend on the polarization of the incident electron, i.e. $\hat{\rho}_{00}(\theta_{RR}, \phi_{RR}) = \hat{\rho}_{kq}^{unp}(\theta_{RR}, \phi_{RR})$. For this reason, moreover, the reduced statistical tensors (6) can be also divided into an unpolarized and a polarized part, similar as in Eq. (2),

$$\mathscr{A}_{kq}(\theta_{RR}, \phi_{RR}) = \mathscr{A}_{kq}^{unp}(\theta_{RR}, \phi_{RR})$$
$$+ P \cdot \mathscr{A}_{kq}^{pol}(\theta_{RR}, \phi_{RR}) \tag{7}$$

and can be used directly in order to derive the angular distribution of the subsequent decay photons. For instance, if we consider the electron capture into the $2p_{3/2}$ state of bare ions, the angular distribution of the Lyman-α_1 ($2p_{3/2} \rightarrow 1s_{1/2}$) radiation is defined by the reduced statistical tensors of the second rank [5]:

$$W_\gamma(\theta, \phi; \theta_{RR}, \phi_{RR})$$
$$= \frac{W_\gamma^0}{4\pi} \left(1 + \sqrt{\frac{4\pi}{5}} \sum_{q=-2}^2 Y_{2q}(\theta, \phi) \frac{\mathscr{A}_{2q}(\theta_{RR}, \phi_{RR})}{2} f(E1, M2) \right), \tag{8}$$

where we referred to $f(E1, M2)$ as the *structure function* [7], which describes the interference between the leading electric dipole ($E1$) and – the much weaker – magnetic quadrupole ($M2$) transition amplitudes. For hydrogen-like uranium, for example, this (dimensionless) function takes the value of about 1.28.

3. Results and discussion

Eq. (8) displays the general *photon–photon angular correlation* between the recombination and the following decay photons and, together with Eq. (7), how this correlation depends on the polarization P of the incident electrons. For the capture into the $2p_{3/2}$ state, for instance, there are five imaginary components of the polarized tensor $\mathscr{A}_{2q}^{pol}(\theta_{RR}, \phi_{RR})$, $q = -2, \ldots, 2$ which are all weighted by the degree of polarization P. In practice, however, only two of these parameters are independent due to the relations: $\mathscr{A}_{21}^{pol} = \mathscr{A}_{2-1}^{pol}$, $\mathscr{A}_{22}^{pol} = -\mathscr{A}_{2-2}^{pol}$ and $\mathscr{A}_{20}^{pol} = 0$. The number of independent *polarization* parameters can be further reduced by making a proper choice of the geometry in the setup of a coincidence experiment. If, for instance, the Lyman-α_1 photons are observed perpendicular to the *reaction* plane (i.e. the plane which is formed by the directions of the beam and the recombination photon), the corresponding angular distribution simplifies to:

$$W_\gamma(\theta, \phi = \pi/2; \theta_{RR}, \phi_{RR})$$
$$= \frac{W_0}{4\pi} \left[1 + \frac{1}{2}\sqrt{\frac{3}{2}} \left(\frac{1}{\sqrt{6}}(3\cos^2\theta - 1) \right.\right.$$
$$\times \mathscr{A}_{20}^{unp}(\theta_{RR}, \phi_{RR}) - \sin^2\theta \mathscr{A}_{22}^{unp}(\theta_{RR}, \phi_{RR})$$
$$\left.\left. - iP \cdot \sin 2\theta \mathscr{A}_{21}^{pol}(\theta_{RR}, \phi_{RR}) \right) f(E1, M2) \right], \tag{9}$$
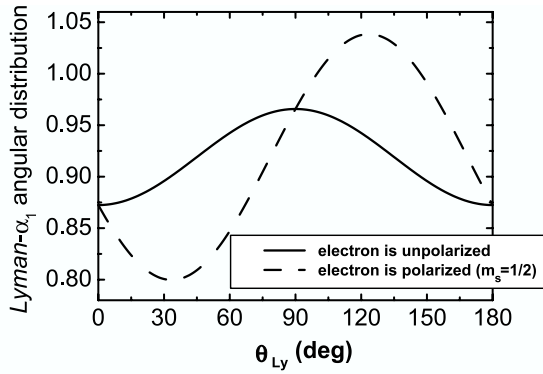
Fig. 1. Angular distributions of the Lyman-α_1 radiation following the radiative recombination of a free electron into the $2p_{3/2}$ state of bare uranium projectile with energy $T_p = 310$ MeV/u, taken for the emission of the *recombination* photon perpendicular to the electron beam ($\theta_{RR} = 90°$). Calculations have been carried out in the projectile frame for the emission of the Lyman-α_1 photons in the plane, perpendicular to the *reaction* one ($\phi = 90°$).

where only one term depends linearly on the degree of polarization P and component of the polarized tensor $\mathscr{A}_{21}^{pol}$. Obviously, this single term reflects the polarization properties of the incident electrons. While the other two (unpolarized) terms describe the angular distribution of the Lyman-α_1 radiation which is *symmetrical* with respect to the plane perpendicular to the beam axis ($\theta = 90°$), the polarized term gives rise to an *asymmetrical* shift in the emission pattern and, hence, to a clear signature of the electron polarization P. Fig. 1 shows the two Lyman-α_1 angular distributions following (i) the capture of unpolarized electrons (solid line) and (ii) of completely polarized electrons (dashed line) into the $2p_{3/2}$ state of bare uranium projectile ions with an energy $T_p = 310$ MeV/u. All calculations have been carried out in the projectile frame for the case of *perpendicular* geometry, i.e. when the characteristic photon is detected in the plane which is perpendicular to the reaction plane. As seen from the Fig. 1, a complete polarization of the incident electrons results in strongly asymmetrical angular distribution of the Lyman-α_1 radiation. Moreover this asymmetrical shift is proportional to the degree P of the electron polarization and, therefore, can be applied as a precise tool in coincidence (e, 2γ) experiment for studying the polarization of the incident particles.

In the near future, the coincidence experiments as planned at the GSI storage ring in Darmstadt are, most likely, to be carried out in a *coplanar* geometry (that is, when both photons are detected within the same plane). In this case, however, the angular distribution of the Lyman-α_1 photons does not depend on the polarization of the incident electrons:

$$W_\gamma(\theta, \phi = 0; \theta_{RR}, \phi_{RR})$$
$$= \frac{W_0}{4\pi}\left[1 + \frac{1}{2}\sqrt{\frac{3}{2}}\left(\frac{1}{\sqrt{6}}(3\cos^2\theta - 1)\right.\right.$$
$$\times \mathscr{A}_{20}^{unp}(\theta_{RR}, \phi_{RR}) - \sin 2\theta \mathscr{A}_{21}^{unp}(\theta_{RR}, \phi_{RR})$$
$$\left.\left. + \sin^2\theta \mathscr{A}_{22}^{unp}(\theta_{RR}, \phi_{RR})\right)f(E1, M2)\right] \quad (10)$$

and hence, cannot be used for deriving the polarization properties of the (target) electrons. To obtain information about the polarization of the electrons (and/or the projectile ions) also in coplanar geometry, the setup of the coincidence experiment needs to be modified. For such a geometry, one possibility consists in measuring the *angle-polarization* correlation, i.e. the polarization of the Lyman-α_1 radiation in coincidence with (the angle of) the recombination photon. By using a new position-sensitive germanium X-ray detectors, such angle-polarization coincidence studies may become likely to be carried out at the GSI storage ring. The density matrix approach will certainly help to analyze such type of experiments. A more detailed investigation of the angle-polarization correlation function is currently under work.

References

[1] Th. Stöhlker, Phys. Scr. T 80 (1999) 165.
[2] Th. Stöhlker, F. Bosch, A. Gallus, C. Kozhuharov, G. Menzel, P.H. Mokler, H.T. Prinz, J. Eichler, A. Ichihara, T. Shirai, et al., Phys. Rev. Lett. 79 (1997) 3270.
[3] J. Eichler, W. Meyerhof, Relativistic Atomic Collisions, Academic Press, San Diego, 1995.
[4] J. Eichler, A. Ichihara, T. Shirai, Phys. Rev. A 58 (1998) 2128.
[5] A. Surzhykov, S. Fritzsche, Th. Stöhlker, J. Phys. B: At. Mol. Opt. Phys. 35 (2002) 3713.
[6] V.V. Balashov, A.N. Grum-Grzhimailo, N.M. Kabachnik, Polarization and Correlation Phenomena in Atomic Collisions, Kluwer Academic, Plenum Publishers, New York, 2000.
[7] A. Surzhykov, S. Fritzsche, A. Gumberidze, Th. Stöhlker, Phys. Rev. Lett. 88 (2002) 153001.

8.5 Polarization studies on the radiative recombination of highly charged ions

Polarization studies on the radiative recombination of highly charged bare ions

Andrey Surzhykov* and Stephan Fritzsche

Universität Kassel, Heinrich-Plett-Strasse 40, D-34132 Kassel, Germany

Thomas Stöhlker and Stanislav Tachenov

Gesellschaft für Schwerionenforschung (GSI), D-64291 Darmstadt, Germany

(Received 29 April 2003; published 27 August 2003)

The polarization of the emitted photons is studied for the radiative recombination of free electrons into the bound states of bare, highly charged ions. We apply density matrix theory in order to investigate how the photon polarization is affected if the incident electrons are themselves spin polarized. For K-shell electron capture, for instance, the linear polarization of the light, which is measured out of the reaction plane, is defined by the degree of polarization of the electrons and may be used as a tool for studying the polarization properties of the electron targets and/or the projectile ions. Detailed computations of the Stokes parameters of x-ray emission following the radiative recombination of bare uranium ions U^{92+} are carried out for a wide range of projectile energies and for different polarization states of the incident electrons.

I. INTRODUCTION

With the recent experimental advances in heavy-ion accelerators and ion storage rings, more possibilities arise to study ion-electron and ion-atom collisions. For the relativistic collisions of highly charged ions with low-Z target atoms (or free electrons), for instance, a number of case studies on radiative electron capture, K-shell Coulomb excitation and ionization of projectiles, electron bremsstrahlung, and even correlated two-electron capture have proceeded in recent years at the GSI storage ring in Darmstadt [1]. So far, however, most of these experiments have dealt with target atoms (or electrons) and ion beams that are both unpolarized. A wide range of qualitatively different *polarization* studies will be opened up by using spin-polarized projectile ions or/and target atoms. Such experiments are very likely to be carried out at the future GSI facilities which will be installed within the next ten years.

Polarization collision experiments, however, require an effective tool for diagnostics the polarization properties of the beam as well as of the target atoms (or electrons). It is necessary, therefore, to find a *probe* process whose characteristics are sensitive to the polarization states of the collision system. One such probe process, which we suggest from the theoretical viewpoint, is the capture of a free (or quasifree) electron into a bound state of the projectile ion with the simultaneous emission of a photon which carries away the excess energy and momentum. This capture process, denoted *radiative recombination*, has been intensively studied during recent years in the relativistic collisions of high-Z projectile ions with low-Z target atoms (or free electrons). A series of experiments, for instance, has been carried out at the GSI storage ring [1,2] in order to explore the total and angle-differential recombination cross sections, which were found to be in good agreement with theoretical predictions based on relativistic Dirac theory [3–5]. However, neither the total

recombination cross section nor the angular distribution of the emitted photons was found to be (much) dependent on the polarization of the ion beam or atomic target and therefore they cannot be used for polarization studies.

In contrast to the total and angle-differential cross sections, the polarization of the emitted photons may appear very sensitive to the particle polarization. A similar effect, for instance, has long been known for the atomic photoeffect [6,7], where the spin polarization of the emitted electron is strongly affected by the polarization of the incident photon. Since the photoeffect is the time-inverse process of radiative recombination, we can expect that measurements of the polarization of the recombination photons will provide us with information on the spin polarization of the target electrons (atoms) or ion beam. In fact, such measurements are possible nowadays for the *linear* polarization of x-ray photons due to the recent improvements in position sensitive polarization detectors. In the last year, for instance, measurements of the linear polarization of K-shell recombination photons have been carried out for electron capture into bare uranium ions U^{92+}.

In this paper, we study the linear polarization of the photons that are emitted due to the capture of free polarized electrons into bound states of bare, high-Z ions. For such investigations of the angular distribution and polarization properties of the emitted radiation, density matrix theory has been found to be the appropriate framework in order to accompany the system through the collision process [8]. Since, however, the concept of density matrix theory has been presented elsewhere in a number of places [8–10], we may restrict ourselves to rather a short outline of the basic relations within the two following sections. Starting from the basic representation of the density matrix, we first derive the explicit expressions for the Stokes parameters of the recombination photons and simplify them by using the parity properties of the levels involved. In Sec. II D, moreover, we introduce a (so-called) *polarization ellipse*, which helps us to discuss and better understand the linear polarization of the emitted x-ray radiation. This representation in terms of an ellipse also shows explicitly how the polarization of the x
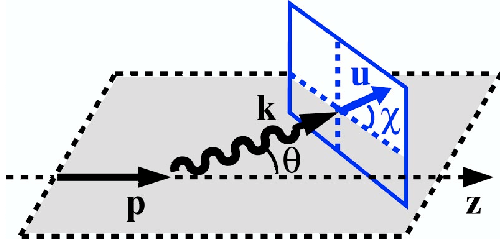
---

*Electronic address: surz@physik.uni-kassel.de

FIG. 1. The unit vector $\mathbf{u}(\chi)$ of the linear polarization is defined in the plane that is perpendicular to the photon momentum $\mathbf{k}$, and is characterized by an angle χ with respect to the reaction plane.

rays is affected if the incident electrons are also polarized. In Sec. III, we describe a series of computations that were carried out for the linear polarization of the emitted photons following the capture of an electron into the K shell of bare uranium (projectile) ions U^{92+}. As seen from this computation, polarization of the incident electrons generally leads also to a rotation of the polarization vector of the light *out of the reaction plane*. A summary of this important result and its implication for future experiments is finally given in Sec. IV.

II. BASIC FORMULAS

A. Polarization vector of the photon

For the radiative recombination of free electrons into bare, high-Z ions, several case studies are known today, which are based on Dirac's equation [4,11–13]. In such a relativistic treatment of the electronic capture, Dirac-Coulomb wave functions are usually applied throughout the computations, both for the incident (free) electron with well defined asymptotic momentum $\mathbf{p}$ and spin projection m_s as well as for the final *bound* state $|n_b j_b \mu_b\rangle$ of the electron. In addition, the emitted—or recombination—photon is typically described in terms of a plane wave with wave vector $\mathbf{k}$ ($k = \omega/c$) and with a polarization that points perpendicular to $\mathbf{k}$ along some unit vector $\mathbf{u}$. The wave vector $\mathbf{k}$ and the electron momentum $\mathbf{p}$ span the reaction plane in the experiment. Of course, the (polarization) vector $\mathbf{u}$ can always be rewritten in terms of any two (linearly independent) basis vectors, such as the *circular-polarization* vectors $\mathbf{u}_{\pm 1}$, which are perpendicular to the wave vector $\mathbf{k}$ and which for $\mathbf{u}_{+1}$ and $\mathbf{u}_{-1}$ refer to right- and left-circularly polarized photons [9], respectively. In such a basis, the unit vector for the linear polarization of the emitted x rays can be written as

$$\mathbf{u}(\chi) = \frac{1}{\sqrt{2}}(e^{-i\chi}\mathbf{u}_{+1} + e^{i\chi}\mathbf{u}_{-1}), \tag{1}$$

where χ is the angle between $\mathbf{u}(\chi)$ and the reaction plane (see Fig. 1).

B. Density matrix approach

While the definition (1) of the polarization vector $\mathbf{u}$ is appropriate to describe the linear polarization of photons in a pure polarization state, it is not sufficient if several photons with different polarization states are emitted in the course of

a capture or collision process. If, for example, we consider a photon beam in some mixed state, the polarization of the photons is then better described in terms of the spin-density matrix. Since the photon (with spin $S=1$) has only two allowed spin (or helicity) states $|\mathbf{k}\lambda\rangle$, $\lambda = \pm 1$, the spin-density matrix of the photon is a 2×2 matrix and, hence, can be parametrized by the three (real) *Stokes parameters* [8,9]

$$\langle \mathbf{k}\lambda | \hat{\rho}_\gamma | \mathbf{k}\lambda' \rangle = \frac{1}{2}\begin{pmatrix} 1+P_3 & P_1 - iP_2 \\ P_1 + iP_2 & 1 - P_3 \end{pmatrix}. \tag{2}$$

In fact, these parameters are often utilized in experiments in order to characterize the degree of polarization of the emitted light; while the Stokes parameter P_3 reflects the degree of circular polarization, the two parameters P_1 and P_2 together denote the (degree and direction of the) linear polarization of the light in the plane perpendicular to the photon momentum $\mathbf{k}$. Experimentally, these Stokes parameters are determined simply by measuring the intensities of the light I_χ, linearly polarized at different angles χ with respect to the reaction plane. For instance, the parameter P_1 is given by the intensity ratio

$$P_1 = \frac{I_0 - I_{90}}{I_0 + I_{90}}, \tag{3}$$

while the parameter P_2 is obtained from a very similar ratio at angles $\chi = 45°$ and $\chi = 135°$, respectively (see Fig. 1):

$$P_2 = \frac{I_{45} - I_{135}}{I_{45} + I_{135}}. \tag{4}$$

As seen from Eq. (2), the three Stokes parameters can obviously also be expressed in terms of the matrix elements of the photon spin-density matrix. For electron capture into a bound state $|n_b j_b \mu_b\rangle$ of a (subsequently hydrogenlike) projectile ion, an expression for these matrix elements was derived previously [11]:

$$\langle \mathbf{k}\lambda | \hat{\rho}_\gamma | \mathbf{k}\lambda' \rangle = \sum_{\nu\mu} D^\nu_{0\mu}(0,\theta,0) \sum_{L\pi L'\pi'} \beta^{\nu\mu}_{L\pi L'\pi'}(\lambda,\lambda'), \tag{5}$$

where θ denotes the angle of the photons with respect to the momentum $\mathbf{p}$ of the (incoming) electrons (see Fig. 1). The angular parameters $\beta^{\nu\mu}_{L\pi L'\pi'}(\lambda,\lambda')$ refer to the contributions of the different multipoles of the radiation field to the polarization state of the emitted photons and can be written as

$$\beta^{\nu\mu}_{L\pi L'\pi'}(\lambda,\lambda') = \sum_{m_s \mu_b} i^{L'+\pi'-L-\pi}(-1)^{m_s - \mu_b}[L,L']^{1/2}$$

$$\times \langle \mathbf{p}m_s | \hat{\rho}_e | \mathbf{p}m_s \rangle \lambda^\pi \lambda'^{\pi'} \langle L'\lambda' L - \lambda | \nu\mu \rangle$$

$$\times \langle L'm_s - \mu_b L \mu_b - m_s | \nu 0 \rangle$$

$$\times \langle \mathbf{p}m_s | \boldsymbol{\alpha} \mathbf{A}^{\pi'}_{L'm_s - \mu_b} | \kappa_b \mu_b \rangle$$

$$\times \langle \mathbf{p}m_s | \boldsymbol{\alpha} \mathbf{A}^\pi_{Lm_s - \mu_b} | \kappa_b \mu_b \rangle^*, \tag{6}$$

where $[L]=2L+1$ and $\langle \mathbf{p}m_s|\alpha\mathbf{A}_{LM}^{\pi}|\kappa_b\mu_b\rangle$ denotes the matrix element for either the electric ($\pi=1$) or magnetic ($\pi=0$) multipole *free-bound* transition of the electron. The explicit separation of the transition amplitudes into their electric and magnetic components, as displayed in Eqs. (5) and (6), will help us later in simplifying the expressions for the Stokes parameters. Of course, the angular coefficient (6) still depends on the (initially prepared) spin-density matrix $\langle \mathbf{p}m_s|\hat{\rho}_e|\mathbf{p}m_s\rangle$, i.e., on the polarization state of the incident electrons.

The transition matrix elements in the last two lines of expression (6) contain the wave function $|\mathbf{p}m_s\rangle$ of a free electron with a definite asymptotic momentum. For further simplification of the spin-density matrix (5), it is therefore necessary to decompose this continuum wave into partial waves $|E\kappa j m_s\rangle$, in order to apply later the standard techniques from the theory of angular momentum. As discussed previously [11–13], however, special care has to be taken about the choice of the quantization axis since this directly influences the particular form of the partial wave decomposition. Using, for example, the electron momentum **p** as the quantization axis, the full expansion of the continuum wave function is given by [4]

$$|\mathbf{p}m_s\rangle = \sum_{\kappa} i^l e^{i\Delta_\kappa}\sqrt{4\pi(2l+1)}\langle l01/2m_s|jm_s\rangle|E\kappa j m_s\rangle,$$

(7)

where the summation runs over all partial waves $\kappa=\pm 1,\pm 2,\ldots$, i.e., along all values of (Dirac's) angular momentum quantum number $\kappa=\pm(j+1/2)$ for $l=j\pm 1/2$. In this notation, the (nonrelativistic orbital) momentum l now represents the parity of the partial waves $|E\kappa jm_s\rangle$, and Δ_κ is the Coulomb phase shift.

Using the decomposition (7) of the continuum wave function together with the Wigner-Eckart theorem [8], the angular parameters (6) can be rewritten in the form

$$\beta_{L\pi L'\pi'}^{\nu\mu}(\lambda,\lambda')$$

$$=\sum_{\kappa\kappa'} i^{L'+\pi'-L-\pi} i^{l-l'} e^{i(\Delta_\kappa-\Delta'_\kappa)}[L,L',l,l']^{1/2}$$

$$\times \begin{Bmatrix} L & L' & \nu \\ j' & j & j_b \end{Bmatrix} \lambda^\pi \lambda'^{\pi'} \langle L'\lambda'L-\lambda|\nu\mu\rangle$$

$$\times \langle E\kappa'j'||\alpha\mathbf{A}_{L'}^{\pi'}||n_b j_b\rangle\langle E\kappa j||\alpha\mathbf{A}_L^\pi||n_b j_b\rangle^* C_{\kappa\kappa'}^\nu,$$

(8)

where the polarization properties of the incident electron now occur only in the coefficient

$$C_{\kappa\kappa'}^\nu = \sum_{m_s}(-1)^{-m_s}\langle \mathbf{p}m_s|\hat{\rho}_e|\mathbf{p}m_s\rangle\langle l01/2m_s|jm_s\rangle$$

$$\times\langle l'01/2m_s|j'm_s\rangle\langle j'-m_s jm_s|\nu 0\rangle.$$

(9)

Therefore, making use of these last two expressions, the evaluation of the spin-density matrix can be traced back to just the computation of the reduced matrix elements $\langle E\kappa j||\alpha\mathbf{A}_L^\pi||n_b j_b\rangle$ which describe the interaction of an electron with the radiation field for a (standard) free-bound transition. The computation of these matrix elements within the framework of Dirac theory was discussed elsewhere at several places in the past [5,13].

C. Symmetry properties of the Stokes parameters

The decomposition of the continuum wave functions in Eqs. (8) and (9) helps analyze the symmetry properties of the two Stokes parameters P_1 and P_2 and, hence, of the linear polarization of the emitted light. As seen from the expression (8), for instance, the helicity quantum numbers λ and λ', which characterize the different partial waves of the outgoing photon, appear only in the phase and in the single Clebsch-Gordan coefficient $\langle L'\lambda'L-\lambda|\nu\mu\rangle$. From the symmetry properties of the Clebsch-Gordan coefficients, it therefore follows immediately that the $\beta_{L\pi L'\pi'}^{\nu\mu}(\lambda,\lambda')$ angular coefficients must also obey the symmetry

$$\beta_{L\pi L'\pi'}^{\nu\mu}(-1,+1)=(-1)^f\beta_{L\pi L'\pi'}^{\nu-\mu}(+1,-1),\quad (10)$$

where the proper phase is given by $f=L+\pi+L'+\pi'-\nu$. The symmetry of the angular coefficients enables one, in turn, to express the two Stokes parameters P_1 and P_2 in a simpler form:

$$P_1 = \frac{\langle \mathbf{k}+1|\hat{\rho}_\gamma|\mathbf{k}-1\rangle + \langle \mathbf{k}-1|\hat{\rho}_\gamma|\mathbf{k}+1\rangle}{\langle \mathbf{k}+1|\hat{\rho}_\gamma|\mathbf{k}+1\rangle + \langle \mathbf{k}-1|\hat{\rho}_\gamma|\mathbf{k}-1\rangle}$$

$$= \frac{\sum_\nu D_{02}^\nu(0,\theta,0)\sum_{L\pi L'\pi'}\beta_{L\pi L'\pi'}^{\nu 2}(-1,1)[1+(-1)^f]}{2\sum_\nu P_\nu(\cos\theta)\sum_{L\pi L'\pi'}\beta_{L\pi L'\pi'}^{\nu 0}(+1,+1)}$$

(11)

and

$$P_2 = -i\frac{\langle \mathbf{k}-1|\hat{\rho}_\gamma|\mathbf{k}+1\rangle - \langle \mathbf{k}+1|\hat{\rho}_\gamma|\mathbf{k}-1\rangle}{\langle \mathbf{k}+1|\hat{\rho}_\gamma|\mathbf{k}+1\rangle + \langle \mathbf{k}-1|\hat{\rho}_\gamma|\mathbf{k}-1\rangle}$$

$$= -i\frac{\sum_\nu D_{02}^\nu(0,\theta,0)\sum_{L\pi L'\pi'}\beta_{L\pi L'\pi'}^{\nu 2}(-1,1)[1-(-1)^f]}{2\sum_\nu P_\nu(\cos\theta)\sum_{L\pi L'\pi'}\beta_{L\pi L'\pi'}^{\nu 0}(+1,+1)},$$

(12)

which, however, still includes a summation over all the possible multipoles in the electron-photon interaction. Owing to parity conservation in the interaction of the electron with the radiation field, of course, not all of these multipoles will

contribute in practice to the polarization properties of the photons, as is reflected above by the phase factor $(-1)^f \equiv (-1)^{L+\pi+L'+\pi'-\nu} = \pm 1$. Therefore, in order to understand the effects of parity conservation, we shall return to expression (8) for the angular parameters $\beta_{L\pi L'\pi'}^{\nu\mu}(\lambda,\lambda')$ and analyze it in some more detail.

In expression (8), of course, the parity selection rules apply to both of the reduced matrix elements and do require that the parities of the (electric and magnetic) multipole fields must be equal to (-1) times the product of the parities that are associated with the bound state and the (outgoing) partial wave, respectively,

$$(-1)^{L+\pi} = -\pi_{n_b j_b} \pi_{\kappa j} = (-1)^{l_b+l+1},$$

$$(-1)^{L'+\pi'} = -\pi_{n_b j_b} \pi_{\kappa' j'} = (-1)^{l_b+l'+1}, \qquad (13)$$

which immediately leads to the relation

$$(-1)^{L+\pi+L'+\pi'-\nu} = (-1)^{l+l'-\nu}. \qquad (14)$$

However, before we continue with the discussion of the Stokes parameters, let us first reconsider the coefficient (9), i.e., that part of the $\beta_{L\pi L'\pi'}^{\nu\mu}$ parameter which depends explicitly on the electron density matrix $\langle \mathbf{p}m_s | \hat{\rho}_e | \mathbf{p}m_s \rangle$ of the incident electrons. Since, in the relativistic theory, the projection of the electron spin has a sharp value only along the electron momentum, the quantization axis (z axis) is chosen parallel to $\mathbf{p}$. For spin-1/2 particles, moreover, a single parameter $-1 \leq \mathcal{P} \leq 1$ is of course sufficient to describe the polarization of the electrons and hence can be used to express the *electron* spin-density matrix

$$\langle \mathbf{p}m_s | \hat{\rho}_e | \mathbf{p}m_s \rangle = \frac{1}{2}(I + \mathcal{P}\sigma_z) = \frac{1}{2}\begin{pmatrix} 1+\mathcal{P} & 0 \\ 0 & 1-\mathcal{P} \end{pmatrix} \quad (15)$$

in terms of the unit matrix I and the Pauli matrix σ_z. In this parametrization of the initial spin-density matrix, obviously, a degree of polarization $\mathcal{P} = 0$ corresponds to a beam of *unpolarized* electrons, while $\mathcal{P} = \pm 1$ refers to a *completely polarized* electron beam with spin projections $m_s = \pm 1/2$.

We are now prepared to study the influence of an initially polarized electron beam on the angular and Stokes parameters. By inserting expression (15) into Eq. (9), we first see that the coefficient $C_{\kappa\kappa'}^{\nu}$ can be decomposed into an "unpolarized" and a "polarized" component

$$C_{\kappa\kappa'}^{\nu} = C_{\kappa\kappa'}^{\nu}(\text{unpol}) + \mathcal{P}C_{\kappa\kappa'}^{\nu}(\text{unpol}), \qquad (16)$$

which, due to the parity rules, behave quite differently under a (sign) change in the spin state of the electron (in either its initial or final state). Taking into account the properties of the Clebsch-Gordan coefficients in Eq. (9), we find that these two parts obey the symmetry relations

$$C_{\kappa\kappa'}^{\nu}(\text{unpol}) = (-1)^{l+l'-\nu} C_{\kappa\kappa'}^{\nu}(\text{unpol}), \qquad$$

$$C_{\kappa\kappa'}^{\nu}(\text{pol}) = (-1)^{l+l'-\nu+1} C_{\kappa\kappa'}^{\nu}(\text{pol}). \qquad (17)$$

A similar decomposition as found for the $C_{\kappa\kappa'}^{\nu}$ coefficients applies of course also to the $\beta_{L\pi L'\pi'}^{\nu\mu}(\lambda,\lambda')$ angular parameters in Eq. (8):

$$\beta_{L\pi L'\pi'}^{\nu\mu}(\lambda,\lambda') = \beta_{L\pi L'\pi'}^{\nu\mu}(\lambda,\lambda';\text{unpol})$$

$$+ \mathcal{P}\beta_{L\pi L'\pi'}^{\nu\mu}(\lambda,\lambda';\text{pol}), \qquad (18)$$

where, using Eqs. (14) and (17), the corresponding "unpolarized" and "polarized" parts satisfy the two symmetry relations

$$\beta_{L\pi L'\pi'}^{\nu\mu}(\lambda,\lambda';\text{unpol})$$

$$= (-1)^{L+\pi+L'+\pi'-\nu} \beta_{L\pi L'\pi'}^{\nu\mu}(\lambda,\lambda';\text{unpol}),$$

$$\beta_{L\pi L'\pi'}^{\nu\mu}(\lambda,\lambda';\text{pol})$$

$$= (-1)^{L+\pi+L'+\pi'-\nu+1} \beta_{L\pi L'\pi'}^{\nu\mu}(\lambda,\lambda';\text{pol}). \quad (19)$$

That is, while the unpolarized part of the $\beta_{L\pi L'\pi'}^{\nu\mu}$ parameter is always *zero* if the phase f is odd, the same is true for the polarized part for even f. Making use of this property of the angular parameter (18), we can now simplify the expressions (11) and (12) for the Stokes parameters to

$$P_1 = \frac{\sum_\nu D_{02}^\nu(0,\theta,0) \sum_{L\pi L'\pi'} \beta_{L\pi L'\pi'}^{\nu 2}(-1,1;\text{unpol})}{\sum_\nu P_\nu(\cos\theta) \sum_{L\pi L'\pi'} \beta_{L\pi L'\pi'}^{\nu 0}(+1,+1)},$$

$$(20)$$

$$P_2 = -i\mathcal{P}\frac{\sum_\nu D_{02}^\nu(0,\theta,0) \sum_{L\pi L'\pi'} \beta_{L\pi L'\pi'}^{\nu 2}(-1,1;\text{pol})}{\sum_\nu P_\nu(\cos\theta) \sum_{L\pi L'\pi'} \beta_{L\pi L'\pi'}^{\nu 0}(+1,+1)},$$

$$(21)$$

which shows us immediately that only the P_2 parameter depends on the polarization $\mathcal{P}$ of the incident electrons and that this parameter is simply proportional to $\mathcal{P}$. Therefore, the Stokes parameter P_2 vanishes identically if the electrons are initially unpolarized and hence can be used as a very valuable tool for studying the polarization of the incident electron (and/or ion) beam. A measurement of the Stokes parameter P_1, in contrast, will not be affected by the polarization of the incoming electrons and depends only on the nuclear charge Z, the projectile energy, and the geometry in the setup of the photon detectors [11,12].

D. Polarization ellipse of the photons

The two Stokes parameters P_1 and P_2 specify the linear polarization of the radiation completely, i.e., both the *degree* of the polarization as well as its *direction* in the plane perpendicular to the photon momentum $\mathbf{k}$. Instead of the Stokes parameters, however, we may represent the linear polarization of the emitted x rays also in terms of a polarization
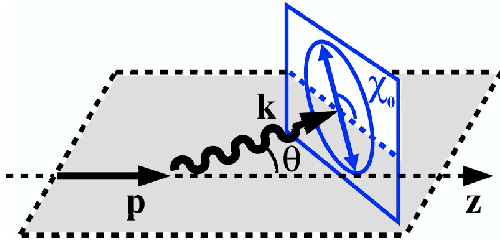
FIG. 2. Definition of the polarization ellipse; its principal axis is characterized by χ_0, the angle with respect to the reaction plane in the given measurement.

ellipse which is defined in this plane (perpendicular to **k**). In such a representation, the degree of linear polarization

$$P_L = \sqrt{P_1^2 + P_2^2} \qquad (22)$$

is characterized by the relative length of the principal axis (of the ellipse), and the direction by its angle χ_0 with respect to the reaction plane. Figure 2 shows the concept of the polarization ellipse and how χ_0 is defined; when expressed in terms of the Stokes parameters, this angle is given by the two ratios [8]

$$\cos 2\chi_0 = \frac{P_1}{P_L}, \quad \sin 2\chi_0 = \frac{P_2}{P_L}, \qquad (23)$$

and can be used to interpret the measurements. While, obviously, an angle $\chi_0 = 0$ or $\chi_0 = \pi/2$ corresponds to a linear polarization of the x rays within or perpendicular to the reaction plane (and with degree $P_L = |P_1|$), any contribution from a nonzero P_2 parameter will rotate the polarization vector (i.e., $\chi_0 \neq 0$ and $\chi_0 \neq \pi/2$). Recalling, moreover, the linear dependence of $P_2 \sim \mathcal{P}$ on the polarization of the incident electrons, we can therefore conclude that any polarization vector that is not in the reaction plane or perpendicular to it reflects a polarization of the (incident) electrons.

For the case of a polarized electron target (and for unpolarized ions), we can express the angle χ_0 of the polarization ellipse also directly in terms of the polarization $\mathcal{P}$ and the $\beta_{L\pi L'\pi'}^{\nu\mu}(\lambda,\lambda')$ angular parameters:

$$\cos 2\chi_0 = \frac{\text{sign}(P_1)}{\sqrt{1 + \mathcal{P}^2 \mathcal{R}^2}}, \qquad (24)$$

$$\sin 2\chi_0 = \frac{\text{sign}(P_2)|\mathcal{P}|\mathcal{R}}{\sqrt{1 + \mathcal{P}^2 \mathcal{R}^2}}, \qquad (25)$$

where

$$\mathcal{R} = \left| \frac{i \sum_\nu D_{02}^\nu(0,\theta,0) \sum_{L\pi L'\pi'} \beta_{L\pi L'\pi'}^{\nu 2}(-1,1;\text{pol})}{\sum_\nu D_{02}^\nu(0,\theta,0) \sum_{L\pi L'\pi'} \beta_{L\pi L'\pi'}^{\nu 2}(-1,1;\text{unpol})} \right| \qquad (26)$$
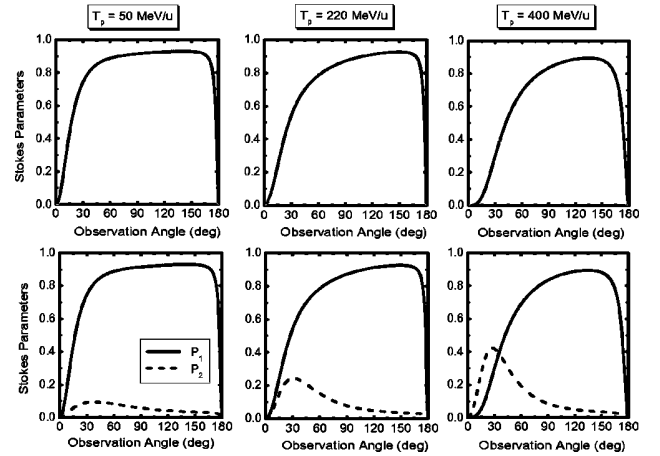

FIG. 3. The Stokes parameters P_1 and P_2 of the x-ray photons that are emitted in electron capture into the K shell of bare uranium ions. The Stokes parameters are shown for the capture of unpolarized (top panels) and completely polarized (bottom panels) electrons. Calculations are presented in the laboratory frame (i.e., the rest frame of the electron target).

denotes some ratio of the "polarized" and "unpolarized" components of the $\beta_{L\pi L'\pi'}^{\nu\mu}$ parameters. In experiments with highly charged ions, it is this representation of the angle χ_0 which, along with theoretical data, may help determine immediately the degree of polarization of the incident electrons without any need to measure the linear polarization in detail.

III. RESULTS AND DISCUSSION

Measurements on the linear polarization of x-ray radiation following the capture of electrons into highly charged ions are no longer impractical today. For the K-shell recombination of bare uranium ions U^{92+}, for example, experiments on the polarization of the photons were carried out at the GSI storage ring in Darmstadt during the last year. These studies on the x-ray polarization became possible owing to the use of position sensitive germanium detectors. These detectors enable one to obtain information not only on the degree of x-ray polarization but also concerning its direction within the detector plane. They may be used therefore for studying the polarization of electron (or atom) targets or even the polarization properties of ion beams at storage rings in the future.

In the following, we analyze the linear polarization of the photons that are emitted in the radiative recombination of bare uranium ions with energies in the range $50 \leq T_p \leq 400$ MeV/u. Detailed calculations have been carried out, in particular, for electron capture into the K shell of U^{92+} projectiles. To explore the effects of a polarized electron target on the (linear) polarization of the recombination photons, two cases are considered: the capture of (i) unpolarized and (ii) completely polarized electrons. For these two cases, Fig. 3 displays the Stokes parameters as a function of the observation angle θ of the recombination photons. In the upper panels of this figure, the P_1 parameter for the capture of unpolarized electrons ($\mathcal{P}=0$) is shown; it is positive and quite large for most angles apart from the forward and back-
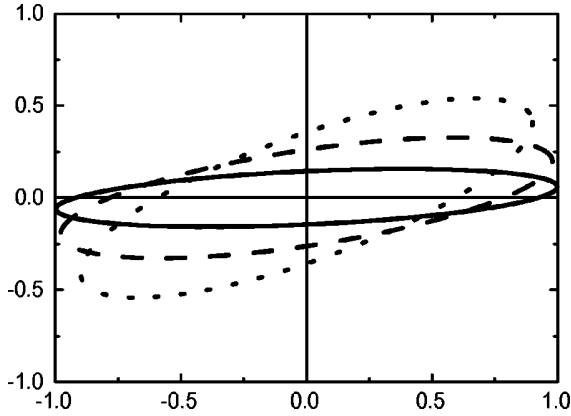
FIG. 4. Rotation of the polarization ellipses of the recombination photons, calculated for the three projectile energies T_p = 50 MeV/u (—), 220 MeV/u (– –), and 400 MeV/u (- - -) at the photon emission angle $\theta = 30°$.

ward directions of emission. As seen from Eq. (21), the Stokes parameter P_2 must vanish identically in the case of unpolarized electrons; since, moreover, $P_1 > 0$ for projectile energies $T_p \lesssim 400$ MeV/u, the principal axis of the polarization ellipse always lies within the reaction plane, $\chi_0 = 0$, for all angles of observation of the recombination photons and for unpolarized electrons.

A rather different situation arises in the second case (ii) for the capture of completely polarized electrons ($\mathcal{P} = 1$) as shown in the lower panels of Fig. 3. Here, a nonvanishing Stokes parameter P_2 appears, which peaks at around $\theta = 30°$ and becomes larger for increasing projectile energies, while the P_1 parameter remains unaffected by the polarization of the electron target. As mentioned above, a nonzero value of P_2 also leads to a rotation of the polarization ellipse out of the reaction plane. This rotation is seen in Fig. 4, which displays the polarization ellipses of the recombination photons at the observation angle $\theta = 30°$, calculated for the three projectile energies $T_p = 50$, 220 and 400 MeV/u. According to the increase of the Stokes parameter P_2 at this angle, the (rotation) angle χ_0 of the polarization ellipse increases from 3.5° for $T_p = 50$ MeV/u to almost 30° for $T_p = 400$ MeV/u. As seen from Figs. 3 and 4, therefore, the effects of the target polarization become apparently more pronounced if the projectile energy is increased.

So far, we have analyzed the linear polarization of the recombination photons for the two limiting cases of either unpolarized or completely polarized electrons. As discussed above, these two cases can be easily distinguished by the polarization ellipse whose principal axis must always lie within or perpendicular to the reaction plane for the capture of unpolarized electrons. As seen from Eqs. (24)–(26), however, observation of the rotation angle χ_0 may provide information on both the degree as well as the direction of the electron polarization $\mathcal{P}(-1 \leqslant \mathcal{P} \leqslant +1)$ and hence can be used for studying the spin polarization of the electrons and atomic targets, respectively. Figure 5 displays the rotation angle χ_0 of the polarization ellipse for various degrees of the electron polarization $\mathcal{P}$, following the capture of electrons into the K shell of bare uranium ions at a projectile energy
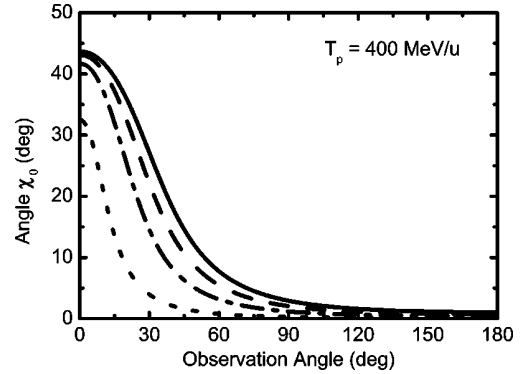

FIG. 5. Rotation angle χ_0 of the polarization ellipse in dependence on the observation angle of the recombination photons. The angle χ_0 is calculated for the capture of longitudinally polarized electrons into the K shell of a bare uranium projectile U^{92+} and is shown for four different degrees of the electron polarization: $\mathcal{P} = 1.0$ (—), $\mathcal{P} = 0.7$ (– –), $\mathcal{P} = 0.4$ (– – –), and $\mathcal{P} = 0.1$ (- - -).

$T_p = 400$ MeV/u. In this figure, the rotation angle χ_0 is shown as a function of the observation angle θ of the recombination photons (in the laboratory frame, i.e., the rest frame of the electron target); for a given energy of the projectiles, apparently, the maximal rotation of the polarization ellipse arises in the forward direction for the emission of recombination photons. Note, however, that χ_0 is not defined at the emission angles $\theta = 0$ and $\theta = 180°$, because photon emission in either the forward or backward direction does not break the *axial* symmetry for the collision system. At these two angles, therefore, the linear polarization of the light must always be zero (see Fig. 3). For the same reason also, all polarization measurements at angles near $\theta = 0$ will become difficult as the degree of linear polarization $P_L = \sqrt{P_1^2 + P_2^2} \ll 0.1$ in this range. For larger emission angles, however, the (degree of) linear polarization increases and may become as large as $P_L \approx 0.5$ for emission angles around $\theta = 30°$. At these angles, the effect from the polarization of the incident electrons is still quite sizable and leads, for $\theta = 30°$ and $T_p = 400$ MeV/u, to a decrease of the rotation angle χ_0 from 27.4° for the capture of completely polarized electrons to 4.0° if the polarization of the incident electrons is $\mathcal{P} = 0.1$.

IV. SUMMARY AND OUTLOOK

Density matrix theory has been applied for studying the polarization of the emitted photons following the radiative recombination of bare, high-Z ions. In our theoretical analysis, emphasis was placed particularly on the two questions of (i) how the polarization of the incident electrons affects the linear polarization of the recombination photons and (ii) how this polarization of the electrons (or of any atomic target) can be observed by experiment. As seen from these investigations, the linear polarization of the recombination photons may serve as a valuable tool for "measuring" the polarization properties of the electrons: While the capture of unpolarized electrons always leads to x-ray photons that are polarized within or perpendicular to the reaction plane, a rotation of the polarization ellipse occurs for polarized elec-

trons. Calculations of this (linear) effect have been carried out especially for the capture of longitudinally polarized electrons into the K shell of bare uranium projectiles U^{92+}.

For the sake of simplicity, here we considered the case of polarized electrons, while the ion beam has been assumed unpolarized throughout the analysis. Owing to the symmetry of the collision system "ion plus electron," however, similar effects on the polarization of the recombination photons as found for a polarized electron target can also be expected if the ion beam is polarized. Of course, for a nuclear spin $I > 1/2$, an enlarged parametrization of the ion density matrix will be required [cf. Eq. (15)]. Investigations along these lines are currently under way and will provide, together with proper measurements of the photon polarization, a method of determining the polarization of (heavy-)ion beams—up to the present a rather unresolved problem in the physics at storage rings.

[1] Th. Stöhlker, Phys. Scr. **T80**, 165 (1999).

[2] Th. Stöhlker, C. Kozhuharov, P. Mokler, A. Warczak, F. Bosch, H. Geissel, R. Moshammer, C. Scheidenberger, J. Eichler, A. Ichihara, T. Shirai, Z. Stachura, and P. Rymuza, Phys. Rev. A **51**, 2098 (1995).

[3] R. Pratt, A. Ron, and H. Tseng, Rev. Mod. Phys. **45**, 273 (1973).

[4] J. Eichler and W.E. Meyerhof, *Relativistic Atomic Collisions* (Academic, San Diego, 1995).

[5] J. Eichler, A. Ichihara, and T. Shirai, Phys. Rev. A **58**, 2128 (1998).

[6] R. Pratt, R. Levee, R. Pexton, and W. Aron, Phys. Rev. **134**, A916 (1964).

[7] J. Scofield, Phys. Rev. A **40**, 3054 (1989).

[8] V.V. Balashov, A.N. Grum-Grzhimailo, and N.M. Kabachnik, *Polarization and Correlation Phenomena in Atomic Collisions* (Kluwer Academic/Plenum, New York, 2000).

[9] K. Blum, *Density Matrix Theory and Applications* (Plenum, New York, 1981).

[10] U. Fano and G. Racah, *Irreducible Tensorial Sets* (Academic, New York, 1959).

[11] A. Surzhykov, S. Fritzsche, and Th. Stöhlker, Phys. Lett. A **289**, 213 (2001).

[12] J. Eichler and A. Ichihara, Phys. Rev. A **65**, 052716 (2002).

[13] A. Surzhykov, S. Fritzsche, and Th. Stöhlker, J. Phys. B **35**, 3713 (2002).

8.6 Polarization of the Lyman−α_1 emission following the radiative recombination of bare, high−Z ions

Polarization of the Lyman–α_1 line following the radiative recombination of bare, high–Z ions

A. Surzhykov (`surz@physik.uni-kassel.de`), S. Fritzsche
Fachbereich Physik, Universität Kassel, Heinrich-Plett-Str. 40, D–34132 Kassel, Germany

Th. Stöhlker
Gesellschaft für Schwerionenforschung, Planckstr. 1, D–64291 Darmstadt, Germany

Abstract.
The radiative recombination of a free electron into the $2p_{3/2}$ state of bare, highly–charged ions and the subsequent *Lyman–α_1* ($2p_{3/2} \rightarrow 1s_{1/2}$) decay are studied theoretically. Special attention is paid to the linear polarization of the characteristic x-ray radiation. In particular, it is found that the *angular distribution* of the *Lyman–α_1* line polarization is remarkably modified by the interference between the leading electric dipole E1 decay channel and – the much weaker – magnetic quadrupole M2 term. Relativistic calculations have been carried out for the electron capture into bare uranium ion for a wide range of projectile energies.

Keywords: radiative recombination, radiative decay, x–ray polarization, E1–M2 interference

1. Introduction

With the recent experimental advances in heavy–ion accelerators and ion storage rings, a number of new possibilities arose to study ion–electron and ion–atom collisions. In these collisions, one of the most basic process is the transfer of an electron from the target atom to the fast moving projectile ion. For high–energy collisions of bare ions, this charge transfer is accompanied by the emission of a photon which carries away the excess energy and momentum. This process, which is known as the radiative recombination (RR) of ions, has been intensively studied during recent years at the GSI storage ring in Darmstadt [1]. So far, however, most of the measurements concerned the capture of an electron into the K–shell of the projectile ions. If, in contrast, the electron is captured into some excited state of the ion, its subsequent decay will lead to the emission of one (or several) photons until the ground state is reached. Such subsequent photon emission is characterized (apart from the well known energies) by its *angular distribution* and *polarization*. Both of these properties are closely related to the magnetic sublevel population of the excited ion as it arises from the electron capture [2, 3]. Several experiments have been carried out during last few years in order to study the angular distribution of the subsequent photons and, therefore, to derive the alignment of the residual ions [4]. Till today, no polarization measurement has yet been performed, mainly because of the lack of efficient x–ray polarization detectors. Owing to recent improvements in the detector techniques, however,

such polarization experiments are likely to be carried out at the GSI storage ring within the next few years.

In this contribution, we study the polarization of the *Lyman–α_1* radiation following the capture of a free electron into the $2p_{3/2}$ state of bare, highly–charged ions. The most natural framework for such polarization studies is given by the density matrix theory [5, 6]. For the sake of brevity, in the present paper, we omit the details of the density matrix formalism when applied to the radiative recombination of bare ions. Instead, we display the *final* formulas for the alignment of the excited ionic state and the polarization of the decay photons in Sections 2 and 3. In Section 4, we describe the computations for the linear polarization of the *Lyman–α_1* radiation following an electron capture into the bare *uranium* ion. A brief summary is given finally in Section 5.

2. Ion alignment following the electron capture

The capture of an *unpolarized* electron into an ionic bound state $|n_b\ j_b\rangle$ leads to an equal population of all pairs of sublevels with the same modulus of the magnetic quantum numbers $|\mu_b|$. Moreover, an ion is said to be *aligned* if, for $j_b > 1/2$, different pairs of such magnetic substates are unequally populated. Usually, the alignment of the residual ion is described in terms of one (or several) parameters $\mathcal{A}_k$ which are related to the total cross sections $\sigma^{RR}(\mu_b)$ for the radiative recombination into the various magnetic sublevels $|n_b\ j_b\ \mu_b\rangle$. For the capture into the $2p_{3/2}$ level, for instance, only one parameter $\mathcal{A}_2$ is nonzero and can be expressed as [2, 3]:

$$\mathcal{A}_2 = \frac{\sigma^{RR}(\mu_b = 3/2) - \sigma^{RR}(\mu_b = 1/2)}{\sigma^{RR}(\mu_b = 3/2) + \sigma^{RR}(\mu_b = 1/2)}. \tag{1}$$

The calculation of the alignment parameter $\mathcal{A}_2$ in the framework of the Dirac theory has been discussed in detail by Eichler and co–workers [2]. It requires the computation of free–bound transition matrix elements for the electron–photon interaction. We calculated these matrix elements and utilized them to obtain both, the partial cross sections and the alignment parameters by using the DIRAC [7] and RACAH [8] programs. The DIRAC package has been developed for studying the properties and behaviour of the hydrogen–like ions and has been used before for investigating the polarization phenomena in the radiative electron capture [9].

3. Polarization of the subsequent photons

The alignment parameter $\mathcal{A}_2$ describes the population of the $2\mathrm{p}_{3/2}$ ionic state as it arises from the electron capture. The subsequent decay of such – an *aligned* – state may lead both, to an anisotropic angular distribution [2, 3] as well as

to a *non–zero* linear polarization of the characteristic x–ray radiation, which is defined in terms of the *degree of polarization* [10]:

$$P_L = \frac{I_\parallel - I_\perp}{I_\parallel + I_\perp}. \tag{2}$$

Here, $I_\parallel$ and $I_\perp$ are the intensities of light, which is linearly polarized in parallel (perpendicular) respectively to the reaction plane, given by the directions of the projectile ion and characteristic photon. Of course, the linear polarization (2) will depend not only on the population of the excited ionic states but also on the angle θ, under which the decay photon is detected with respect to the ion beam. For instance, the linear polarization of the *Lyman–α_1* photons is given in the emitter frame by the standard expression [10, 11]:

$$P_L(\theta) = \frac{-\frac{3}{2}\frac{\mathcal{A}_2}{2}\sin^2\theta}{1 + \frac{\mathcal{A}_2}{2}P_2(\cos\theta)}, \tag{3}$$

where P_2 is the second–order Legendre polynomial.

Equation (3) includes only the dominant electric dipole (E1) decay channel while – the much weaker – magnetic quadrupole component (M2), which also contributes to the *Lyman–α_1* transition, is neglected. Although the electric dipole approximation (3) is certainly appropriate for light ions, it should be questioned for highly–charged ions since the contribution of the magnetic quadrupole term to the properties of the *Lyman–α_1* transition increases dramatically for the higher nuclear charges Z. As we showed recently, for instance, the *angular distribution* of the characteristic radiation is considerably modified by incorporating the magnetic quadrupole (M2) term [3]. Of course, the M2 term must also be taken into account for the *linear polarization* of the decay photons. By using the density matrix theory, Equation (3) can easily be extended to include both, the electric dipole and the magnetic quadrupole components. For the sake of brevity, we leave out the derivation of the following expression and just present the final result:

$$P_L(\theta) = \frac{-\frac{3}{2}\frac{\mathcal{A}_2}{2}\sin^2\theta\left[\frac{|\langle||\mathbf{E1}||\rangle|^2 - |\langle||\mathbf{M2}||\rangle|^2 - \frac{2}{\sqrt{3}}\langle||\mathbf{E1}||\rangle\langle||\mathbf{M2}||\rangle^*}{|\langle||\mathbf{E1}||\rangle|^2 + |\langle||\mathbf{M2}||\rangle|^2}\right]}{1 + \frac{\mathcal{A}_2}{2}P_2(\cos\theta)\left[\frac{|\langle||\mathbf{E1}||\rangle|^2 - |\langle||\mathbf{M2}||\rangle|^2 + 2\sqrt{3}\langle||\mathbf{E1}||\rangle\langle||\mathbf{M2}||\rangle^*}{|\langle||\mathbf{E1}||\rangle|^2 + |\langle||\mathbf{M2}||\rangle|^2}\right]}$$

$$\propto \frac{-\frac{3}{2}\frac{\mathcal{A}_2}{2}\sin^2\theta\left[1 - \frac{2}{\sqrt{3}}\frac{\langle||\mathbf{M2}||\rangle}{\langle||\mathbf{E1}||\rangle}\right]}{1 + \frac{\mathcal{A}_2}{2}P_2(\cos\theta)\left[1 + 2\sqrt{3}\frac{\langle||\mathbf{M2}||\rangle}{\langle||\mathbf{E1}||\rangle}\right]}, \tag{4}$$

where the $\langle||\mathbf{E1}||\rangle \equiv \left\langle 2p_{3/2}\left||\alpha\mathbf{A}_{\mathbf{L=1}}^{(\mathbf{e})}\right||1s_{1/2}\right\rangle$ and $\langle||\mathbf{M2}||\rangle \equiv \left\langle 2p_{3/2}\left||\alpha\mathbf{A}_{\mathbf{L=2}}^{(\mathbf{m})}\right||1s_{1/2}\right\rangle$ are the reduced matrix elements for the electric dipole and magnetic quadrupole transitions, respectively [3].
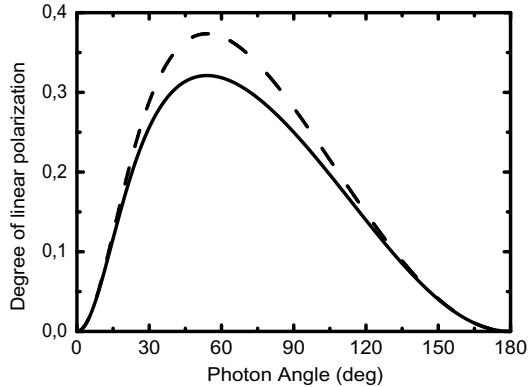
Figure 1. Degree of linear polarization $P_L(\theta)$ of the *Lyman–α_1* radiation following the electron capture into the $2p_{3/2}$ state of bare uranium projectile with energy $T_p = 220$ MeV/u. The dashed line represents the results within the electric dipole approximation, i.e. when the magnetic quadrupole term M2 is neglected. The solid line shows the degree of linear polarization as defined by Eq. (4)

As seen from Eq.(4), the main correction due to the magnetic quadrupole decay channel arises from the term which is proportional to the ratio of the transition amplitudes. For high–Z ions, this ratio is of the order $\propto 0.1$, which may lead to the 10–15 % magnetic quadrupole correction over the electric dipole approximation (3). Moreover, due to the Z scaling rule for the ratio of the transition amplitudes $\langle ||\mathbf{M2}|| \rangle / \langle ||\mathbf{E1}|| \rangle \propto Z^{2.2}$, the non–negligible effect of a few percent remains even for the medium–Z ions. For instance, for the hydrogen–like xenon Xe^{53+} this contribution is still about 4 %.

4. Calculations and discussion

Experimental studies on the linear polarization of the characteristic *Lyman–α_1* radiation are currently planned to be carried at the GSI storage ring within the next few years. As seen from the Eqs.(3–4), such polarization measurements can provide detailed information on the population of the magnetic substates, which is produced by the electron capture processes. However, for a proper interpretation of the experimental data, the magnetic quadrupole correction (M2) should be taken into account since it modifies the linear polarization of the emitted photons. Figure 1, for instance, shows the degree of linear polarization of the *Lyman–α_1* radiation as a function of the photon emission angle, drawn for the electron
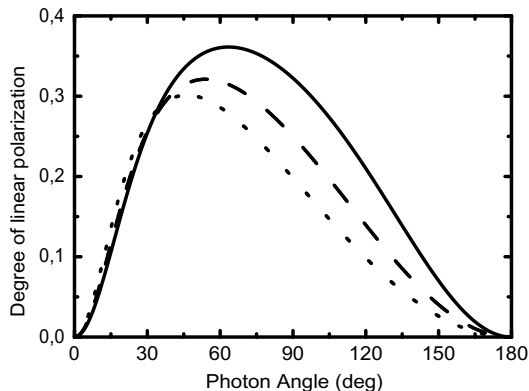
Figure 2. Degree of linear polarization $P_L(\theta)$ of the *Lyman–α_1* radiation following the electron capture into the $2p_{3/2}$ state of bare uranium ion. Results are shown for the projectile energies: $T_p = 110 MeV/u$ (——), $T_p = 220 MeV/u$ (– –) and $T_p = 358 MeV/u$ (- -).

capture into the $2p_{3/2}$ state of bare *uranium* ion with energy $T_p = 220$ MeV/u. Two different approximations are shown: while the dashed line corresponds to the electric dipole approximation (i.e. when the magnetic quadrupole term is neglected), the solid line represents the degree of linear polarization $P_L(\theta)$ as defined by Equation (4). Since, moreover, the radiative recombination of ions is usually studied experimentally by collisions of high–Z projectiles with (low–Z) target atoms, the linear polarization in Figure 1 is presented for angles as measured in the *laboratory system* (the rest frame of the target atoms). As seen from the Figure, the strongest effect due to the magnetic quadrupole term arises around the angle of 54 degrees, which corresponds to an angle of $\theta = 90$ degree in the projectile ion system. At this angle, the degree of linear polarization is 33 %, which is less than the 38 % as obtained from the electric dipole approximation (3).

Until now, we studied the degree of linear polarization $P_L(\theta)$ for the electron capture into bare uranium projectile with energy $T_p = 220$ MeV/u. Apart from the photon emission angle, of course, the linear polarization also depends on the projectile energy. As seen from Eqs. (3–4), the energy dependence is given by the alignment parameter (1), which decreases for the energy range of $T_p = 110...358$ MeV/u from $\mathcal{A}_2 = $ - 0.655 to $\mathcal{A}_2 = $ - 0.528 [2]. Of course, decrease of the alignment parameter also leads to a smaller degree of the linear polarization for high projectile energies. Figure 2, for instance, shows the degree of linear polarization (4), drawn for three typical projectile energies. As seen from the

Figure, the – maximal – linear polarization decreases by one sixth from 36 % to 30 % for the projectile energies $T_p = 110...358$ MeV/u.

5. Summary

In this contribution, we studied the linear polarization of the $Lyman–\alpha_1$ photons following the radiative recombination of a free electron into the $2p_{3/2}$ state of high–Z, bare ions. This polarization is found to be significantly affected by the interference between the leading electric dipole (E1) decay channel and the weak magnetic quadrupole branch (M2). For the hydrogen–like uranium, the E1–M2 interference leads to the 15 % enhancement of the linear polarization when compared with the dipole approximation.

Similar interference effects can be expected also for the polarization of the the characteristic radiation in few–electron heavy ions. Two interest cases of this type are, for instance, the radiative decays in the He–like ions following the KLL–dielectronic recombination [11] or the electron–impact excitation [12, 13].

Acknowledgements

References

1. Stöhlker, Th., Physica Scripta **T80** (1999) 165.
2. Eichler, J., Ichihara, A. and Shirai, T., Phys. Rev. A **58** (1998) 2128.
3. Surzhykov, A., Fritzsche, S., Stöhlker, Th., and Gumberidze, A., Phys. Rev. Lett. **88** (2002) 153001
4. Stöhlker, Th., Bosch, F., Gallus, A., Kozhuharov, C., Menzel, G., Mokler, P.H., Prinz, H.T., Eichler, J., Ichihara, A., Shirai, T., Dunford, R.W., Ludziejewski, T., Rymuza, P., Stachura, Z., Swiat, P. and Warczak, A., Phys. Rev. Lett. **79** (1997) 3270.
5. Balashov, V.V., Grum–Grzhimailo, A.N. and Kabachnik, N.M., *Polarization and Correlation Phenomena in Atomic Collisions* (Kluwer Academic Plenum Publishers, New York, 2000)
6. Berezhko, E.G. and Kabachnik N.M., J. Phys. B **10** (1977) 2467.
7. Surzhykov, A. and Fritzsche, S., to be published (2003).
8. Inghoff, T., Fritzsche, S. and Fricke, B. Comput. Phys. Commun. **139** (2001) 297.
9. Surzhykov, A., Fritzsche, S. and Stöhlker, Th., Phys. Lett. A **289** (2001) 213.
10. Percival, I.C. and Seaton, M.J., Phil. Trans. R. Soc. A **251** (1958) 113.
11. Chen, M.H. and Scofield, J.H., Phys. Rev. A **52** (1995) 2057.
12. Reed, K.J. and Chen, M.H., Phys. Rev. A **48** (1993) 3644.
13. Inal, M.K. and Dubau, J., J. Phys. B **20** (1987) 4221.

Acknowledgments

First of all, I would like to express very special thanks to my supervisor **Dr. Stephan Fritzsche** for the skilful guidance and constant support during all period of my PhD study. His help, suggestions and encouragement were crucial for the development of the whole work. Moreover, the warm and friendly relations which have been settled down between us within these years were also extremely important for my scientific research.

I direct may thanks to **Prof. Dr. Burkhard Fricke** for accepting me in the theoretical physics group at Kassel University and for giving me unique opportunity to fulfill this thesis work.

For the close collaboration and fruitful discussions I gratefully acknowledge **Dr. Thomas Stöhlker**. His suggestions and comments were very useful for my understanding the cases of experimental interest in heavy ion collisions.

I would like to appreciate very much **Dr. Wolf–Dieter Sepp** for his friendly help in scientific as well as "daily life" difficulties. This help was very important for me and for my family.

A special place in my acknowledgments I want to reserve for my *"alma mater"* – Moscow State University where I started my education in physics. I remember and thank a lot **Prof. Dr. Vsevolod V. Balashov** for guiding my first steps towards the world of physics.

For the friendly environment and for the great help I would like to thank my past and present colleagues from the theoretical physics group in Kassel: **Dr. Josef Anton**, **Dr. Turgut Bastug**, **Gabriel Cristache**, **Dr. Chenzhong Dong**, **Lars Haag**, **Thorsten Inghoff**, **Dr. Timo Jacob**, **Peter Koval**, **Ekaterina Rykhlinskaia**, **Cristina Sarpe–Tudoran** and **Alexander Uvarov** as well as the external collaborators: **Dr. Gediminas Gaigalas** and **Dr. Tomohiko Ishii**.

While working on this thesis, I had a few opportunities to visit the Center for Heavy Ion Research (Gesellschaft für Schwerionenforschung) in Darmstadt. I am very grateful for the hospitality to all members of atomic physics group of GSI and especially to my colleagues and friends: **Dr. Dariusz Banas**, **Dr. Alexandre Gumberidze**, **Andreas Orsic–Muthig**, **Dominik Sierpowski** and **Stanislav Tachenov**.

I would like to express my very special gratefulness to **my parents** for their love and support. Finally, thanks to **Katja** and **Liza** that we were together these three years in Kassel.

Curriculum Vitae

Name	**Andrey Surzhykov**
Born	18 January 1977 in Moscow, Russia

School education

Sep. 1984 – May 1987	primary school, Moscow
Sep. 1987 – May 1992	secondary school, Moscow
Sep. 1992 – June 1994	higher school, Moscow

University education

Sep. 1994 – Jan. 2000	Physics Department, Moscow State University named by M. V. Lomonosov
Jan. 2000	Diploma *(with honor)*, speciality "Physics", major "Theoretical Physics"

Employment

from Oct. 2000	Scientific collaborator at University of Kassel, Germany

Erklärung

Hiermit versichere ich, daß ich die vorliegende Dissertation selbständig und ohne unerlaubte Hilfe angefertigt und andere als die in der Dissertation angegebenen Hilfsmittel benutzt habe. Alle Stellen, die wörtlich oder sinngemäß aus veröffentlichten oder unveröffentlichten Schriften entnommen sind, habe ich als solche kenntlich gemacht. Kein Teil dieser Arbeit ist in einem anderen Promotions- oder Habilitationsverfahren verwendet worden.

October 2003, Kassel

Andrey Surzhykov